



LABORATÓRIO NACIONAL  
DE ENGENHARIA CIVIL

## **DEVELOPMENT OF DamDamage3D1.0**

**A MATLAB program for non-linear analysis of arch  
dams using a damage model**

Work carried out under the project P2I/LNEC, DAMFA  
"Cutting-edge solutions for sustainable assessment  
of concrete dam foundations"

Lisbon • November 2019

**R&D CONCRETE DAMS**

**REPORT 381/2019 – DBB/NMMR**

## **Title**

### **DEVELOPMENT OF DamDamage3D1.0**

A MATLAB program for non-linear analysis of arch dams using a damage model

## **Authors**

CONCRETE DAMS DEPARTMENT

### **André Filipe Moreira Alegre**

Doctoral Research Fellow, Modelling and Rock Mechanics Unit

### **Sérgio Bruno Martins de Oliveira**

Assistant Researcher, Modelling and Rock Mechanics Unit

Copyright © LABORATÓRIO NACIONAL DE ENGENHARIA CIVIL, I. P.

AV DO BRASIL 101 • 1700-066 LISBOA

e-mail: [lnec@lnec.pt](mailto:lnec@lnec.pt)

[www.lnec.pt](http://www.lnec.pt)

Report 381/2019

File no. 0402/112/2075501

## DEVELOPMENT OF DamDamage3D1.0

A MATLAB program for non-linear analysis of arch dams using a damage model

### Abstract

---

The main goal of this report is to present **DamDamage3D1.0**, a 3D finite element-based program for non-linear static analysis of arch dams, developed using MATLAB. The non-linear simulations are performed using a damage law and an iterative numerical method based on the stress-transfer technique, considering the redistribution of unbalanced forces in each iteration due to material damage. The concrete's non-linear behaviour up to failure is simulated using an isotropic damage model with softening, considering two independent scalar damage variables:  $d^+$  for tension damage and  $d^-$  for compression damage.

The implemented code was verified and optimized for a simple test structure, more specifically a concrete frame structure with three columns. According to the defined material properties for the structural elements, the concrete failure is expected to occur only at the central column without causing the collapse of the structure, which remains in equilibrium.

**DamDamage3D1.0** is used to evaluate the structural safety of Cabril arch dam (132 m high) for the concrete strength decrease scenario, considering the material deterioration under tension and compression. This failure scenario is usually considered in the scope of the safety control of dams, and the main goal is to obtain a global safety factor  $\lambda_s$  that indicates how many times the material's resistance can be reduced without causing the dam's structural collapse. This way  $\lambda_s$  is the maximum admissible multiplying factor of the applied loads.

The non-linear behaviour of the dam is analysed for the load combination with the self-weight (SW) and the hydrostatic pressure (HP) at the upstream face (full reservoir), using a 3D finite element mesh with three elements in thickness. The numerical simulations are performed using two different constitutive damage laws to evaluate the influence of the compression softening phenomenon in the global resistant capacity of the dam. The main results include displacements and stress fields and the distributions of tension and compression damage in the dam body.

Keywords: DamDamage3D1.0 / MATLAB 3DFEM program / Concrete arch dams / Cabril dam / Non-linear behaviour / Concrete strength decrease scenario / Damage model / Tension damage / Compression damage

## DESENVOLVIMENTO DO PROGRAMA DamDamage3D1.0

Um programa em MATLAB para análise não-linear de barragens abóbada usando um modelo de dano

### Resumo

---

O principal objetivo deste relatório é apresentar o programa de elementos finitos 3D **DamDamage3D1.0**, desenvolvido em MATLAB para análise da resposta estática não-linear de barragens abóbada usando uma lei constitutiva de dano. Os cálculos não-lineares são realizados com um método numérico iterativo baseado na técnica de *stress-transfer*, em que se considera a redistribuição de tensões desequilibradas em cada iteração devido ao dano. O comportamento não-linear do betão até à rotura é simulado com base num modelo de dano isotrópico de duas variáveis escalares de dano, independentes:  $d^+$  para o dano à tração e  $d^-$  para o dano à compressão.

O código desenvolvido foi calibrado e otimizado para o caso de uma estrutura simples, mais especificamente um pórtico com três pilares. De acordo com as propriedades atribuídas aos vários elementos estruturais, é esperada a rotura do betão apenas no pilar central sem levar ao colapso da estrutura, a qual permanece em equilíbrio.

O programa **DamDamage3D1.0** é utilizado para avaliar a segurança estrutural da barragem do Cabril (132 m de altura) para o cenário de decréscimo da resistência do betão, considerando a deterioração do material sob tensões de tração e de compressão. Este cenário de rotura é um dos mais importantes no âmbito do controlo da segurança estrutural de barragens, e tem como objetivo a determinação de um coeficiente de segurança global que indica quantas vezes a resistência do material pode diminuir sem que ocorra o colapso global da obra (este é calculado como o valor máximo do fator de amplificação das cargas).

O comportamento não-linear da barragem é analisado para a combinação de ações com o peso próprio (PP) e a pressão hidrostática (PH) no paramento de montante (albufeira cheia), utilizando um modelo de elementos finitos 3D refinado com três elementos em espessura. As simulações numéricas são realizadas utilizando duas leis constitutivas de dano diferentes para avaliar a influência do fenómeno de enfraquecimento em compressão na capacidade resistente global da barragem. Os principais resultados incluem os campos de deslocamentos e tensões e as distribuições de dano à compressão e à tração no corpo da obra.

Palavras-chave: DamDamage3D1.0 / Programa de elementos finitos 3D em MATLAB / Barragem abóbada de betão / Comportamento não-linear / Cenário de decréscimo da resistência do betão / Modelo de dano / Dano à tração / Dano à compressão



## Table of contents

1	Introduction.....	1
	1.1 General considerations .....	1
	1.2 Framework .....	2
	1.3 Objectives .....	3
	1.4 Report organization.....	4
2	Finite Element Models for concrete arch dams.....	5
	2.1 General considerations .....	5
	2.2 Fundamental equations of Solid Mechanics. Navier's equation .....	5
	2.3 Boundary Values Problem .....	9
	2.4 The Finite Element Method.....	10
	2.4.1 Navier's equation: from the strong to the weak formulation .....	11
	2.4.2 The discrete problem .....	11
	2.4.3 Finite element formulation. Governing equations .....	12
	2.4.4 Structural analysis.....	17
3	Constitutive damage model to simulate the non-linear behaviour of concrete .....	23
	3.1 General considerations .....	23
	3.2 Concrete non-linear behaviour.....	23
	3.3 Continuum Damage Mechanics.....	24
	3.3.1 Damage models.....	25
	3.3.2 Plasticity and damage.....	25
	3.3.3 Scalar damage variable .....	26
	3.3.4 Effective stress.....	27
	3.3.5 Constitutive relations for damaged materials.....	28
	3.4 Fracture Mechanics .....	29
	3.4.1 Types of crack models.....	29
	3.4.2 Fracture Process Zone (FPZ) .....	31
	3.4.3 Fracture energy.....	31
	3.4.4 Softening and strain localization .....	32
	3.5 Development of a constitutive damage model for the concrete.....	34
	3.5.1 Thermodynamic consistency: free energy potential .....	35
	3.5.2 Damage criteria and damage evolution laws.....	36
	3.5.3 Constitutive damage law with two independent damage variables .....	41
4	Development of a 3D FE program for non-linear analysis of arch dams .....	46
	4.1 General considerations .....	46
	4.2 DamDamage3D1.0 .....	46
	4.3 Code validation. Test with a 3D structure .....	50
5	Non-linear analysis of a large arch dam. Study for the concrete strength decrease scenario .....	56
	5.1 General considerations .....	56
	5.2 The concrete strength decrease scenario for arch dams .....	56
	5.2.1 Structural behaviour and damaged zones .....	58
	5.2.2 Compression damage in arch dams and its importance for the concrete strength decrease scenario. Numerical issues due to strain-softening .....	58
	5.3 Case study: Cabril arch dam (132 m high) .....	59
	5.4 3DFE model, material properties and constitutive laws.....	62
	5.5 Static load combination and structural analysis.....	65

5.6 Safety verification for the concrete strength decrease scenario .....67  
6| Conclusions .....75  
References .....78

## List of figures

Figure 1.1 – Cabril arch dam. View and 3DFE model (dam-reservoir-foundation system) .....	1
Figure 1.2 – Study of the concrete deterioration scenario: a) reduced scale physical model of an arch dam used in a failure test and schematic representation of the hydraulic jacks used to simulate the hydrostatic pressure; b) example of a 3DFE mesh and of a constitutive law used to perform non-linear analysis.....	2
Figure 1.3 – Inputs and outputs of DamDamage3D1.0. a) Cabril arch dam FE discretization using 3D cubic elements of 20 nodes; b) Constitutive damage law; c) Example of tension and compression damage for the main static load combination (self-weight and hydrostatic pressure) using an amplification factor $\lambda=7$ .....	3
Figure 2.1 – Generic 3D problem: gravity dam. Main unknowns: displacements, stresses and strains ..	6
Figure 2.2 – 3D problem. Fundamental equations of Solid Mechanics and Navier’s differential equation .....	9
Figure 2.3 – Example of 3DFE meshes for an arch dam. 20 node cubic FE and 16 node joint FE (global and local axis) used in DamDamage3D1.0 .....	12
Figure 2.4 – Polynomial interpolation functions. Graphical representation for 2D and 3D elements.....	13
Figure 2.5 – Example of 3DFE used in DamDamage3D1.0. Cubic element with 20 nodal point (global coordinates system), “master” element (local coordinates) with node numbering and Gauss points (adapted from [Oliveira, 2000, 2011]) .....	16
Figure 2.6 – Use of the FEM to solve the BVP posed by Navier’s differential equation and boundary conditions. Application of the FE basic approximation in the integral (weak) formulation to obtain the global stiffness matrix and load vector .....	17
Figure 2.7 – Linear FEM analysis of an arch dam. Displacement and stress fields .....	18
Figure 2.8 – Stress-transfer iterative method. Representation of the global force-displacement equilibrium for convergent and divergent processes .....	22
Figure 3.1 – Concrete behaviour up to failure under tension and compression (adapted from [Oliveira, S. 2000]) [Coutinho & Gonçalves, 1994] .....	23
Figure 3.2 – a) Biaxial stress state: failure surface; b) Concrete compressive strength for a triaxial stress state (adapted from [Oliveira, S. 2000]) [Coutinho & Gonçalves, 1994] .....	24
Figure 3.3 – Internal damage (microcracks and microvoids) and evolution to macroscopic cracks.....	24
Figure 3.4 – Plasticity and damage state (adapted from [Oliveira, S. 2000]).....	25
Figure 3.5 – Damaged and undamaged areas in a portion of material (adapted from [Oliveira, 2000])	26
Figure 3.6 – Real stress (damaged) and effective stress (undamaged) (adapted from [Faria, R. 1994]) .....	27
Figure 3.7 – Non-linear stress-strain constitutive relation for a damaged material.....	28
Figure 3.8 – Crack propagation and strain softening constitutive law.....	29
Figure 3.9 – Crack development and strain distribution for: a) discrete crack model; b) smeared crack model. Respective simulation using a FE mesh (adapted from [Oliveira, S. 2000]) .....	30
Figure 3.10 – Fracture Process Zone (FPZ). Representation of different strain-stress states near the damaged zone (adapted from [Oliveira, S. 2000]) .....	31
Figure 3.11 – Schematic representation of the different phases of a concrete’s behaviour up to failure. Unidimensional stress-strain diagrams and definition of the specific fracture energy (adapted from [Oliveira, S. 2000]) .....	32
Figure 3.12 – Failure localization for small-scale problems .....	33
Figure 3.13 – Failure localization for large-scale problems.....	34
Figure 3.14 – Elastic domain bounding surface, as defined by the stress thresholds [Faria & Oliver, 1993] .....	38
Figure 3.15 – Concrete behaviour under tension. Constitutive law with different types of softening branches: a) linear, b) bilinear and c) exponential (adapted from [Oliveira, 2000]).....	40
Figure 3.16 – Concrete behaviour under compression. Constitutive laws to represent different types of softening (adapted from [Oliveira, 2000]) .....	40

Figure 3.17 – Implemented constitutive law. Stress-strain diagrams for uniaxial tension and compression.....	42
Figure 3.18 – Computational algorithm used to obtain unidimensional stress-strain diagrams (damage law).....	44
Figure 3.19 – Computed stress-strain diagrams for uniaxial strain increments: a) tension, b) compression and c) alternate tension and compression .....	45
Figure 4.1 – a) Computational algorithm developed for DamDamage3D1.0 in MATLAB.....	48
Figure 4.2 – Test structure: 3D FE mesh, properties and constitutive damage law for the central column.....	50
Figure 4.3 – Tension damage test. First iteration: displacement and elastic stress fields, tension damage values (d+) and real stress field.....	52
Figure 4.4 – Tension damage test. End of stress-transfer: displacement field, convergence test, tension damage values (d+) and real stress field .....	53
Figure 4.5 – Compression damage test. First iteration: displacement and elastic stress fields, compression damage values (d-) and real stress field .....	54
Figure 4.6 – Compression damage test. End of stress-transfer: displacement field, convergence test, compression damage values (d-) and real stress field .....	55
Figure 5.1 – Study of the concrete strength decrease scenario for Cabril dam: a) reduced scale physical model used in a failure test; and b) 3D FE model of Cabril dam and the material constitutive law.....	57
Figure 5.2 – Cabril dam (132 m high). Aerial view, downstream views, example of a 3DFE model and cracked zone detail .....	60
Figure 5.3 – Cabril dam. Technical drawings: Plan, upstream face elevation and central cantilever's cross section .....	61
Figure 5.4 – Cabril dam. The concrete strength decrease scenario: a) reduced scale model for failure tests; and b) 3DFE model used in previous numerical studies.....	62
Figure 5.5 – Cabril dam: 3D FE mesh, material properties and constitutive law (type I and type II) .....	64
Figure 5.6 – Schematic representation of the static load combination SW+HP for an arch dam and the corresponding deformed shape .....	65
Figure 5.7 – Linear analysis. Static load combination SW+HP132. Displacement and stress fields....	66
Figure 5.8 – Non-linear response: type I constitutive law ( $\lambda_s = 7.4$ ): evolution of the radial displacements (central cantilever) and displacement field at the end of the stress-transfer process.....	69
Figure 5.9 – Non-linear response: type I constitutive law ( $\lambda_s = 7.4$ ): tension damage distributions .....	70
Figure 5.10 – Non-linear response: type I constitutive law ( $\lambda_s = 7.4$ ): compression damage distributions .....	71
Figure 5.11 – Non-linear response: type II constitutive law ( $\lambda_s = 8.1$ ): evolution of the radial displacements (central cantilever) and displacement field at the end of the stress-transfer process.....	72
Figure 5.12 – Non-linear response: type II constitutive law ( $\lambda_s = 8.1$ ): tension damage distributions ...	73
Figure 5.13 – Non-linear response: type II constitutive law ( $\lambda_s = 8.1$ ): compression damage distributions .....	74

# 1| Introduction

## 1.1 General considerations

The safety control of important structures, such as dams, bridges or tunnels, should be performed during their whole life cycle, since the design phase until the end of their useful life. In what concerns large concrete dams, structures of high potential risk [RSB, 2018], it is necessary to increase knowledge about their performance under several accident/incident scenarios, in order to meet the increasingly demanding requirements for structural safety and hence prevent incidents and accidents. This is valid for new dams and old dams, built several decades ago, with evolutionary deterioration problems (e.g. swelling reactions).

In this context, it is essential to invest in the development of accurate numerical models (Figure 1.1) to simulate the structural behaviour of dams and to support safety control studies, considering the effects of static loads (self-weight, hydrostatic pressure, thermal variations, swelling, etc.) or dynamic loads like earthquakes, and the effects of evolutionary deterioration processes, involving the dam and/or foundation materials. These numerical models for dam behaviour analysis are often based on the Finite Element Method (FEM) [Zienkiewicz, 1967, 1977; Pedro, 1977; Zienkiewicz, Taylor & Zu, 2005] using iterative numerical techniques for the simulation of different scenarios of accident/incident, under static and/or dynamic loads.

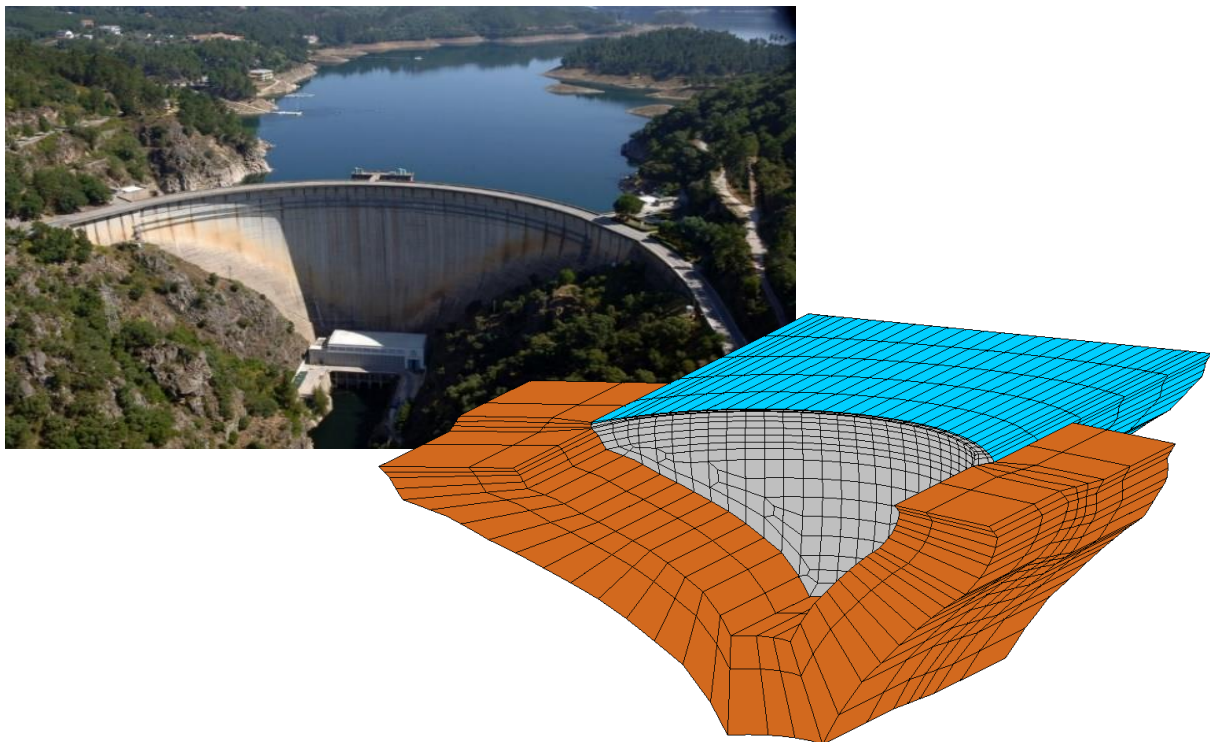


Figure 1.1 – Cabril arch dam. View and 3DFE model (dam-reservoir-foundation system)

## 1.2 Framework

In order to evaluate the global performance of dams, scenarios concerning the stability of the foundation and the dam body resistance must be studied [Pina, 1988]. These scenarios include a failure scenario concerning the concrete strength decrease under the main static loads (self-weight and hydrostatic pressure), which is to be studied in this work for a large concrete arch dam (Cabril dam, Portugal). This scenario is used by the designers to the comparison of different dams in what concerns the relationship between dam body geometry (design options) and the overall performance under a concrete strength deterioration scenario.

The concrete strength decrease scenario has been analysed in the CDD since the 1960s [Rocha & Serafim, 1960]: at first, by performing failure tests on physical models (made of gypsum and diatomite), and since the 1980s also based on numerical simulations, enabling to further understand the observed behaviour and to calibrate the FE models (Figure 1.2). The non-linear response is usually analysed for a static load combination considering the dam self-weight (SW) and the hydrostatic pressure (HP) at the upstream face (water at the crest level). As for the numerical studies, the non-linear calculations have been performed using 3DFEM based codes, while the concrete deterioration under tension and compression is based on isotropic damage models with two independent scalar damage variables [Oliveira, 2000].

For this scenario simulation the main goal is to compute a global safety factor  $\lambda_s$  that represents the maximum concrete strength decrease that can occur without causing the dam's collapse. Due to the impracticability of reducing the material resistance in the experimental tests with physical models, which were performed by assuming a proportional amplification to the applied loads<sup>1</sup>, the safety factor was obtained as the maximum multiplying factor of the applied forces  $\lambda$ . The same assumptions have been made in the numerical studies.

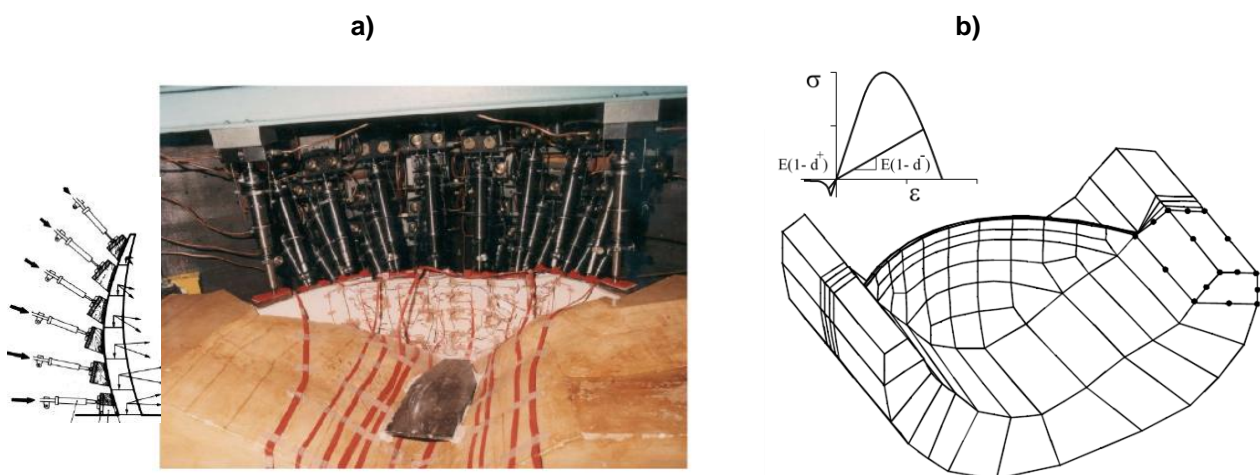


Figure 1.2 – Study of the concrete deterioration scenario: a) reduced scale physical model of an arch dam used in a failure test and schematic representation of the hydraulic jacks used to simulate the hydrostatic pressure; b) example of a 3DFE mesh and of a constitutive law used to perform non-linear analysis

<sup>1</sup> The equivalent forces were applied to the physical dam model using a system of hydraulic jacks.

### 1.3 Objectives

In view of the above considerations, the primary focus in this work is to present **DamDamage3D1.0**, a new 3DFEM program developed in MATLAB for non-linear static analysis of arch dams (Figure 1.3), and to demonstrate its potential to evaluate the performance and assess the structural safety of arch dams for the concrete strength decrease scenario. The theoretical foundations on which the implemented formulations are based and the algorithm of the developed code are also presented. The aim is to develop a code based on an iterative numerical method using the *stress-transfer* technique to carry out the non-linear calculations, while the concrete's non-linear behavior up to failure is simulated with an isotropic damage model of two independent damage variables:  $d^+$  for tension damage and  $d^-$  for compression damage.

Considering the importance of the concrete strength decrease scenario, the developed program will be used to evaluate the structural safety of Cabril arch dam (132 m high) for the referred scenario, considering the material deterioration under tension and compression, in view of computing the global safety factor  $\lambda_s$ . The non-linear simulations are to be carried out using two constitutive laws to evaluate the influence of the compression softening phenomenon in the global resistant capacity of the dam.

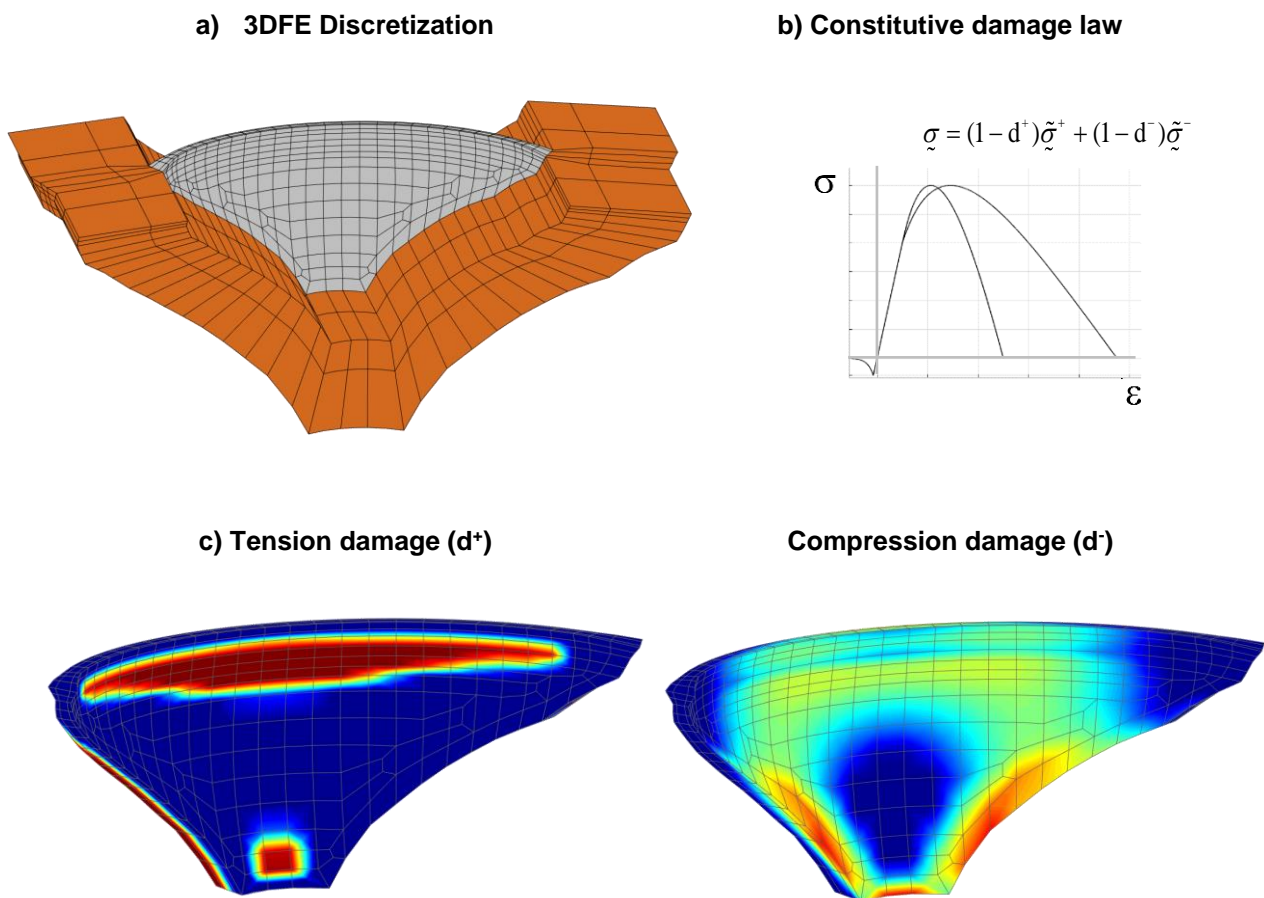


Figure 1.3 – Inputs and outputs of DamDamage3D1.0. a) Cabril arch dam FE discretization using 3D cubic elements of 20 nodes; b) Constitutive damage law; c) Example of tension and compression damage for the main static load combination (self-weight and hydrostatic pressure) using an amplification factor  $\lambda=7$

## 1.4 Report organization

This report comprises six chapters, including this introduction chapter and the final chapter for conclusions.

Chapter 2 addresses the development of FE models to simulate the response of concrete arch dams, with focus on the fundamental equations of Solids Mechanics and referring the basics of Finite Element Method and their application to structural analysis.

In Chapter 3 the key concepts of Continuum Damage Mechanics and Fracture Mechanics are summarised. The developed constitutive damage model and its fundamentals are presented in detail, followed by the computational algorithm implemented in MATLAB.

The developed program ***DamDamage3D1.0*** is presented in chapter 4, including its main features and an abridged version of its algorithm. Aiming to calibrate and verify the code, a non-linear analysis is carried out for a simple test structure (a concrete frame with three columns).

Finally, the developed program is used to study the non-linear behaviour of Cabril arch dam for the static load combination including the self-weight and the hydrostatic pressure. The goal is to simulate the concrete strength decrease scenario, considering the material deterioration under tension and compression, in order to obtain the corresponding global safety factors. The non-linear calculations are performed using two types of strain-softening constitutive laws to assess the influence of compression softening in the dam's global resistant capacity. The numerical results include displacements and stresses and the distribution of tension and compression damage in the dam body.



## 2| Finite Element Models for concrete arch dams

### 2.1 General considerations

The numerical models based on the FEM are of great use to simulate the structural response and to perform safety verifications of concrete dams under static and dynamic loads, considering linear or non-linear behaviour for dam body, for foundation materials and for existing joints. Aiming to achieve reliable numerical results, it is fundamental to develop robust numerical models that properly represent the dam behavior.

In this chapter the fundamental equations of Solid Mechanics and the key concepts and the formulation of the Finite Element Method (FEM) and their application for static analysis are presented. Some important aspects regarding the development of *DamDamage3D1.0* are also addressed.

### 2.2 Fundamental equations of Solid Mechanics. Navier's equation

For a structural analysis problem, the main goal is to calculate the displacements, stresses and strains in each point of the dam body, knowing its geometry, material properties, mass forces and the outlined boundary conditions. Considering a generic three-dimensional (3D) problem (Figure 2.1), the main unknown for a given point P are the displacement vector

$$\underline{u} = \underline{u}(x_1, x_2, x_3) = \begin{bmatrix} u_1(x_1, x_2, x_3) \\ u_2(x_1, x_2, x_3) \\ u_3(x_1, x_2, x_3) \end{bmatrix} \quad (2.1)$$

The tensors that define the strain and stress state at point P can be represented by symmetric matrices (in the reference axes  $(x_1, x_2, x_3)$  )

$$\underline{\varepsilon} = \begin{bmatrix} \varepsilon_{11} & \varepsilon_{12} & \varepsilon_{13} \\ \varepsilon_{21} & \varepsilon_{22} & \varepsilon_{23} \\ \varepsilon_{31} & \varepsilon_{32} & \varepsilon_{33} \end{bmatrix} \quad (2.2)$$

$$\underline{\sigma} = \begin{bmatrix} \sigma_{11} & \sigma_{12} & \sigma_{13} \\ \sigma_{21} & \sigma_{22} & \sigma_{23} \\ \sigma_{31} & \sigma_{32} & \sigma_{33} \end{bmatrix} \quad (2.3)$$

The normal and shear stress components are represented by  $\sigma_{ii}$  and  $\sigma_{ij}$ . The normal strains  $\varepsilon_{ii}$  are associated with length variations while the shear strains  $\varepsilon_{ij}$  are related to angle variations (distortions). Both tensors can be presented in a compact vector format

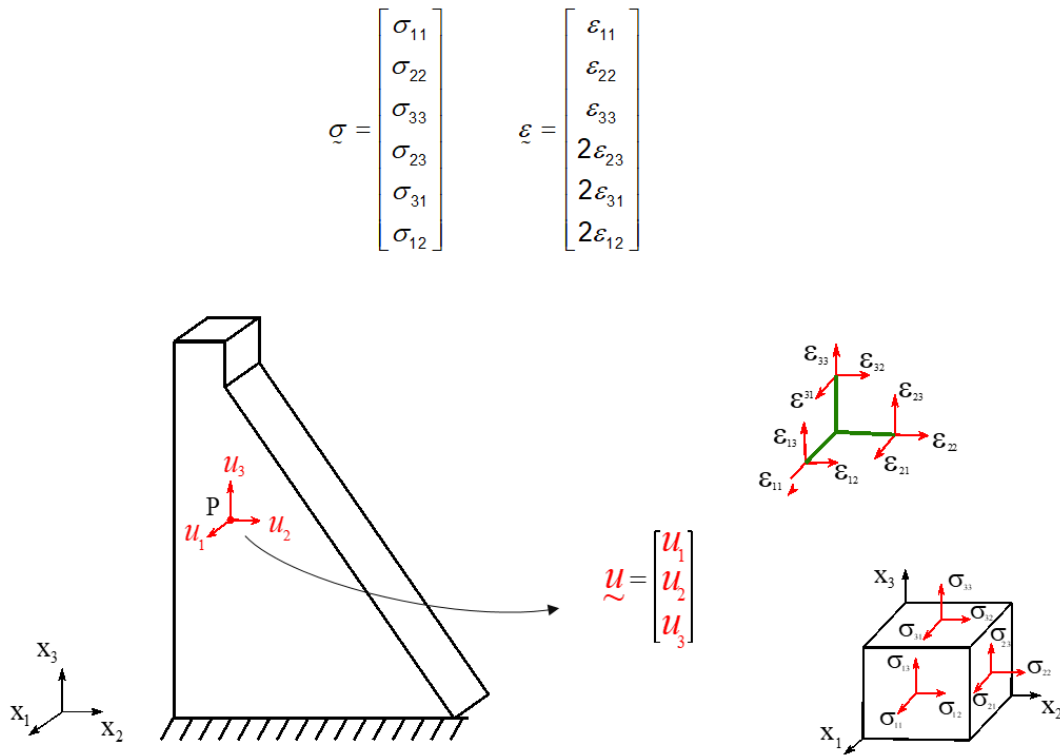


Figure 2.1 – Generic 3D problem: gravity dam. Main unknowns: displacements, stresses and strains

The fundamental equations of Solid Mechanics are used to establish the relations between displacements, stresses and strains. Aiming at solving a 3D structural analysis problem, a total of 15 equations are defined, including: six compatibility differential equations, that relate displacements and strains, six algebraic constitutive equations for the stress-strain relations, and three differential equilibrium equations between mass forces and stresses.

Concerning the displacement-strains relations, the differential equations for normal and shear strain components are

$$\varepsilon_{ii} = \frac{\partial u_i}{\partial x_i} \quad (2.5)$$

$$\varepsilon_{ij} = \frac{1}{2} \cdot \left( \frac{\partial u_i}{\partial x_j} + \frac{\partial u_j}{\partial x_i} \right) \quad (2.6)$$

Thus, the relation between the strain tensor and the displacement vector is given by

$$\underline{\varepsilon} = \begin{bmatrix} \varepsilon_{11} \\ \varepsilon_{22} \\ \varepsilon_{33} \\ 2\varepsilon_{23} \\ 2\varepsilon_{31} \\ 2\varepsilon_{12} \end{bmatrix} = \begin{bmatrix} \frac{\partial}{\partial x_1} & 0 & 0 \\ 0 & \frac{\partial}{\partial x_2} & 0 \\ 0 & 0 & \frac{\partial}{\partial x_3} \\ 0 & \frac{\partial}{\partial x_3} & \frac{\partial}{\partial x_2} \\ \frac{\partial}{\partial x_3} & 0 & \frac{\partial}{\partial x_1} \\ \frac{\partial}{\partial x_2} & \frac{\partial}{\partial x_1} & 0 \end{bmatrix} \begin{bmatrix} u_1 \\ u_2 \\ u_3 \end{bmatrix} \quad (2.7)$$

which defines the compatibility equation with  $\underline{L}$  as a matrix differential operator,

$$\underline{\varepsilon} = \underline{L} \cdot \underline{u} \quad (2.8)$$

$\begin{matrix} (6 \times 1) & & (6 \times 3) & (3 \times 1) \end{matrix}$

Regarding the stress-strain relations, the differential equations for normal and shear stresses yield

$$\varepsilon_{ii} = \frac{\sigma_{ii}}{E} - \nu \frac{\sigma_{jj}}{E} - \nu \frac{\sigma_{kk}}{E} \quad (2.9)$$

$$2\varepsilon_{ij} = \frac{\sigma_{ij}}{G} \quad (2.10)$$

where E is Young's modulus and  $\nu$  is Poisson's ratio. Based on the above expressions and knowing that the shear modulus G and the bulk modulus K are obtained in function of E and  $\nu$ ,

$$G = \frac{E}{2(1+\nu)} \quad (2.11)$$

$$K = \frac{E}{3(1-2\nu)} \quad (2.12)$$

then the stress-strain constitutive equation is established

$$\underline{\sigma} = \underline{D} \cdot \underline{\varepsilon} \quad (2.13)$$

$\begin{matrix} (6 \times 1) & (6 \times 6) & (6 \times 1) \end{matrix}$

where  $\underline{D}$  is the elasticity matrix that relates all six stress and strain components

$$\underline{\sigma} = \begin{bmatrix} \sigma_{11} \\ \sigma_{22} \\ \sigma_{33} \\ \sigma_{23} \\ \sigma_{31} \\ \sigma_{12} \end{bmatrix} = \begin{bmatrix} K + \frac{4}{3}G & K - \frac{2}{3}G & K - \frac{2}{3}G & & & \\ K - \frac{2}{3}G & K + \frac{4}{3}G & K - \frac{2}{3}G & & & \\ K - \frac{2}{3}G & K - \frac{2}{3}G & K + \frac{4}{3}G & & & \\ & & & 0 & & \\ & & & & G & 0 & 0 \\ & & & & 0 & G & 0 \\ & & & & 0 & 0 & G \end{bmatrix} \begin{bmatrix} \varepsilon_{11} \\ \varepsilon_{22} \\ \varepsilon_{33} \\ 2\varepsilon_{23} \\ 2\varepsilon_{31} \\ 2\varepsilon_{12} \end{bmatrix} \quad (2.14)$$

From the force-stress equilibrium at point P, expressed as a sum of all forces in the i-direction

$$\sum F_{x_i} = 0 \rightarrow \frac{\partial \sigma_{ii}}{\partial x_i} + \frac{\partial \sigma_{ji}}{\partial x_j} + \frac{\partial \sigma_{ki}}{\partial x_k} + f_i = 0 \quad (2.15)$$

the equilibrium equation that relates the stresses and mass body forces is obtained

$$\underline{L}^T \cdot \underline{\sigma} + \underline{f} = \underline{0} \quad (2.16)$$

$\begin{matrix} (3 \times 6) & (6 \times 1) & (3 \times 1) & (3 \times 1) \end{matrix}$

The term  $\underline{L}^T \cdot \underline{\sigma}$  represents the stress gradient and  $\underline{f} = \underline{f}(x_1, x_2, x_3)$  is the body force vector. For a static analysis the body force is given by the gravity forces<sup>2</sup>,  $\rho \underline{g}$ , where  $\rho$  is the material density (kg/m<sup>3</sup>) and  $\underline{g} = [0 \ 0 \ -9.81]^T$  is the gravity acceleration vector (m/s<sup>2</sup>). The initial strain-thermal effects are omitted herein.

By substituting eq. 2.8 into eq. 2.14, and the latter into eq. 2.16 (Figure 2.2), the equilibrium between internal elastic forces and body forces, to be verified for all points belonging to the domain  $\Omega$ , is defined by Navier's differential equation in terms of the material properties, the problem unknowns (displacements) and the body forces,

$$\underline{L}^T (\underline{D} \underline{L} \underline{u}) + \underline{f} = \underline{0}, \quad \forall P(x_1, x_2, x_3) \in \Omega \quad (2.17)$$

---

<sup>2</sup> For dynamic analysis, the mass forces induced by dynamic motion (damping and inertia) would be considered.

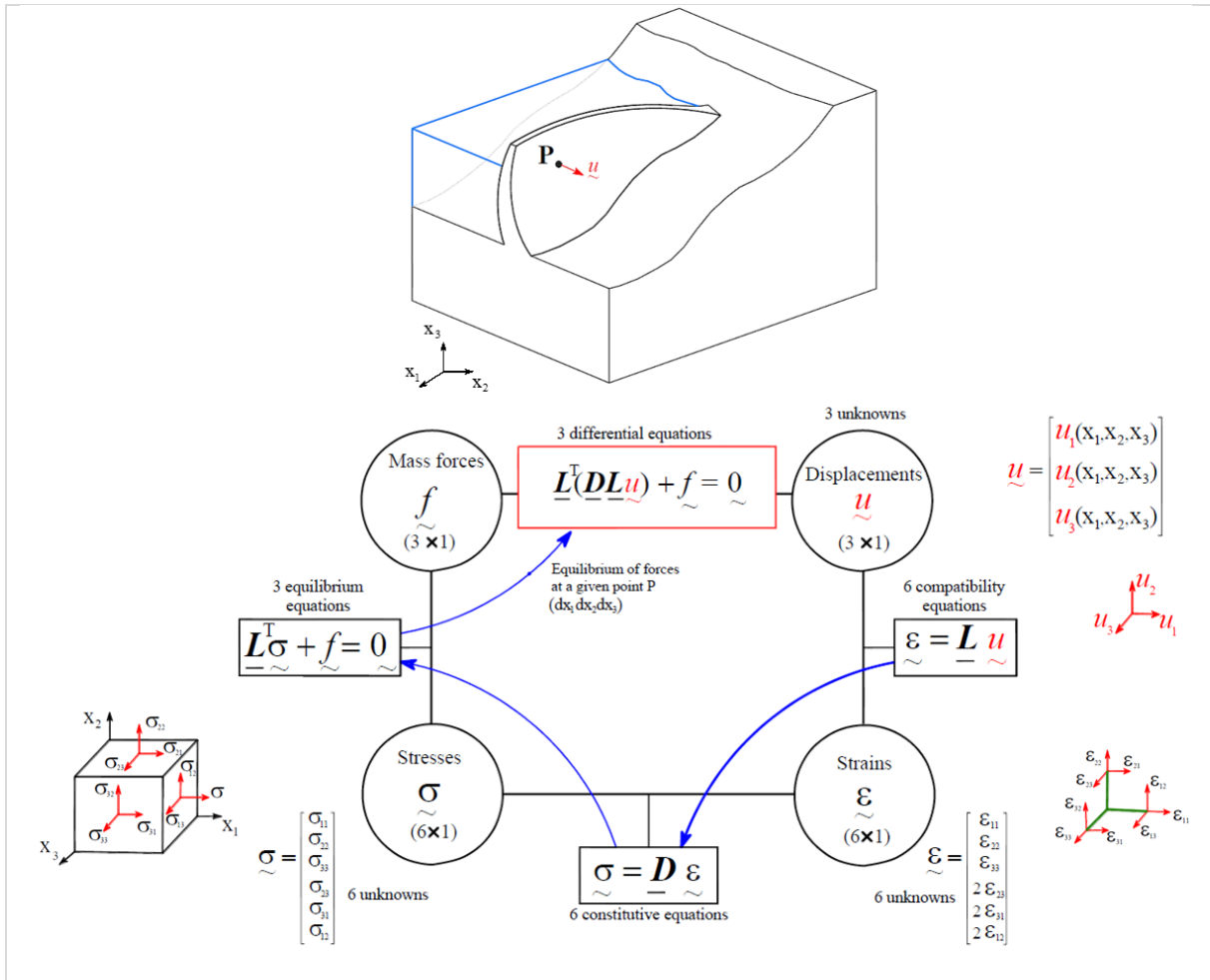


Figure 2.2 – 3D problem. Fundamental equations of Solid Mechanics and Navier's differential equation

### 2.3 Boundary Values Problem

To completely define the BVP for the structure under analysis, boundary conditions must be specified for each point at the boundaries  $\Gamma$  of the domain  $\Omega$  where these are applicable. Two types of boundary conditions can be considered: displacement and traction boundary conditions [Zienkiewicz et al. 2005], Displacement boundary conditions are specified for each point of the boundary  $\Gamma_u$  by prescribing known displacement values  $\bar{u}$  (e.g. null displacements on nodal points where elastic supports exist),

$$u = \bar{u}, \quad \forall P(x_1, x_2, x_3) \in \Gamma_u \quad (2.18)$$

Traction boundary conditions are prescribed at each point of the boundary  $\Gamma_t$  and are given in terms of stresses  $\bar{t}$  (force per unit area) applied in the boundary surface (e.g. water pressure on the upstream face of a dam),

$$\underline{t} = \bar{t}, \quad \forall P(x_1, x_2, x_3) \in \Gamma_t \quad (2.19)$$

being

$$\underline{t} = \underline{G}^T \cdot \underline{\sigma} = \underline{G}^T \cdot \underline{D}(\underline{L}\underline{u}) \quad (2.20)$$

where  $\underline{G}^T$  is a matrix containing the direction cosines for the normal direction to the traction boundary  $\Gamma_t$ ,

$$\underline{G}^T = \begin{bmatrix} n_x & 0 & 0 & n_y & 0 & n_z \\ 0 & n_y & 0 & n_z & n_z & 0 \\ 0 & 0 & n_z & 0 & n_y & n_x \end{bmatrix} \quad (2.21)$$

Finally, the BVP for linear structural analysis is posed by Navier's differential equation and specific boundary conditions,

$$\begin{cases} \underline{L}^T (\underline{D}\underline{L}\underline{u}) + \underline{f} = 0, & \forall P(x_1, x_2, x_3) \in \Omega \\ \underline{u} = \bar{u}, & \forall P(x_1, x_2, x_3) \in \Gamma_u \\ \underline{t} = \bar{t}, & \forall P(x_1, x_2, x_3) \in \Gamma_t \end{cases} \quad (2.22)$$

## 2.4 The Finite Element Method

The use of an analytical approach to solve Navier's differential is only possible for simple elementary problems, e.g the case of a column supporting its self-weight or the deflection of an elastic beam. However, more complex problems involving 2D or 3D analysis require the use of numerical methods to obtain approximate solutions for the corresponding differential equations [Oliveira & Pedro, 1986]. The FEM [Zienkiewicz, et al., 2005] is widely used to solve problems in several fields, including structural analysis, fluid behaviour, heat conduction, etc., due to the potential of the finite element process to simulate an extensive range of boundary and/or initial value problems.

Furthermore, the classic displacement formulation [Oliveira, 1975] ensures computational robustness when applied to large structures, as is the case of arch dams, which are simulated using models comprising a great amount of data. For these above reasons and considering the previous experience in working with FEM based codes, this was the chosen method in the development of **DamDamage3D1.0** (to be presented in chapter 4).

So, in order to obtain an approximate solution to a continuum problem using the FEM, some standard steps have to be followed: i) first, the equilibrium equations, such as Navier's equation for structural analysis, should be transformed from the strong formulation (differential form) to the corresponding weak form (integral form); ii) second, the continuous domain is discretized into finite elements, enabling the application of the finite element formulation to establish the equilibrium equations at an elementary level; iii) third, the global equilibrium equation for the complete discretized system is obtained by assembling the element contributions; iv) finally, the solution can be calculated, allowing linear or non-linear simulations to be performed.

#### 2.4.1 Navier's equation: from the strong to the weak formulation

The first step in the finite element process consists in constructing the integral or weak form of the BVP, including Navier's differential equation and the boundary conditions (eq. 2.22). The integral form can be reached using the Variational Formulation (involving the Fundamental Lemma of Calculus of Variations and the Green-Gauss Theorem) or the Virtual Work Principle [Zienkiewicz et al.,2005]. Therefore, the weak form of the governing equilibrium equation yields

$$\int_{\Omega} \delta_u^T [\underline{L}^T \underline{\sigma} - \underline{f}] d\Omega - \int_{\Gamma_t} \delta_u^T \underline{t} d\Gamma = 0 \quad (2.23)$$

$$\int_{\Omega} (\underline{L} \delta_u)^T \cdot (\underline{D} \underline{L} u) d\Omega - \int_{\Omega} \delta_u \underline{f} d\Omega - \int_{\Gamma_t} \delta_u^T \underline{t} d\Gamma = 0 \quad (2.24)$$

The displacement boundary condition  $u = \bar{u}$  for all points on  $\Gamma_u$  is omitted from this formulation and is latter introduced in the solution for the unknown displacements vector. The term  $\delta_u$  indicates a set of arbitrary functions (sometimes referred to as virtual displacements) or test functions that satisfy the equilibrium differential equations for all points in the problem's domain  $\Omega$ . This weak form will enable the incorporation of the finite element approximation, to obtain the solution element by element and the subsequent assembly for the global system.

#### 2.4.2 The discrete problem

To solve the structural problem using the FEM it is necessary to divide the structure into a finite number of elements, connected by common nodal points, which results in the definition of a mesh. Considering the displacement formulation for 3D structural analysis, each nodal point has three displacement degrees of freedom (DOF).

For the discrete system, the weak form of the governing equation can be approximated by dividing the integrals on the global domain  $\Omega$  and the respective boundaries  $\Gamma$  (eq. 2.24) into sums over each element

$$\sum_e \int_{\Omega_e} (\underline{L}\underline{\delta}_u)^T \cdot (\underline{D}\underline{L}\underline{u}) d\Omega - \sum_e \int_{\Omega_e} \underline{\delta}_u^T \underline{f} d\Omega - \sum_e \int_{\Gamma_{t,e}} \underline{\delta}_u^T \underline{\bar{t}} d\Gamma = 0 \quad (2.25)$$

where  $\Omega_e$  indicates the element domain and  $\Gamma_{t,e}$  denotes the part of the boundary for elements where traction boundary conditions are applied. In short, for each element we can write

$$\int_{\Omega_e} (\underline{L}\underline{\delta}_u)^T \cdot (\underline{D}\underline{L}\underline{u}) d\Omega - \int_{\Omega_e} \underline{\delta}_u^T \underline{f} d\Omega - \int_{\Gamma_{t,e}} \underline{\delta}_u^T \underline{\bar{t}} d\Gamma = 0 \quad (2.26)$$

For the FE discretization can be used different types of elements, with varying shapes and number of nodal points. In **DamDamage3D1.0**, can be use discretizations with serendipity FE: i) 3D isoparametric elements with twenty nodal points for the continuum (e.g. dam body and foundation); and ii) compatible joint (or surface) elements with sixteen nodes to define discontinuities (e.g. contraction joints or existing cracks). Thus, all vectors and matrix dimensions henceforth indicated refer to this type of FE.

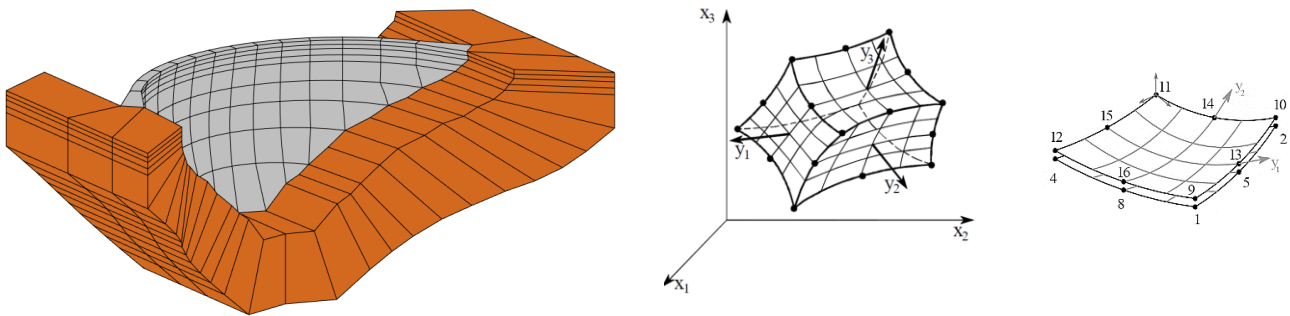


Figure 2.3 – Example of 3DFE meshes for an arch dam. 20 node cubic FE and 16 node joint FE (global and local axis) used in DamDamage3D1.0

### 2.4.3 Finite element formulation. Governing equations

#### Displacement approximation

Aiming to achieve an approximate numerical solution at each modal point of the global discrete domain, the approximation functions for the main unknown  $\underline{u}$  need to be defined [Zienkiewicz et al., 2005], knowing that these functions must satisfy the requirement of continuity between adjacent elements.

In the finite element procedure, the solution for the unknown displacement vector  $\underline{u}$  at a generic point P, located in a FE of domain  $\Omega^e$ , is approximated by

$$\underline{u} = \hat{\underline{u}} = \underline{N}_u \cdot \underline{u}^e \quad (2.27)$$



$$\underline{u} = \begin{Bmatrix} u^1 \\ u^2 \\ u^3 \end{Bmatrix}_{(3 \times 1)} = \begin{bmatrix} N_{u,1} & 0 & 0 & N_{u,2} & 0 & 0 & \ddots & N_{u,20} & 0 & 0 \\ 0 & N_{u,1} & 0 & 0 & N_{u,2} & 0 & \ddots & 0 & N_{u,20} & 0 \\ 0 & 0 & N_{u,1} & 0 & 0 & N_{u,2} & \ddots & 0 & 0 & N_{u,20} \end{bmatrix} \cdot \begin{Bmatrix} u_1^{e1} \\ u_1^{e2} \\ u_1^{e3} \\ \vdots \\ u_{20}^{e1} \\ u_{20}^{e2} \\ u_{20}^{e3} \end{Bmatrix}_{(60 \times 1)} \quad (2.28)$$

where  $u^e$  (60×1) are the nodal parameters or nodal displacement values and  $N_u$  (3×60) are matrices containing the interpolation (or shape) functions, defined in terms of the local coordinates  $(y_1, y_2, y_3)$  in the master element (Figure 2.4). This approximation is valid for the arbitrary functions, using the same shape functions (Galerkin method),

$$\hat{\delta}_u = \hat{\delta}_u^e = N_u \cdot \delta_u^e \quad (2.29)$$

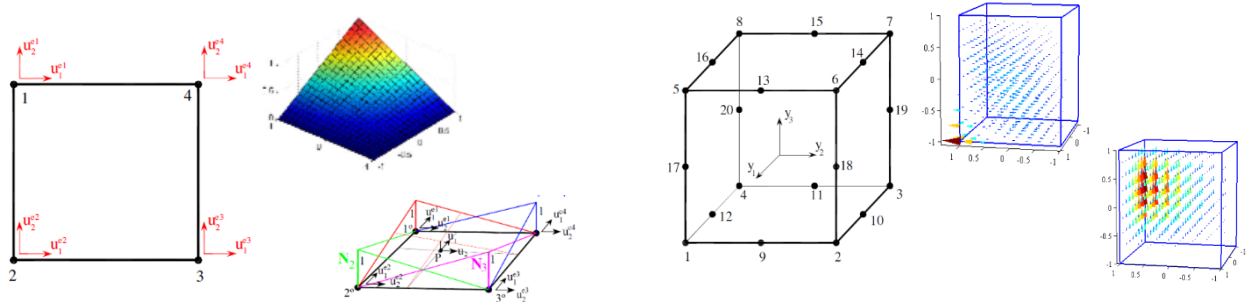


Figure 2.4 – Polynomial interpolation functions. Graphical representation for 2D and 3D elements

### Strain and stress approximations

Considering the infinitesimal strain theory and the hypothesis of linear-elastic behaviour, eq. (2.27) can then be introduced into the constitutive and compatibility relations to obtain the approximate solutions for stresses and strains,

$$\varepsilon = \underline{L} N_u u^e = \underline{B}_u u^e \quad (2.30)$$

$$\sigma = \underline{D} \underline{B}_u u^e \quad (2.31)$$

where  $\underline{B}_u = \underline{L} N_u$  (6×60) is the matrix with the derivatives of the interpolation functions.

### Element stiffness matrices and load vectors

Based on the standard Galerkin discretization [2] and substituting the above approximations for displacements, stresses and strains in the weak form of the finite element equilibrium equation (eq. 2.25), the elementary equilibrium yields

$$\int_{\Omega_e} \delta_u^{eT} \underline{B}_u^T \underline{D} \underline{B}_u \underline{u}^e d\Omega - \int_{\Omega_e} \delta_u^{eT} \underline{N}_u^T \underline{f} d\Omega - \int_{\Gamma_{t,e}} \delta_u^{eT} \bar{\underline{t}} d\Gamma = 0 \quad (2.32)$$

from which we can write

$$\underline{k}^e \cdot \underline{u}^e = \underline{f}^e \quad (2.33)$$

Therefore, the elementary stiffness matrices  $\underline{k}^e$  (60×60) and the body load vectors  $\underline{f}^e$  (60×1) can be obtained by calculating the integrals

$$\underline{k}^e = \int_{\Omega_e} \underline{B}_u^T \underline{D} \underline{B}_u \underline{u}^e d\Omega \quad (2.34)$$

$$\underline{f}^e = \underline{f}_{\Omega_e}^e + \underline{f}_{\Gamma_{t,e}}^e \quad (2.35)$$

being

$$\underline{f}_{\Omega_e}^e = \int_{\Omega_e} \underline{N}_u^T \underline{f} d\Omega \quad \text{and} \quad \underline{f}_{\Gamma_{t,e}}^e = \int_{\Gamma_{t,e}} \underline{N}_u^T \cdot \bar{\underline{t}} d\Gamma \quad (2.36)$$

As mentioned above, the displacement boundary conditions are incorporated by prescribing known displacement values  $\bar{\underline{u}}$  for nodal points where that conditions are applied, while the traction boundary forces are obtained the surface integral (over  $\Gamma_{t,e}$ ).

**DamDamage3D1.0** was developed to perform structural analysis of arch dams considering the main static loads, namely the combination including the dam self-weight (SW) and the hydrostatic pressure (HP). Regarding the implemented finite element procedure, the nodal forces corresponding to the dam weight are computed as the nodal forces equivalent to the body forces in all elements,

$$\underline{f} = \rho \underline{g} \rightarrow \underline{f}_{sw}^e = \rho \int_{\Omega_e} \underline{N}_u^T \underline{g} d\Omega \quad (2.37)$$

The external nodal forces due to the hydrostatic pressure (boundary condition at the upstream dam face  $\Gamma_t$ ) are calculated on the corresponding boundary nodes, by considering the water pressure on the surface,

$$\bar{\mathbf{t}} = \mathbf{N}_{\Gamma_e}^T \gamma_w h_w \rightarrow \mathbf{f}_{\Gamma_{t,e}}^e = \gamma_w \int_{\Gamma_{t,e}} \mathbf{N}_U^T \cdot \mathbf{N}_{\Gamma_e}^T h_w d\Gamma \quad (2.38)$$

where  $\gamma_w$  denotes the water specific weight and  $h_w$  is the water height above each boundary surface point.

### Numerical integration

The integration over each element domain  $\Omega_e$  can be computed by numerical quadrature [Zienkiewicz et al., 2005], accounting for the mapping from local coordinates, at the element level, to global coordinates, at the global structure level. Therefore, volume integrals (or surface integrals) are approximated as the sum of Q components associated with each quadrature point q,

$$\int_V (\cdot) dV \approx \sum_{q=1}^Q (\cdot)_q J_q W_q \quad (2.39)$$

where  $J_q$  is the determinant of the jacobian matrix that transforms local to global coordinates at point q and  $W_q$  is the weight (associated volume) for each quadrature point q.

These integrals are commonly calculated based on the Gauss integration method and using serendipity type elements, which are idealized at the local coordinate system as a perfectly dimensioned cube with local coordinates  $(y_1, y_2, y_3)$  that vary from -1 to +1 [Zienkiewicz, et al., 2005]. Therefore, based on Gauss quadrature, the elementary stiffness matrices and load vectors are computed as

$$\underline{\mathbf{k}}^e = \int_{\Omega_e} \underline{\mathbf{B}}_U^T \underline{\mathbf{D}} \underline{\mathbf{B}}_U d\Omega = \sum_{n_{GP}=1}^N \underline{\mathbf{B}}_{U,n_{GP}}^T \underline{\mathbf{D}} \underline{\mathbf{B}}_{U,n_{GP}} J_{n_{GP}} W_{n_{GP}} \quad (2.40)$$

$$\underline{\mathbf{f}}^e = \int_{\Gamma_e} \underline{\mathbf{N}}_U^T \underline{\mathbf{f}} d\Gamma = \sum_{n_{GP}=1}^N \underline{\mathbf{N}}_{n_{GP}}^T \underline{\mathbf{f}} J_{n_{GP}} W_{n_{GP}} \quad (2.41)$$

$$\mathbf{f}_{\Gamma_{t,e}}^e = \int_{\Gamma_{t,e}} \underline{\mathbf{N}}_U^T \cdot \bar{\mathbf{t}} d\Gamma = \sum_{n_{GP,\Gamma}=1}^{N_\Gamma} \underline{\mathbf{N}}_{U,n_{GP,\Gamma}}^T \bar{\mathbf{t}} J_{n_{GP,\Gamma}} W_{n_{GP,\Gamma}} \quad (2.42)$$

where  $\underline{\mathbf{N}}_{n_{GP}}^T$  and  $\underline{\mathbf{B}}_{U,n_{GP}}^T$  are, respectively, the matrices with the values of the interpolation functions and its derivatives, at the quadrature points.

In *DamDamage3D1.0*, 3D isoparametric cubic elements with 20 nodal points are used and the numerical integration is performed using 27 quadrature Gauss points ( $n_{gp}$ ) per element (Figure 2.5) to obtain the stiffness matrices and load vectors over each element. Similarly, the surface integral of the external boundary forces is computed with the Gauss integration method, using 9 face Gauss points ( $n_{gp,\Gamma}$ ).

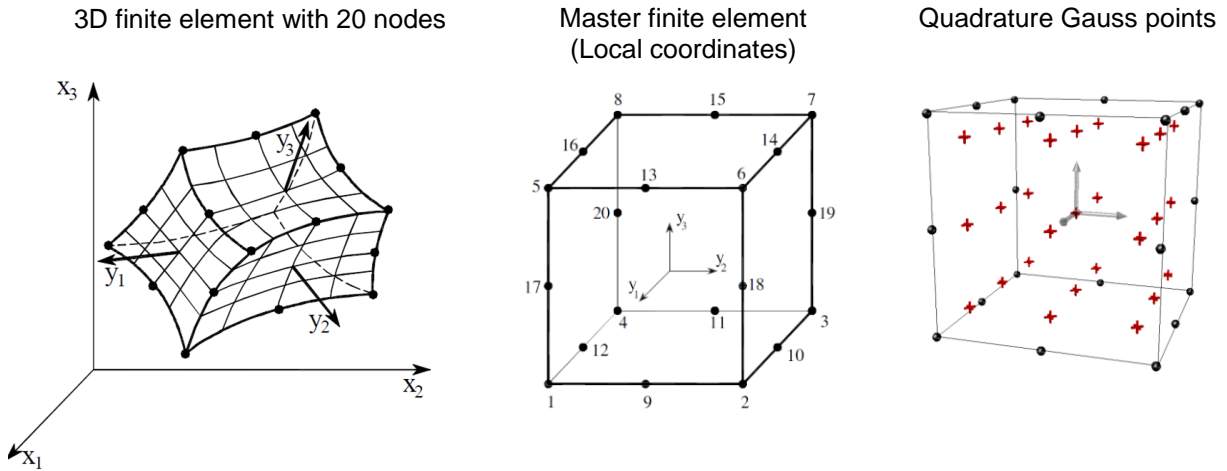


Figure 2.5 – Example of 3DFE used in *DamDamage3D1.0*. Cubic element with 20 nodal point (global coordinates system), “master” element (local coordinates) with node numbering and Gauss points (adapted from [Oliveira, 2000, 2011])

### Global stiffness matrix and load vector

The global stiffness matrix and load vector (including body forces and surface forces) for the complete discrete structure are obtained by assembling ("Σ") the element contributions,

$$\underline{\mathbf{K}}_{(N_{DOF} \times N_{DOF})} = \sum_e \underline{\mathbf{k}}^e \quad (2.43)$$

$$\underline{\mathbf{F}}_{(N_{DOF} \times 1)} = \sum_e \underline{\mathbf{f}}^e + \sum_{\Gamma_t} \underline{\mathbf{f}}_{\Gamma_t}^e \quad (2.44)$$

Finally, after considering the displacement boundary conditions using, for example, the penalty method, the global static equilibrium equation for the discretized system (Figure 2.6) is given by

$$\underline{\mathbf{K}} \cdot \underline{\mathbf{u}} = \underline{\mathbf{F}} \quad (2.45)$$

where  $\underline{\mathbf{u}}$  ( $N_{DOF} \times 1$ ) is the global displacements vector of the discrete system (with 3 displacement components for each nodal point).

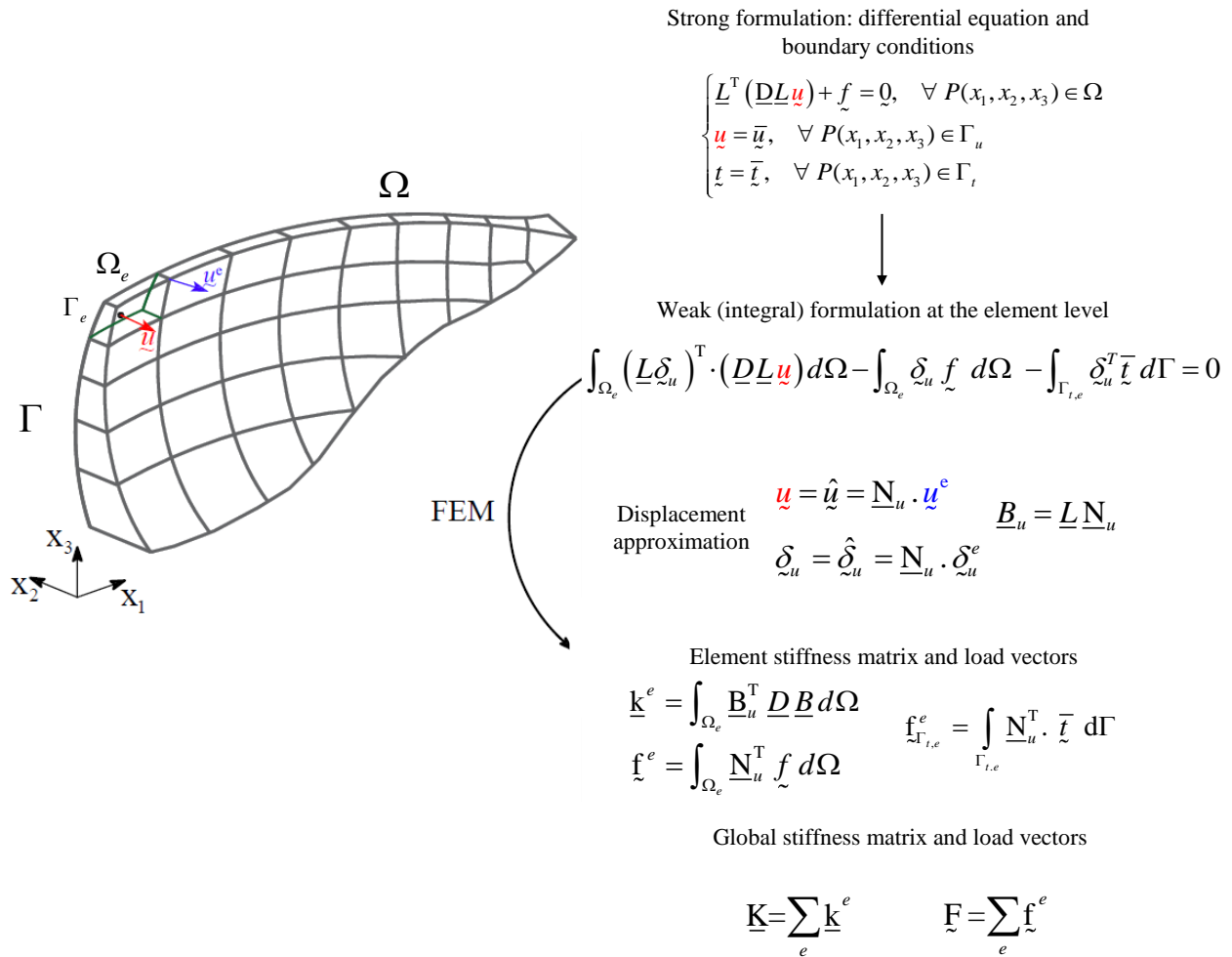


Figure 2.6 – Use of the FEM to solve the BVP posed by Navier’s differential equation and boundary conditions. Application of the FE basic approximation in the integral (weak) formulation to obtain the global stiffness matrix and load vector

## 2.4.4 Structural analysis

### Linear analysis

Based on the FEM procedure, the 3D structural analysis problem posed by Navier’s differential equation and the boundary conditions (eq. 2.22) is transformed into a set of linear algebraic equations (eq. 2.45). Considering a linear elastic analysis, the displacements are computed by solving (eq. 2.45), being

$$\underline{u} = \underline{K}^{-1} \cdot \underline{F} \quad (2.46)$$

The finite element formulation, based on the approximation of the solution (displacements  $\underline{u}$  at a generic point P), results in a realistic representation of the displacement field over the discrete system domain by computing the displacements in each node. Regarding the strains and stresses, which tend to be

continuous within the material, one should ensure that the strain and stress fields are computed in a realistic and accurate way. This can be achieved through several methods [Zienkiewick et al., 2005]. One of these methods, which was implemented in **DamDamage3D1.0**, consists in assuming that these quantities can be approximated in points inside the element domain by interpolation in the same manner as the displacements, using the constitutive and compatibility relations with the displacement approximation (eqs. 2.26 and 2.27). Therefore, using the Gauss integration method, the strain and stress tensors are computed for every Gauss point ( $n_{GP}$ ) of all elements,

$$\underline{\varepsilon}_{n_{GP}} = \underline{L} \underline{N}_{u,n_{GP}} \underline{u}^e = \underline{B}_{u,n_{GP}} \underline{u}^e \quad (2.47)$$

$$\underline{\sigma}_{n_{GP}} = \underline{D} \underline{\varepsilon}_{n_{GP}} \quad \Rightarrow \quad \underline{\sigma}_{n_{GP}} = \underline{D} \underline{B}_{u,n_{GP}} \underline{u}^e \quad (2.48)$$

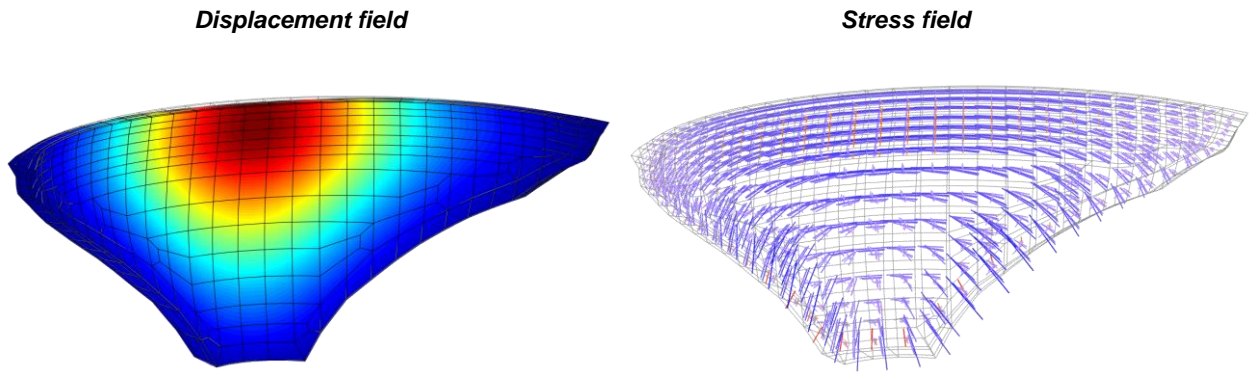


Figure 2.7 – Linear FEM analysis of an arch dam. Displacement and stress fields

### Non-linear analysis. Stress-transfer method

For non-linear structural analysis, the global equilibrium might be influenced by a stiffness decrease due to local material damage, which means that the global stiffness matrix will depend on the displacement field,  $\underline{K} = \underline{K}(\underline{u})$ , and consequently on the installed stresses. Using a FEM formulation, the resulting non-linear equation yields

$$\underline{K}(\underline{u}) \cdot \underline{u} = \underline{F} \quad (2.49)$$

To solve this non-linear problem, it is usual to adopt an iterative calculation process. There are various methods to do this [de Borst & Sluys, 1999; Faria, 1994; Oliveira, 2000], some of which include the re-calculation of the global stiffness matrix in every iteration or once every  $n$  iterations. However, the implementation of such methods can be significantly demanding in terms of computational performance and data storage, particularly for problems of great dimensions.

In **DamDamage3D1.0**, the non-linear analysis is carried out through an iterative numerical method using the stress-transfer procedure, which only requires the stiffness matrix to be calculated once, at the 1<sup>st</sup> iteration. The stress-transfer method is based on the redistribution of the unbalanced stresses which arise due to local ruptures. The goal is to compute the displacements field and the real stress tensors at each point over the domain, in order to assess the resistant capacity of the structure for an applied load  $\underline{F}_{ap}$ .

Numerically, the implemented method seeks to simulate the non-linear response by solving the following equation

$$\underline{K}_0 \cdot \underline{u}_n = \underline{F}_{ap} + \underline{\Psi} \quad (2.50)$$

With this approach, the global stiffness matrix  $\underline{K}_0$  remains unchanged throughout the whole iterative process and is obtained initially for the undamaged structure (linear elastic state). In order to account for the stress redistribution process, the vector of forces equivalent to the unbalanced stresses  $\underline{\Psi}$  is summed to the applied load  $\underline{F}_{ap}$ , which is imposed at the beginning of the calculation. In every iteration  $n$ , the stress-transfer's loading term is obtained by consecutively summing previous unbalanced forces

$$\underline{F}_{ap} + \underline{\Psi} = \underline{F}_{ap} + \sum_{i=1}^{n-1} \underline{\Psi}_i \quad (2.51)$$

Therefore, the equilibrium equation (eq. 2.50) is solved to obtain the displacements vector for the complete discrete system at iteration  $n$ , being

$$\underline{u}_n = \underline{K}_0^{-1} \cdot (\underline{F}_{ap} + \sum_{i=1}^{n-1} \underline{\Psi}_i) \quad (2.52)$$

To evaluate if structural equilibrium is achieved, the actual resistant forces  $\underline{F}_{R,n}$  and the new "partial" unbalanced forces  $\underline{\Psi}_n$  must be computed. The resistant forces represent the structure's real resistant capacity, and thus correspond to real stresses  $\underline{\sigma}$  installed over the structure's domain - to simulate the material's non-linear behaviour, the real stresses are calculated from the elastic stresses based on a constitutive damage model (this subject is addressed in detail in Chapter 3). Based on a FEM formulation, the real stress tensors  $\underline{\sigma}_{n_{gp}}$  are computed for every quadrature point of all elements from the "fictitious" elastic stress tensors, which are calculated for the total forces  $\underline{F}_{ap} + \underline{\Psi}$  using eq. 2.47. Accordingly, the elementary nodal resistant forces are achieved through the Gauss integration method over each FE as

$$\underline{f}_R^e = \int_{\Omega_e} \underline{B}_u^T \underline{\sigma} d\Omega = \sum_{n_{GP}=1}^N \underline{B}_{u,n_{GP}}^T \underline{\sigma}_{n_{GP}} J_{n_{GP}} W_{n_{GP}} = \sum_{n_{GP}=1}^N \underline{B}_{u,n_{GP}}^T \underline{D} \underline{B}_{u,n_{GP}} \underline{u}_n^e J_{n_{GP}} W_{n_{GP}} \quad (2.53)$$

and the global resistant load vector is obtained by summing all the element contributions

$$\underline{F}_{R,n} = \sum_e \underline{f}_R^e \quad (2.54)$$

( $N_{DOF} \times 1$ )

Finally, the new partial unbalanced forces  $\underline{\Psi}_n$ , arising due to material deterioration, are computed as the difference between the applied forces  $\underline{F}_{ap}$  and the real resistant forces  $\underline{F}_{R,n}$ ,

$$\underline{\Psi}_n = \underline{F}_{ap} - \underline{F}_{R,n} \quad (2.55)$$

( $N_{DOF} \times 1$ )

At the end of every iteration, the convergence (or divergence) of the non-linear calculations must be verified, by analysing the unbalanced forces  $\underline{\Psi}_n$  or the corresponding displacements  $\underline{u}_{\Psi_n}$ . In terms of structural safety, two scenarios can occur (Figure 2.8): i) the structure has enough resistant capacity to support the applied load, meaning that it is capable to withstand a certain amount of damage and of redistributing unbalanced stresses; global equilibrium is achieved and the stress-transfer process is convergent; and ii) the structure is not capable of supporting the applied loads and to redistribute the arising unbalanced forces due significant material deterioration, resulting in global collapse – global equilibrium is not achieved and the stress transfer process is divergent.

In **DamDamage3D1.0**, the convergence of the iterative process was controlled through a specific criterion based on the partial displacements vector  $\underline{u}_{\Psi,n}$  calculated from the corresponding unbalanced forces in iteration  $n$ . These displacements are compared to the ones obtained at the end of the first iteration  $\underline{u}_{\Psi,1}$  to check if equilibrium was achieved. In terms of the computational algorithm, the following procedure is established. First, the preliminary calculation (iteration  $n = 1$ ), is performed (eq. 2.56). If the applied forces  $\underline{F}_{ap}$  cause a stress state that falls within the linear-elastic domain for all quadrature points over the structure domain, the unbalanced stresses are equal to zero and thus the actual stress-transfer process does not begin. Thus, a linear analysis is enough. Otherwise, if unbalanced stresses exist after the preliminary non-linear calculation the stress-transfer process is performed to simulate the non-linear response (eq. 2.57). Again, two scenarios can occur: i) the unbalanced forces and corresponding displacements decrease from iteration to iteration and, consequently, the value of  $Norm_n$  will decrease - if this value is lower than a predefined tolerance, global equilibrium was achieved and the calculation is terminated (convergent process); and ii) the unbalanced forces increase for several consecutive



iterations and so does the  $Norm_n$  value until the tolerance is exceeded (divergent process). In **DamDamage3D1.0** a standard tolerance of 0,1% is defined and a maximum number of iterations  $n_{iter,max}$  is established to stop the calculation for divergent processes and prevent it from continuing indefinitely.

$$\begin{aligned} \underline{u}_{\Psi_1} &= \underline{K}_0^{-1} \cdot (\underline{\Psi}_1) = \underline{K}_0^{-1} \cdot (\underline{F}_{ap} - \underline{F}_{R,1}) \\ &\Downarrow \\ n=1 &\left\{ \begin{array}{l} |\underline{u}_{\Psi_1}| = 0 \Rightarrow Norm_1 = 0 < Tol \quad (\text{stop non-linear calculation}) \\ |\underline{u}_{\Psi_1}| > 0 \Rightarrow Norm_1 = \frac{|\underline{u}_{\Psi_1}|}{|\underline{u}_{\Psi_1}|} \times 100 = 100 > Tol \quad (\text{begin stress-transfer}) \end{array} \right. \end{aligned} \quad (2.56)$$

$$\begin{aligned} \underline{u}_{\Psi_n} &= \underline{K}_0^{-1} \cdot (\underline{\Psi}_n) = \underline{K}_0^{-1} \cdot (\underline{F}_{ap} - \underline{F}_{R,n}) \\ &\Downarrow \\ n=2, \dots, n_{iter,max} &\Rightarrow Norm_n = \frac{|\underline{u}_{\Psi_n}|}{|\underline{u}_{\Psi_1}|} \times 100 \left\{ \begin{array}{l} > Tol \quad (\text{continue stress-transfer}) \rightarrow n > n_{iter,max} \quad (\text{stop; divergence}) \\ < Tol \quad (\text{stop; convergence}) \end{array} \right. \end{aligned} \quad (2.57)$$

In resume, the stress-transfer method involves the following main steps:

1. Preliminary calculation (iteration 1)
  - i. Impose the applied load and compute the displacements and stresses (linear response)
  - ii. Calculate the real stresses using a constitutive damage model (non-linear material behaviour)
  - iii. Compute the resistant forces from the real stresses
  - iv. Calculate the unbalanced forces
  - v. Check convergence. If convergence is not reached, perform the stress-transfer iterative process.
2. Stress transfer. For every iteration  $n+1$ 
  - vi. Calculate the new loading term by summing the (initial) applied load and the unbalanced forces
  - vii. Calculate the new displacement vector and the corresponding fictitious elastic stresses
  - viii. Calculate the real stresses using a constitutive damage model (non-linear material behaviour)
  - ix. Compute the resistant forces from the real stresses
  - x. Calculate the unbalanced forces
  - xi. Repeat steps vi) to x) until convergent or divergent process is reached.

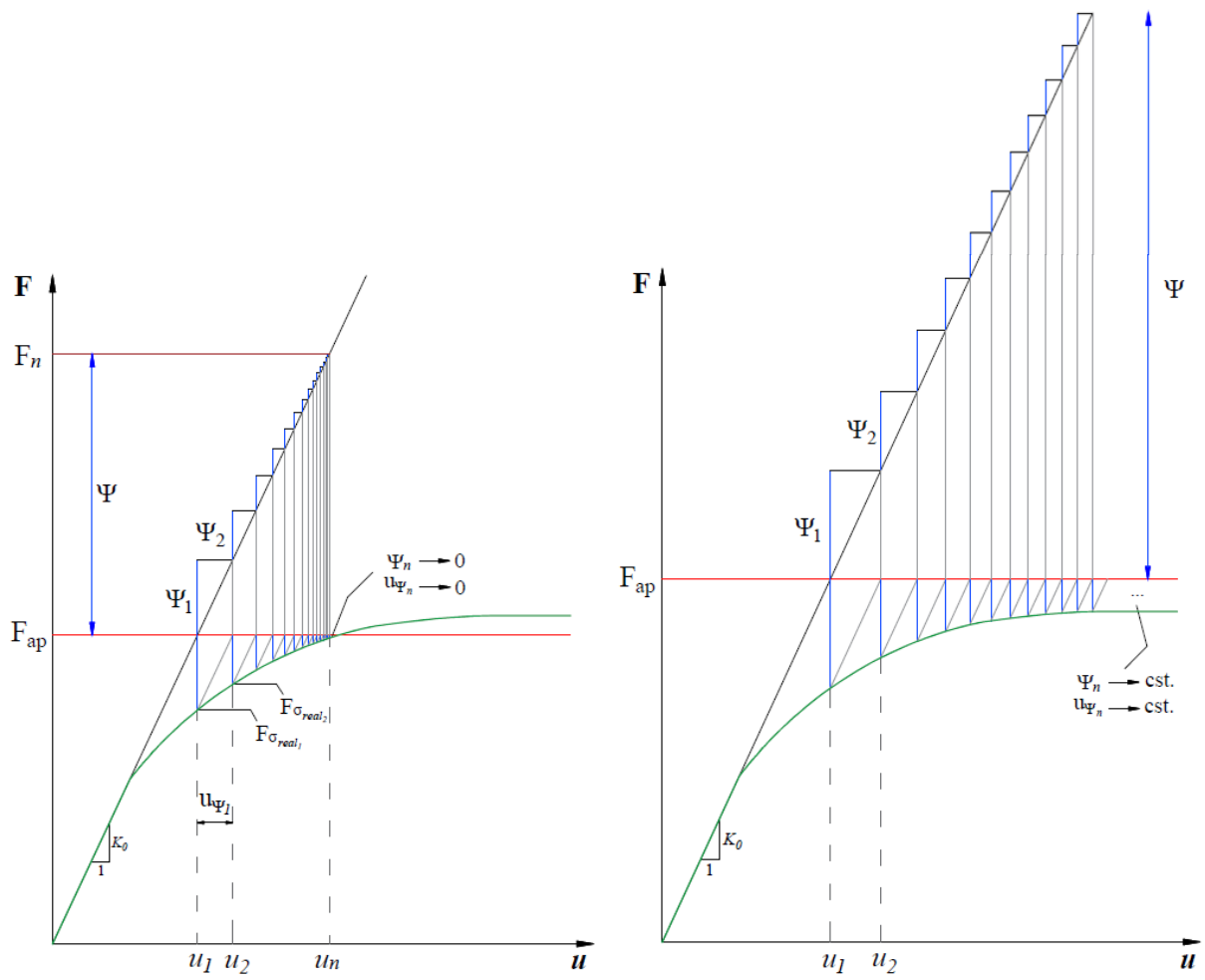


Figure 2.8 – Stress-transfer iterative method. Representation of the global force-displacement equilibrium for convergent and divergent processes

### 3| Constitutive damage model to simulate the non-linear behaviour of concrete

#### 3.1 General considerations

In view to perform non-linear structural analysis and assess the structural safety of concrete arch dams, it is essential not only to develop robust 3DFEM models but also to adopt realistic constitutive models, both in the dam body (concrete and contraction joints) and/or in the foundation (rock mass and existing discontinuities).

The basic concepts regarding the non-linear behaviour of concrete are presented, and the fundamentals of Continuum Damage Mechanics and Fracture Mechanics are addressed in detail. The developed damage model to simulate the non-linear behavior of concrete up to failure is described, with focus on the damage criteria, the respective damage evolution laws and the constitutive damage law for the stress-strain relation. This damage model was developed using MATLAB routine that was incorporated into the program *DamDamage3D1.0*.

#### 3.2 Concrete non-linear behaviour

Concrete is a material with high compressive strength and under tension presents a fragile behavior until failure. Its instantaneous failure process (Figure 3.1) is characterized by a softening phenomenon (i.e. a post-peak stress strength decrease), combined with the formation of microcracks, the consequent continuum damage increase (stiffness decrease) and the accumulation of irreversible strains. Therefore, as referred in [Oliveira, 2000], to fully perceive and correctly simulate the non-linear behaviour of concrete up to failure, it is fundamental to include the key concepts of Continuum Damage Mechanics, Plasticity Theory and Fracture Mechanics.

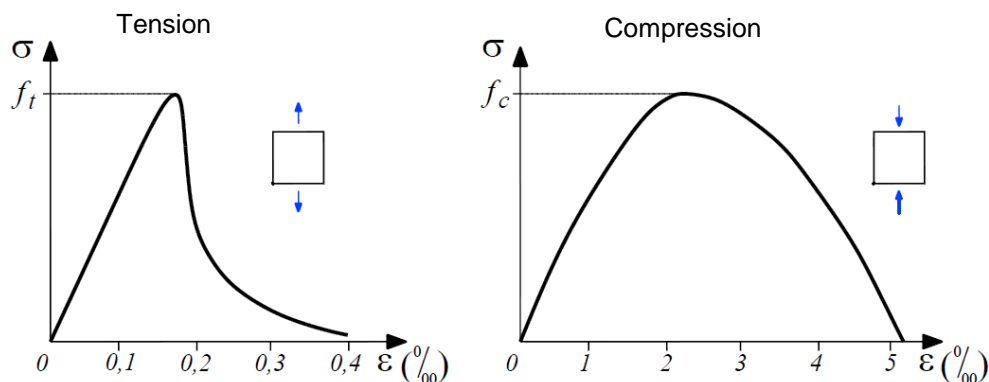


Figure 3.1 – Concrete behaviour up to failure under tension and compression (adapted from [Oliveira, S. 2000])  
[Coutinho & Gonçalves, 1994]

The non-linear behaviour of concrete for uniaxial stress-states is simpler to characterize, although in practice the material used in different structures is commonly under biaxial or triaxial stress-states. Just as for the uniaxial behaviour, it is possible to observe a non-linear development of the stress-strain curves for concrete, with a significant increase of compressive strength for biaxial and mainly for triaxial stress-states (Figure 3.2).

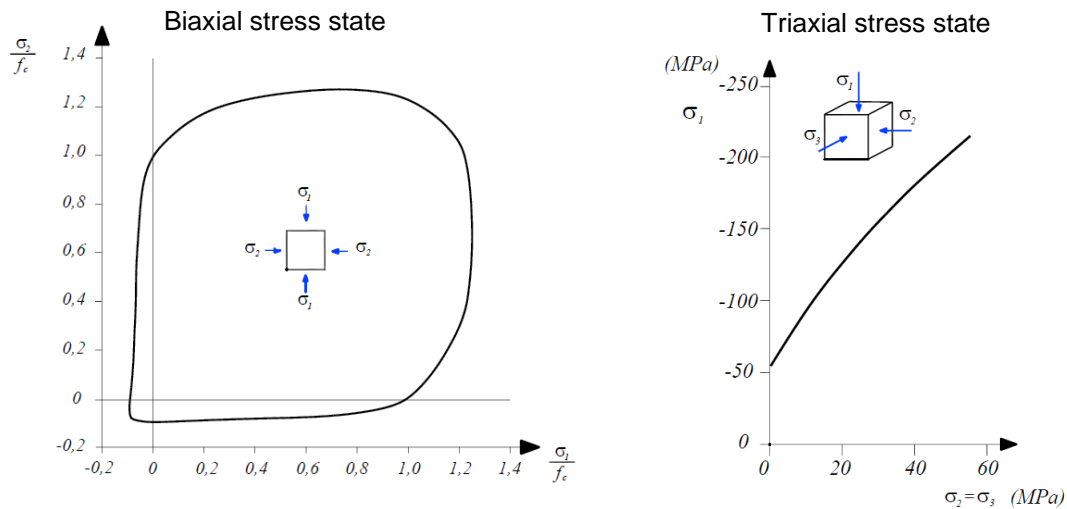


Figure 3.2 – a) Biaxial stress state: failure surface; b) Concrete compressive strength for a triaxial stress state (adapted from [Oliveira, S. 2000]) [Coutinho & Gonçalves, 1994]

### 3.3 Continuum Damage Mechanics

Continuum Damage Mechanics, introduced by Kachanov [Kachanov, 1958], describes the evolution of the irreversible deterioration phenomenon that occurs inside a given material, from the undamaged state to the occurrence of macroscopic cracks (Figure 3.3), under applied forces that exceed its strength. This phenomenon is associated with the formation and evolution of new or existing volume (microvoids) or surface (microcracks) discontinuities and with their coalescence that will eventually lead to macroscopic failure (macrocracks), resulting in a reduction of the material's intrinsic stiffness [de Borst & Sluys, 1999; Faria, 1994; Geers, 1999; Faria, 1994; Oliveira, 2000].

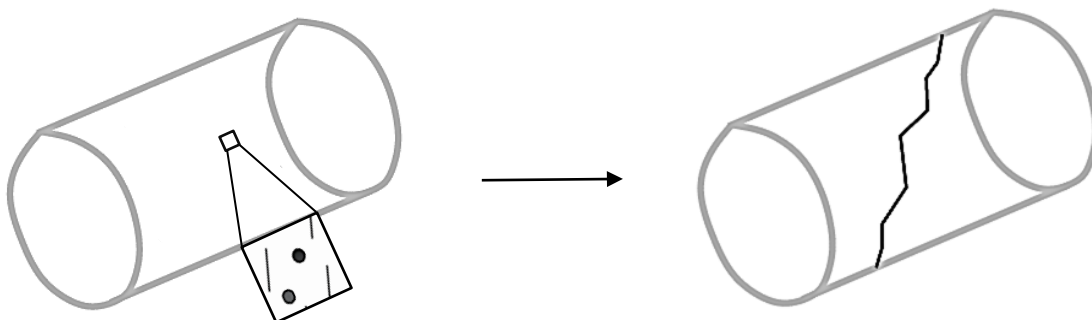


Figure 3.3 – Internal damage (microcracks and microvoids) and evolution to macroscopic cracks

### 3.3.1 Damage models

The evolution of the damage phenomenon in concrete before the initiation of macrocracks, might be simulated based on different types of numerical damage models, according to the definition of appropriate continuum damage variables and their respective evolution laws. Therefore, considering the nature of the damage that might occur and the related propagation mechanisms, one can use: a) scalar damage models, with scalar damage variables [Kachanov 1958; Mazars, 1984; Lemaitre and Chaboche, 1985; Faria, 1994]; or b) vector/tensor damage models, based on vector [Davison & Stevens, 1993] or tensor damage variables [Murakami & Ohno, 1981; Ju, 1989; Ramtani, 1990]. Furthermore, the choice of the damage evolution law is influenced by the material type and the loads to be considered: the formulation can depend solely on the elastic deformation or on the plastic deformation, and it can also incorporate the damage evolution over time, the number of load cycles and swelling effects (alkali-aggregate reactions). In **DamDamage3D1.0**, the non-linear behaviour of concrete is simulated using models with two independent scalar damage variables, which has been the case in several studies carried out in LNEC over the last decades [LNEC, 2003, 2010, 2014]. Thus, this is the type of model addressed in this chapter.

### 3.3.2 Plasticity and damage

While elastic deformations are related to modifications at the atomic level, both plasticity and damage phenomena are associated to energy dissipation processes. These are irreversible phenomena, according to the Clausius-Duhem inequality<sup>3</sup>. In terms of the non-linear behaviour of concrete, plasticity originates the redistribution of inter-crystalline defects and consequently leads to the accumulation of irreversible strains. On the other hand, the damage evolution consists on the initiation of new internal micro cracks and on the growth of the existing ones, resulting in a global material stiffness decrease.

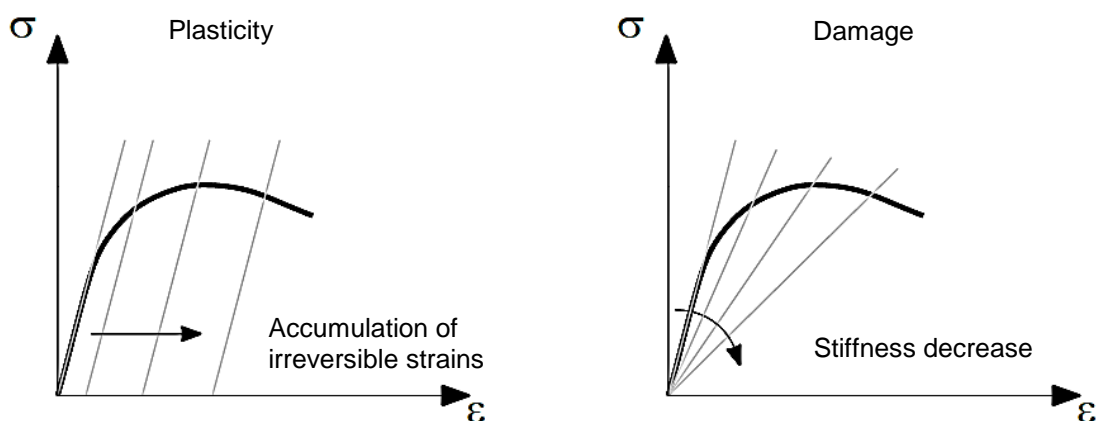


Figure 3.4 – Plasticity and damage state (adapted from [Oliveira, S. 2000])

<sup>3</sup> The Clausius-Duhem inequality expresses the Second Law (or fundamental inequality) of Thermodynamics and it concerns the irreversible nature of natural processes when energy dissipation is involved.

### 3.3.3 Scalar damage variable

In Continuum Damage Mechanics, the state of internal damage for a certain material is characterized through a set of internal variables, referred to as damage variables, usually represented by the letter  $d$ . These damage variables are used to quantify the damage state (Kachanov, 1958, 1986) whose values value ranges from  $d=0$ , representing the undamaged (or intact) material state, to  $d=1$ , when the material is completely damaged, and failure occurs. Given that the evolution of internal deterioration is an irreversible process, the damage value always increases.

To explain the damage variable concept, one can consider an infinitesimal portion of material, located inside a given solid (Figure 3.5). Considering this portion as a surface element of area  $S$  with a normal direction  $\vec{n}$ , small enough to belong to a material point but also sufficiently large to contain damaged sections of total area  $S^d$ , then the undamaged area is given by

$$\tilde{S} = S - S^d \quad (3.1)$$

The damage value represents the surface density of damaged areas, associated with the normal direction  $\vec{n}$ , and is calculated as:

$$d = \frac{S^d}{S} = \frac{S - \tilde{S}}{S} = 1 - \frac{\tilde{S}}{S} \quad (3.2)$$

As stated above, damage variables are associated with a certain direction, so they should be represented by vectors or tensors for all directions at a given material point, particularly in cases where the cracking phenomenon is heavily oriented. However, the implementation and validation of vector/tensor damage models is quite complex and computationally demanding. Also, for many cases in structural analysis the concrete damage phenomena under tension and compression can usually be considered as isotropic, i.e. equal in all directions, and therefore the use of scalar isotropic damage models is assumed to be adequate for simulating the material's non-linear behaviour up to failure.

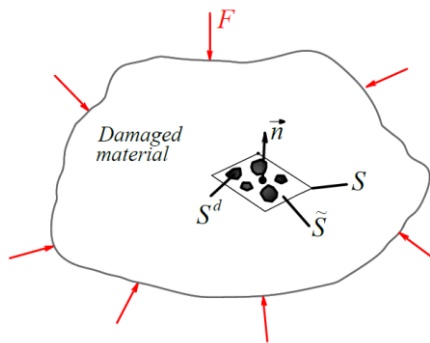


Figure 3.5 – Damaged and undamaged areas in a portion of material (adapted from [Oliveira, 2000])

### 3.3.4 Effective stress

The definition of a damage variable that represents the surface density of damaged areas leads to the concept of effective stress, which is the stress installed in effective resistant area. Considering a unidimensional equilibrium, the applied force  $F$  in a material section of area  $S$  results in a real (or Cauchy) stress value

$$\sigma = \frac{F}{S} \quad (3.3)$$

If the installed stress exceeds the material strength, isotropic damage  $d$  will occur. Thus, the area of the effective resistant section  $\tilde{S}$  becomes equal to the difference between the total area  $S$  and the damaged area  $S^d$ ,

$$\tilde{S} = S - S^d = S(1-d) \quad (3.4)$$

Considering that the section of the material must remain in equilibrium, then the relation between effective and real stress is

$$\sigma \cdot S = \tilde{\sigma} \cdot \tilde{S} = \tilde{\sigma} \cdot S(1-d) \quad (3.5)$$

and finally, the effective stress is determined as [Lemaitre, 1984]

$$\tilde{\sigma} = \frac{\sigma}{(1-d)} \quad (3.6)$$

Therefore, the effective stress  $\tilde{\sigma}$  can be defined as the stress installed in the area  $\tilde{S}$  of the material section that effectively resists to the applied forces (Figure 3.6). So, it is always  $\tilde{\sigma} \geq \sigma$ , with  $\tilde{\sigma} = \sigma$  for intact material ( $d = 0$ ;  $\tilde{S} = S$ ) and  $\tilde{\sigma} \rightarrow \infty$  when failure occurs ( $d \rightarrow 1$ ;  $\tilde{S} \rightarrow 0$ ).

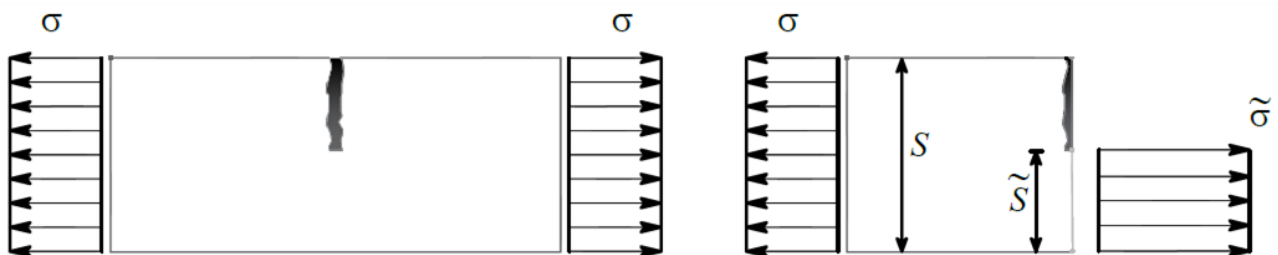


Figure 3.6 – Real stress (damaged) and effective stress (undamaged) (adapted from [Faria, R. 1994])

### 3.3.5 Constitutive relations for damaged materials

The definition of a constitutive stress-strain relation for a material with internal damage is achieved based on the simplifying hypothesis referred to as the Principle of Strain Equivalence [Lemaitre & Chaboche, 1985]. This principle basically states that the strain state of a material with internal damage can be determined through the constitutive relation defined for the undamaged material, with elasticity modulus  $E_0$ , by replacing the usual Cauchy stress with the effective stress.

Considering unidimensional linear elastic behaviour, the constitutive relation for an intact material is

$$\varepsilon = \frac{\sigma}{E_0} \rightarrow \sigma = E_0 \varepsilon \quad (3.7)$$

For a material with internal damage [Faria & Oliver, 1993] a similar law is defined by the linear effective stress-strain relation

$$\varepsilon = \frac{\tilde{\sigma}}{E_0} \rightarrow \tilde{\sigma} = E_0 \varepsilon \quad (3.8)$$

while the Cauchy stress-strain constitutive relation is non-linear (Figure 3.7) and depends on the damage variable

$$\varepsilon = \frac{\sigma}{(1-d)E_0} \rightarrow \sigma = (1-d)E_0 \varepsilon \quad (3.9)$$

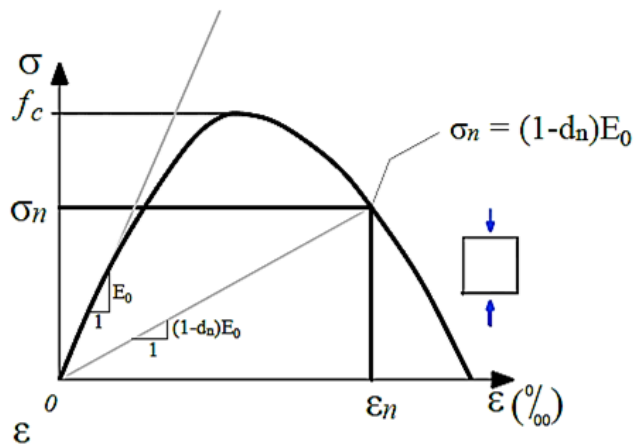


Figure 3.7 – Non-linear stress-strain constitutive relation for a damaged material



Regarding a 3D material with internal isotropic damage, the non-linear linear constitutive relation can be established between the strain tensor and the Cauchy stress tensor,

$$\sigma = (1-d) \tilde{\sigma} = (1-d) \underline{D}_0 \varepsilon \quad (3.10)$$

where  $\underline{D}_0$  is the elasticity matrix for an undamaged state and  $\tilde{\sigma}$  is the effective stress tensor.

### 3.4 Fracture Mechanics

Fracture Mechanics is a field that studies the propagation process of existing cracks in materials (Figure 3.8), accounting for the energy release and softening phenomena, aiming to describe the non-linear behaviour of structural elements with macroscopic discontinuities up to failure. Considering the lower concrete tensile strength, when compared to compression, it is particularly important to address the cracking growth process that leads to fracture under tension and the corresponding effects in its behaviour.

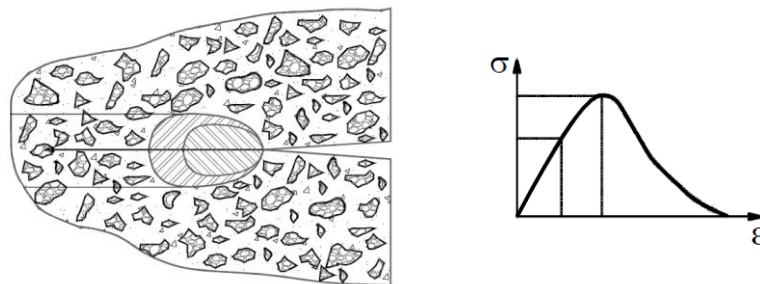


Figure 3.8 – Crack propagation and strain softening constitutive law

#### 3.4.1 Types of crack models

For a concrete sample, cracked under tensile stress, it is usual to note a gradual strain increase due to damage, over a band (Figure 3.9). From a numerical modelling point of view, this is difficult to simulate using a FEM formulation, so it is usual to assume simplified criteria to account for the damage localization in the finite element mesh domain. Generally, two approaches can be adopted:

i) Models based on the discrete crack hypothesis [Ngo & Scordelis, 1967; Ingraffea & Saouma, 1985; Hillerborg, 1985; Alfaiate, 1992]. These consider that damage occurs along a line or surface (for 2D or 3D meshes) between adjacent elements, leading to the simulation of cracking propagation through the elimination of the existing connections between elements and consequently to the creation of new nodal

points at the resulting surfaces. The mesh may remain unaltered or, in alternative, an automatic remeshing procedure can be used; and

ii) Models based on the distributed (or smeared) crack hypothesis [Rashid, 1968; Bazant & Oh, 1983; Bazant, 1986; Belytschko, Fish & Engelman, 1988] and non-local models [Bazant, 1987; Bazant & Pijaudier-Cabot, 1987; Pijaudier-Cabot & Bazant, 1987; Bazant & Lin, 1988]). For these type of models, it is assumed that the cracking is distributed along a band of finite width, inside a set of finite elements. This assumption is particularly useful when using the FEM, while also being advantageous for computational implementation. To simulate the deterioration process, a decrease in the material stiffness is assumed for an element once it is comprised inside the damaged area. Also, these models enable a smooth transition from the pre-cracked to the cracked state without being necessary to adjust the mesh and the material constitutive laws.

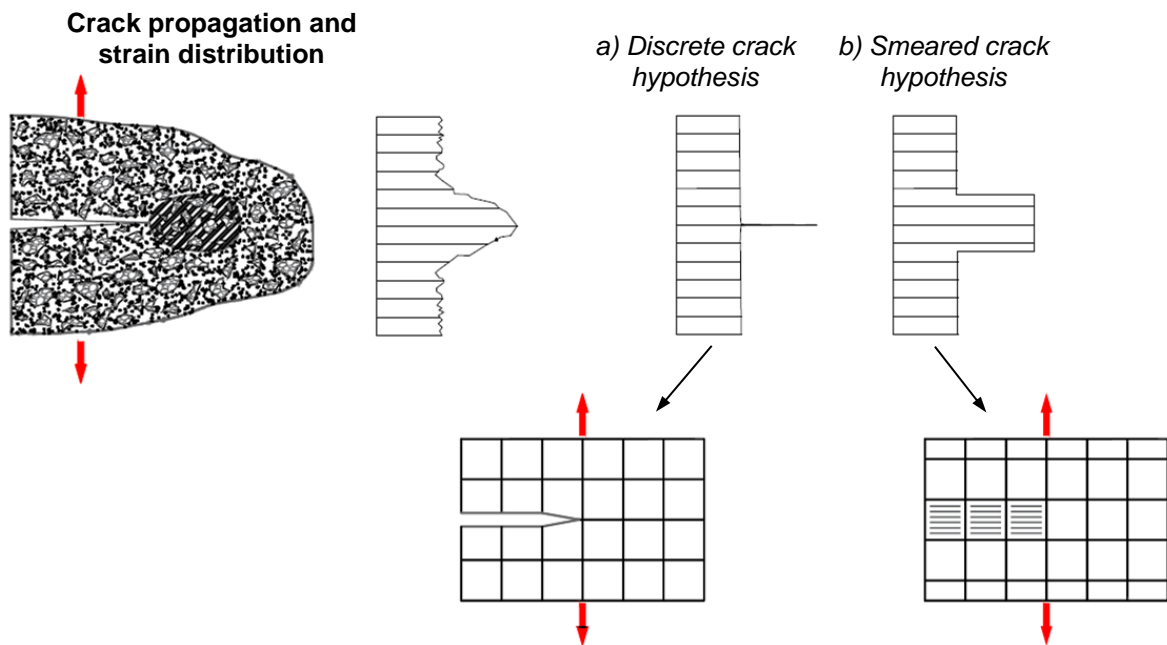


Figure 3.9 – Crack development and strain distribution for: a) discrete crack model; b) smeared crack model. Respective simulation using a FE mesh (adapted from [Oliveira, S. 2000])

For modelling the propagation of cracks in fragile materials, such as concrete, numerical continuum damage models that consider the softening phenomenon and based on the smeared crack hypothesis can be used, provided that the key concepts of Continuum Damage Mechanics and Fracture Mechanics are properly considered. In the FEM program **DamDamage3D1.0**, the non-linear behaviour up to failure of concrete is simulated based on this type of models.

### 3.4.2 Fracture Process Zone (FPZ)

According to the fundamentals of Non-Linear Fracture Mechanics, it is assumed that a micro cracking zone with a finite dimension arises at the crack tip, where the fracture process occurs (Figure 3.10): the FPZ consists on a group of individual microcracks that merge and ensure the propagation of the existing crack. The width of the FPZ ( $w_b$ ) is considered as a constant material property and depends on the maximum aggregate dimension for concrete. This is a zone of non-linear material behaviour, characterized by a gradual material deterioration, and it separates the cracked (or damaged) zone from the undamaged portion of the material (linear elastic behaviour).

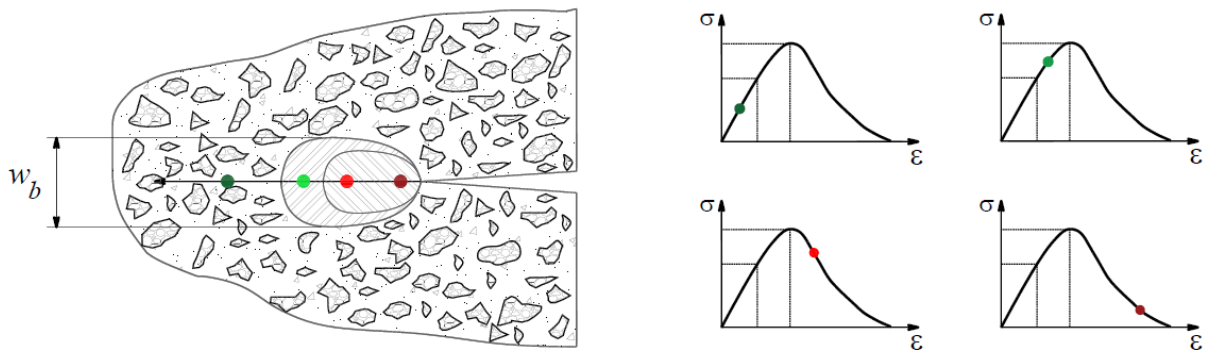


Figure 3.10 – Fracture Process Zone (FPZ). Representation of different strain-stress states near the damaged zone (adapted from [Oliveira, S. 2000])

### 3.4.3 Fracture energy

The crack propagation process includes the rupture of intermolecular forces along the surface of the newly formed or pre-existing crack and thus originates a certain energy dissipation (irreversible process). As stated by Griffith [Griffith, 1921], based on a thermodynamic approach, the surface energy involved in the growth of a crack may be considered as a material property, usually referred to as the fracture energy  $G_f$  (kNm/m<sup>2</sup>), or, when referring to the energy dissipated per volume unit, the specific fracture energy  $g_f$  (kNm/m<sup>3</sup>),

$$g_f = \frac{G_f}{w_b} \quad (3.11)$$

Furthermore, considering the physical behaviour of the material, it is known that the crack propagation phenomenon depends on the stress installed at the crack tip. Consequently, it is possible to establish a

correlation between the installed stress and the specific fracture energy [de Borst & Sluys, 1999], by regarding the area under the stress-strain diagram as a specific material property (Figure 3.11).

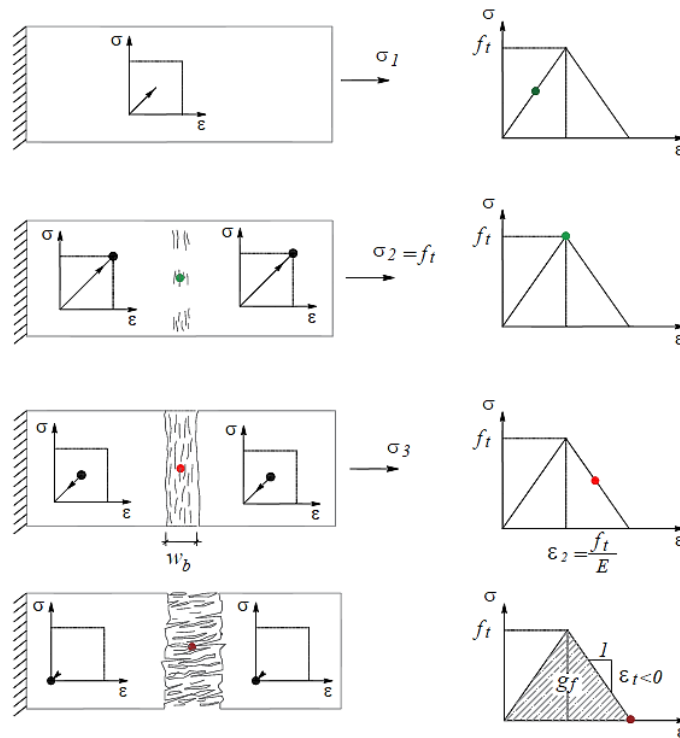


Figure 3.11 – Schematic representation of the different phases of a concrete's behaviour up to failure. Unidimensional stress-strain diagrams and definition of the specific fracture energy (adapted from [Oliveira, S. 2000])

The total amount of energy involved in the cracking process must be fully dissipated in the distributed cracking band, in order to meet the thermodynamic criteria stating that the potential energy initially available in the material must be equal to the amount of energy consumed during the fracture process. Based on a physical approach on the process of concrete fracture under tension [Oliver, 1989], the expended work during this process is proportional to the volume where cracking occurs and to the specific fracture energy,

$$W_{diss} \propto V_f \cdot g_f \quad (3.12)$$

### 3.4.4 Softening and strain localization

As mentioned previously, concrete failure involves the material softening phenomenon, which represents a gradual stress decrease for a strain increase after the linear elastic threshold is exceeded. Therefore, to simulate the crack propagation process up to failure it is necessary to consider a strain-softening branch for the concrete constitutive law. Material softening occurs in the FPZ due to the

strain and damage evolution in that zone, along a band of width  $w_b$ , which will eventually result in concrete failure [Bazant & Oh, 1983].

For FE models based on non-linear structural analysis using constitutive laws with strain-softening, the strain accumulation and material damage is expected to be localized in specific zones of the discrete system, corresponding to the FPZ. The stresses and the values of damage variables are calculated in the integration points (Gauss points, see Chap.2): the volume associated to the points with non-null damage is used to compute the energy release in the fracture process. In this way the problem might be ill-posed, given that the obtained results become dependent on the adopted discretization, i.e. dependent on the finite element's size. Therefore, it is necessary to seek for solutions that ensure the reliability of the obtained numerical results, i.e. results that do not depend on the adopted discretization.

### Small-scale problems

For problems of reduced dimensions (e.g. simple structural elements or small structures), a considerable mesh refinement is used and consequently the FPZ comprises various finite elements (Figure 3.12). In that case, it is numerically possible to obtain failure localization in zones of null volume. Although this is not incoherent from a thermodynamic perspective [Bazant & Planas, 1998], it poses an inaccuracy in terms of the mechanical behaviour of the material. Thus, it is usual to use localization restraints to guarantee that cracking occurs in volumes with a minimum size, as in the case of the smeared crack band and the non-local models.

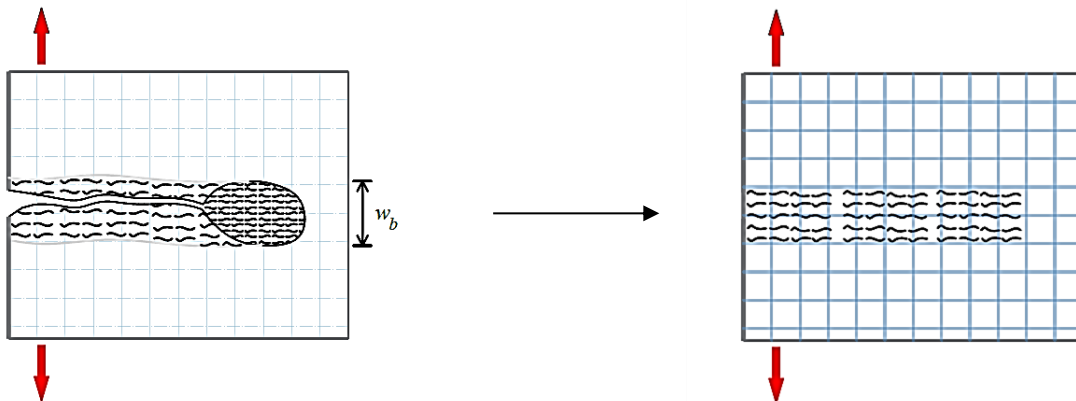


Figure 3.12 – Failure localization for small-scale problems

### Large-scale problems

To study problems of large dimensions (e.g. concrete dams), considering the limitations imposed due to the available computational resources in terms of both data storage and performance, it is common to define discretized systems in which the volume involved in the failure process, i.e. the width  $w_b^*$  associated with the Gauss points, is significantly greater than the actual volume involved in the material cracking phenomenon (Figure 3.13).

The determination of the mesh-dependent width of the FPZ  $w_b^*$  is not a simple process in three-dimensional analysis due to the complexity of the fracture phenomenon, namely concerning the shape and propagation process of cracks. This fact makes it difficult to establish clear scientific criteria to define this parameter, being usual to calculate it based on simplifying hypothesis. For example, some of the used techniques are: i) the width  $w_b^*$  value is estimated by the user, based on the used FE mesh; ii) by considering the size (or volume) of the finite element where failure arises,  $w_b^* = \sqrt{V^e}$ ; and iii) using a consistent formulation, taking into account the cracking orientation and the dimensions of the FE in analysis [Oliver, 1989].

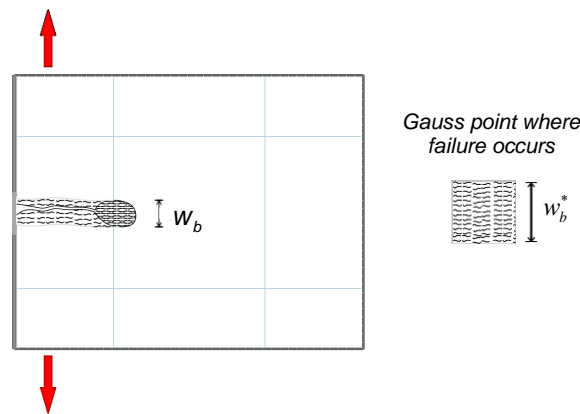


Figure 3.13 – Failure localization for large-scale problems

For such problems, the cracking zone is associated with the volume (or weight) of each quadrature Gauss point  $V_f^*$ , which might be characterized by a width  $w_b^*$  greater than the real FPZ width  $w_b$ . In that case, it is necessary to adopt a corrected specific fracture energy  $g_f^*$ , by using fixed constitutive laws, in order to guarantee that the dissipated fracture energy is calculated in a consistent and realistic way for all quadrature Gauss points where cracking occurs,

$$G_f = w_b \cdot g_f = w_b^* \cdot g_f^* \quad (3.13)$$

In special cases, it might be possible to define a mesh discretization such that the volumes of the Gauss points are of the same order of magnitude as the dimension of the real FPZ, that is  $w_b^* \cong w_b$ . Consequently, the real stress-strain diagrams can be used for all points where material damage occurs, and thus the computed solutions are not mesh-dependent.

### 3.5 Development of a constitutive damage model for the concrete

Aiming to perform FE based non-linear analysis of concrete structures, it is essential to use robust constitutive models for an accurate simulation of concrete's behaviour up to failure, considering the

fundamentals of Continuum Damage Mechanics and Fracture Mechanics. Also, it is important for developed numerical models that ensure a simple analysis of the material's mechanic behaviour under tension and compression, as well as to structure the damage law algorithm based on variables that can be directly calculated from strain tensors, which can be simply computed determined when using FE formulations.

In **DamDamage3D1.0**, the non-linear behaviour of concrete up to failure is simulated based on an isotropic damage model with two independent scalar variables,  $d^+$  for tension damage and  $d^-$  for compression damage [Faria, 1994; Oliveira, 2000], considering the strain-softening phenomenon and the smeared crack hypothesis. This damage model enables the calculation of real stress tensors from effective stress tensors, considering the damage evolution, for applied strain increments. Also, the stiffness reduction associate to damage is considered, while the irreversible plastic strains are not. The main theoretical bases that support the constitutive damage law and its algorithm are presented.

### 3.5.1 Thermodynamic consistency: free energy potential

The formulation of a realistic constitutive model be consistent from a thermodynamic point of view, meaning that the damage evolution laws used to describe the material degradation process must properly represent its irreversible nature. With that aim, a free energy potential  $\psi$  that verifies a thermodynamic fundamental condition  $\dot{\psi} \geq 0$  is postulated, using an expression similar to the specific elastic strain energy [Mazars & Pijaudier-Cabot, 1989; Faria & Oliver, 1993] that represents the area underneath the stress-strain diagram for the uniaxial case,

$$\psi = \frac{1}{2} \sigma \varepsilon \quad (3.14)$$

Generalizing for a triaxial stress state, the stress tensor, defined in the space of principal stresses

$$\underline{\sigma} = \underline{D}_0 \underline{\varepsilon} \quad (3.15)$$

can be decomposed as the sum of tension and compression components [Faria, Oliver & Cervera, 1998]

$$\underline{\sigma} = \underline{\sigma}^+ + \underline{\sigma}^- \quad (3.16)$$

and thus the free energy potential can be rewritten as

$$\Psi = \frac{1}{2}(\sigma^+ \varepsilon + \sigma^- \varepsilon) = \frac{1}{2}\sigma^+ \varepsilon + \frac{1}{2}\sigma^- \varepsilon \quad (3.17)$$

Based on the concept of effective stress (eq. 3.6) and considering that the above decomposition (eq. 3.16) is valid for the effective stress tensor, the tension and compression tensors can be written in terms of the respective damage variables

$$\sigma^+ = (1-d^+) \tilde{\sigma}^+ \quad (3.18)$$

$$\sigma^- = (1-d^-) \tilde{\sigma}^- \quad (3.19)$$

Finally, the free energy potential can be defined in terms of the tension and compression components of the effective stress tensor

$$\Psi = \frac{1}{2}(1-d^+) \tilde{\sigma}^+ \varepsilon + \frac{1}{2}(1-d^-) \tilde{\sigma}^- \varepsilon \quad (3.20)$$

and, considering the effective stress-strain relation for a material with internal damage (eq. 3.7), it yields

$$\Psi = \frac{1}{2}(1-d^+) \tilde{\sigma}^+ D_0^{-1} \tilde{\sigma} + \frac{1}{2}(1-d^-) \tilde{\sigma}^- D_0^{-1} \tilde{\sigma} \quad (3.21)$$

This formulation [Faria, 1994; Oliveira, 2000; Oliveira & Faria, 2006] always assumes nonnegative values [Faria et al., 1998] and hence fulfils the referred thermodynamic condition.

### 3.5.2 Damage criteria and damage evolution laws

In order to simulate the damage evolution, it is essential to establish specific damage criteria, to bound the material linear elastic behaviour, and evolution laws for the internal damage variables  $d^+$  and  $d^-$ , making it possible to control the evolution of the damage variables for each applied strain increment. Additionally, the damage formulation must incorporate a "memory" feature to model the damage process and its irreversible nature throughout the strain's application.

#### Elastic domain and stress thresholds

First, it is necessary to outline the bounding surfaces of the elastic domain and consequently determine the corresponding stress thresholds. Considering the partition of the effective stress tensor into tension



$\tilde{\sigma}^+$  and compression  $\tilde{\sigma}^-$  components, it is convenient to introduce the concept of equivalent stress, given by positive scalar values, to enable the comparison between 3D stress states and the referred linear elastic thresholds.

Assuming the equivalent effective tensile stress [Simu & Ju, 1987] to be equal to

$$\tilde{\tau}^+ = \sqrt{(\tilde{\sigma}^+)^T \underline{D}_0^{-1} \tilde{\sigma}^+} \quad (3.22)$$

then linear tension threshold can be established, using a formulation that was considered to adequately reproduce known experimental results [Faria, R. et al. 1998], that is

$$r_0^+ = \sqrt{f_0^+ \frac{1}{E_0} f_0^+} = \frac{f_0^+}{\sqrt{E_0}} \quad (3.23)$$

where  $f_0^+$  represents the maximum admissible tension for linear elastic behaviour, as determined in a standard uniaxial tensile test.

Regarding the behaviour under compression, it is important to note that concrete presents a greater strength for biaxial or triaxial compression. Therefore, the equivalent effective compressive stress [Faria & Oliver, 1993] is defined as

$$\tilde{\tau}^- = \sqrt{\sqrt{3}(K \tilde{\sigma}_{oct}^- + \tilde{\tau}_{oct}^-)} \quad (3.24)$$

assuming the elastic domain is defined by a bounding surface based on the Drucker-Prager yield criterion. The parameter K is a material property related to the yield surface [Faria, 1994] and it can be obtained experimentally from the maximum admissible compressive stresses for uniaxial  $f_0^-$  and biaxial  $f_{0,2}^-$  tests,

$$R_0 = \frac{f_{0,2}^-}{f_0^-} \quad (3.25)$$

$$K = \sqrt{2} \frac{1-R_0}{1-2R_0} \quad (3.26)$$

The octahedral components of the effective compression tensor  $\tilde{\sigma}^-$  are the mean normal stress  $\tilde{\sigma}_{oct}^-$  (or hydrostatic stress) and the shear stress  $\tilde{\tau}_{oct}^-$ , which are calculated by

$$\tilde{\sigma}_{oct}^- = \frac{1}{3} \text{tr}(\tilde{\sigma}^-) \quad (3.27)$$

$$\tilde{\tau}_{oct}^- = \sqrt{\frac{2}{3} J_2(\tilde{\sigma}^-)} \quad (3.28)$$

where  $J_2$  is the second invariant of the deviatoric stress tensor and it can be calculated in terms of both the principal stresses and the principal deviatoric stresses as shown in [de Borst & Sluys, 1999]. Finally, the linear elastic compressive stress threshold is obtained

$$r_0^- = \sqrt{\frac{\sqrt{3}}{3} (K \cdot f_0^- + \sqrt{2} \cdot |f_0^-|)} \quad (3.29)$$

Based on the tension and compression stress thresholds, a bounding surface defining the elastic domain is established, which is represented (Figure 3.14) in the principal stress space for  $\tilde{\sigma}_2 = 0$ .

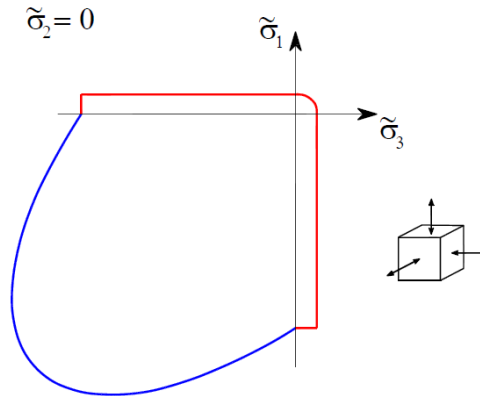


Figure 3.14 – Elastic domain bounding surface, as defined by the stress thresholds [Faria & Oliver, 1993]

### Damage criteria

For a point in a material domain under a given stress state, the damage process begins once the respective linear elastic threshold is exceeded,  $\tilde{\tau}^+ > r^+$ . From that moment on, the analysis is performed in the non-linear domain and the equivalent effective stresses need to be compared with the respective

damage thresholds,  $r^+$  and  $r^-$ , aiming to control the evolution of tension and compression damage. Thus, the following damage criteria can be established [Simu & Ju, 1987]

$$\tilde{\tau}^+ \leq r^+ \quad ; \quad \tilde{\tau}^- \leq r^- \quad (3.30)$$

Assuming that an incremental loading process is implemented, e.g. by applying strain increments in consecutive loading steps, then the damage phenomenon begins, say, at step  $n+1$ , if the linear elastic domain threshold is exceeded,  $\tilde{\tau}_{n+1}^\pm > r_0^\pm$ . Henceforth, damage can only increase, which occurs when the equivalent effective stresses surpass the new thresholds,  $\tilde{\tau}_{n+1}^\pm > r_n^\pm$ . These new thresholds,  $r_n^+$  and  $r_n^-$ , are obtained as the highest values reached by the equivalent stresses until iteration  $n$ . Finally, the intended damage criteria are established [Faria, 1994; Oliveira, 2000; Oliveira & Faria, 2006],

$$\left\{ \begin{array}{l} \text{Linear domain, } \tilde{\tau}_{n+1}^\pm \leq r_0^\pm \rightarrow d^\pm = 0 \rightarrow r_{n+1}^\pm = r_0^\pm \\ \text{Non-linear domain, } \tilde{\tau}_{n+1}^\pm > r_n^\pm \rightarrow d^\pm > 0 \ (d_{n+1}^\pm \geq d_n^\pm) \rightarrow r_{n+1}^\pm = \max(r_n^\pm; \tilde{\tau}_{n+1}^\pm) \end{array} \right. \quad (3.31)$$

ensuring that the stress thresholds and the damage values are constantly updated throughout the loading process, aiming to control the damage phenomenon evolution and to ensure its irreversibility.

#### Damage evolution laws: tension damage $d^+$

Concerning the concrete behaviour under tension, the stress-strain constitutive laws present an ascending branch, representing the linear elastic domain, followed by a post-peak descending branch to simulate material softening until failure occurs, which can be achieved through linear, bilinear or exponential functions (Figure 3.15).

To simulate concrete failure under tension using a constitutive law with an exponential softening branch, the evolution of the tension damage scalar variable  $d^+$  is based on the evolution law [Oliver, Cervera, Oller & Lubliner, 1990; Oliveira & Faria, 2006],

$$\tilde{\tau}^+ > r^+ \rightarrow d^+ = 1 - \frac{r_0^+}{\tilde{\tau}^+} e^{-A^+ \left(1 - \frac{\tilde{\tau}^+}{r_0^+}\right)} \quad (3.32)$$

where  $A^+$  is a parameter given by

$$A^+ = \left( \frac{G_i E}{w_b (f_0^+)^2} - \frac{1}{2} \right)^{-1} \quad (3.33)$$

which is defined to ensure an appropriate energy dissipation during the fracture process, considering the fundamental concepts of Fracture Mechanics.

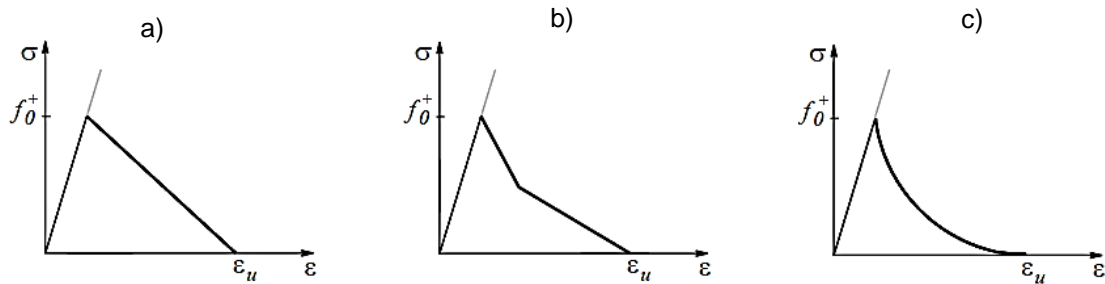


Figure 3.15 – Concrete behaviour under tension. Constitutive law with different types of softening branches: a) linear, b) bilinear and c) exponential (adapted from [Oliveira, 2000])

### Compression damage $d^-$

As for concrete compression behaviour, the constitutive stress-strain relation (Figure 3.16) is characterized by a linear ascending branch that defines the linear elastic domain, until the uniaxial maximum stress is exceeded, followed by a pre-peak hardening curve. After the peak compressive stress is reached, the constitutive law presents a descending curve to simulate softening under compression until the failure state, which is not fragile as in tensile failure.

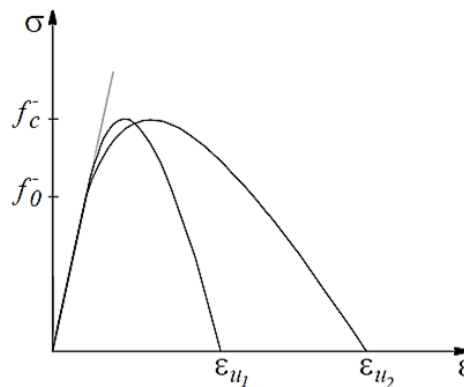


Figure 3.16 – Concrete behaviour under compression. Constitutive laws to represent different types of softening (adapted from [Oliveira, 2000])

The concrete failure under compression is controlled by the progression of the compression damage scalar variable  $d^-$ , based on an evolution law that ensures an accurate simulation of both hardening and softening phenomena of concrete [Mazars & Pijaudier-Cabot, 1989; Faria & Oliver, 1993; Oliveira & Faria, 2006]

$$\tilde{\varepsilon}^- > r^- \rightarrow d^- = 1 - \frac{r_0^-}{\tilde{\varepsilon}^-} (1 - A^-) - A^- e^{B^- (1 - \frac{\tilde{\varepsilon}^-}{r_0^-})} \quad (3.34)$$

where  $A^-$  and  $B^-$  are two parameters calculated from two points  $P_1 (\sigma_1^-; \varepsilon_1^-)$  and  $P_2 (\sigma_2^-; \varepsilon_2^-)$  on the stress-strain diagram [Faria & Oliver, 1993],

$$A^- = \frac{\sigma_1^- - \frac{r_0^-}{\tilde{\varepsilon}_1^-} \tilde{\sigma}_1^-}{\left( e^{B^- (1 - \frac{\tilde{\varepsilon}_1^-}{r_0^-})} - \frac{r_0^-}{\tilde{\varepsilon}_1^-} \right) \tilde{\sigma}_1^-} \quad (3.35)$$

$$B_i^- \rightarrow B_{i+1}^- = B_i^- - \frac{f(B_i^-)}{f'(B_i^-)} \quad (\text{iterative process}) \quad (3.36)$$

$$f(B_i^-) = \left[ \left( \sigma_2^- - \frac{r_0^-}{\tilde{\varepsilon}_2^-} \tilde{\sigma}_2^- \right) \tilde{\sigma}_1^- \right] \left[ e^{B_i^- (1 - \frac{\tilde{\varepsilon}_1^-}{r_0^-})} - \frac{r_0^-}{\tilde{\varepsilon}_1^-} \right] - \left[ \left( \sigma_1^- - \frac{r_0^-}{\tilde{\varepsilon}_1^-} \tilde{\sigma}_1^- \right) \tilde{\sigma}_2^- \right] \left[ e^{B_i^- (1 - \frac{\tilde{\varepsilon}_2^-}{r_0^-})} - \frac{r_0^-}{\tilde{\varepsilon}_2^-} \right] \quad (3.37)$$

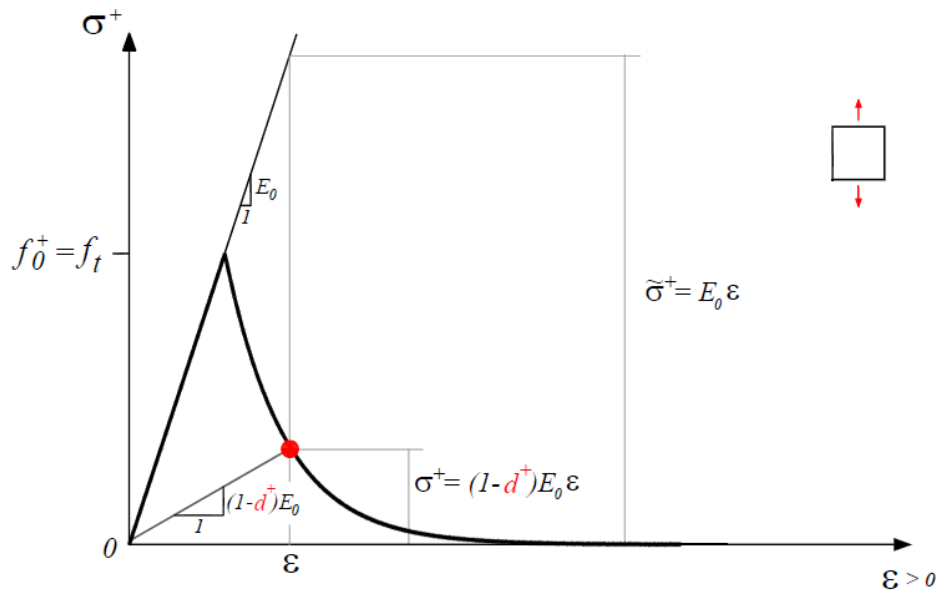
### 3.5.3 Constitutive damage law with two independent damage variables

As mentioned throughout this chapter, during the deterioration process the dissipated energy can never decrease, which the Clausius-Duhem inequality  $-\psi' + \sigma^T \varepsilon' \geq 0$  must be fulfilled. Therefore, considering the postulated free energy potential in eq. 3.21, the constitutive damage law with two independent damage variables [Oliveira, 2000; Oliveira & Faria, 2006] to simulate the concrete's non-linear behaviour up to failure is defined

$$\sigma = (1 - d^+) \tilde{\sigma}^+ + (1 - d^-) \tilde{\sigma}^- \quad (3.38)$$

This damage law enables the calculation of the Cauchy stresses from the effective stresses, considering the damage criteria and the damage evolution laws for the tension and compression damage variables,  $d^+$  and  $d^-$ . The stress-strain diagrams for uniaxial tension and compression are presented in Figure 3.17.

a)



b)

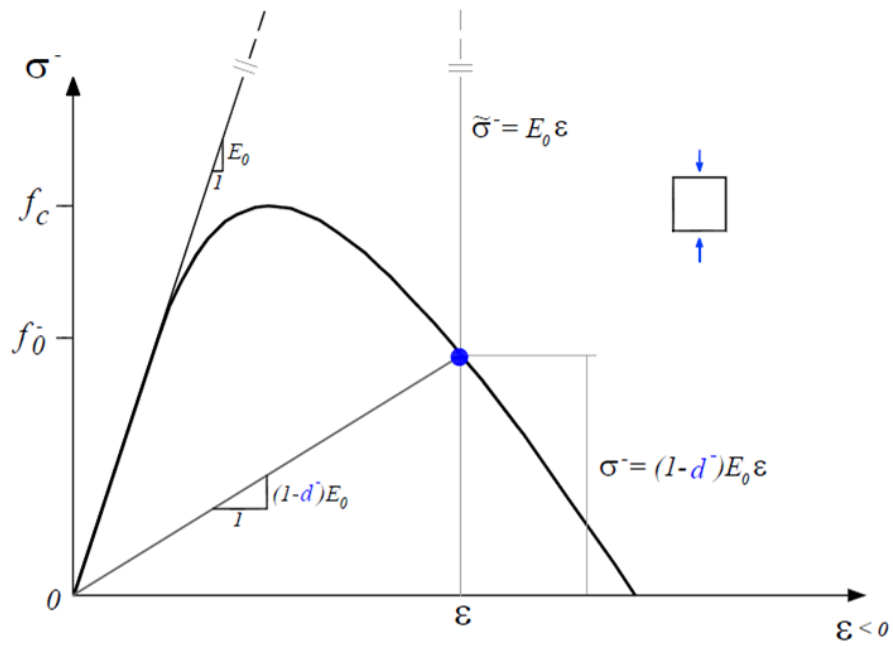


Figure 3.17 – Implemented constitutive law. Stress-strain diagrams for uniaxial tension and compression

Considering that the objective is to incorporate the presented damage model in the 3DFE based program **DamDamage3D1.0**, the developed MATLAB code, *CDamageModel.m*, was structured in order to compute the Cauchy stress tensors from strain tensors, which can be simply obtained from the vector of displacements in the main program. Additionally, an auxiliary code *ParametersCDM.m* was developed to calculate the parameters used in the damage evolution laws.

To calibrate the developed code, some tests were performed to obtain the uniaxial stress-strain diagrams, considering the loading process to be simulated by applying consecutive strain increments until failure occurs ( $\sigma = 0$  and  $d = 1$ ). The algorithm used to obtain unidimensional stress-strain diagrams is presented in Figure 3.18 for a generic 3D analysis, including the algorithm for the constitutive damage model. The computed results are shown in Figure 3.19, namely for positive and negative strain increments, to simulate the evolution of tension and compression damage and to test the memory feature of the damage model.

Based on the computed stress-strain diagrams, the calculated constitutive laws present the intended shape, meeting the stress and strain values that define the linear elastic domain until the maximum admissible stresses, and following the strain-softening branch until failure occurs, under both tension and compression. Also, when alternate positive and negative strain increments are applied to simulate a loading-unloading process, the defined damage evolution laws can simulate the required “memory” feature. To conclude, the implemented code of the constitutive damage model with two independent damage variables is able to properly simulate the concrete’s non-linear behaviour up to failure and its irreversible nature, considering the progression of damage under tension and compression.

### 1. Read input data

1.1. Material properties:  $E, \nu, K, G \rightarrow \underline{D}_0$ ;  $f_0^+, f_0^-, f_{0,2}^-, f_u^-$ ;  $G_f, w_b$ ;  $P_1(\sigma_1^-, \varepsilon_1^-), P_2(\sigma_2^-, \varepsilon_2^-)$

1.2. Strain increment:  $\Delta \varepsilon$

### 2. Run *ParametersCDM.m*: calculate main parameters for the damage evolution laws

2.1. Tension:  $r_0^+, A^+$

2.2. Compression:  $R_0, K, r_0^-, B^-, A^-$

### 3. Initialization of the main variables:

3.1. Stress thresholds  $r_1^\pm = r_0^\pm$

3.2. Scalar damage variables  $d_1^\pm = d_0^\pm$

3.3. Effective stress tensors  $\tilde{\sigma}_1 = \underline{0}$

3.4. Cauchy stress tensors  $\sigma_1 = \underline{0}$

### 4. For each loading step $n+1$ (strain increment $\Delta \varepsilon$ ) $\rightarrow$ run *CDamageModel.m*:

4.1. Compute the effective stress tensors:  $\tilde{\sigma}_{n+1} = \tilde{\sigma}_n + \underline{D}_0 \cdot \Delta \varepsilon$

4.2. Compute equivalent effective stress tensors:  $\tilde{\tau}_{n+1}^+; \tilde{\tau}_{n+1}^-$

4.3. Verify damage criteria and update stress thresholds

. If  $\tilde{\tau}_{n+1}^\pm \leq r_0^\pm \rightarrow d^\pm = 0 \rightarrow r_{n+1}^\pm = r_0^\pm$ ; **repeat 4**

. If  $\tilde{\tau}_{n+1}^\pm > r_n^\pm \rightarrow d^\pm > 0 \rightarrow r_{n+1}^\pm = \max(r_n^\pm, \tilde{\tau}_{n+1}^\pm)$ ; **continue**

4.4. Calculate damage variables

. Tension damage:  $d_{n+1}^+ = 1 - \frac{r_0^+}{\tilde{\tau}_{n+1}^+} e^{A^+ (1 - \frac{\tilde{\tau}_{n+1}^+}{r_0^+})}$

. Compression damage:  $d_{n+1}^- = 1 - \frac{r_0^-}{\tilde{\tau}_{n+1}^-} (1 - A^-) - A^- e^{B^- (1 - \frac{\tilde{\tau}_{n+1}^-}{r_0^-})}$

4.5. Compute Cauchy stress tensor

.  $\sigma_{n+1} = (1 - d_{n+1}^+) \tilde{\sigma}_{n+1}^+ + (1 - d_{n+1}^-) \tilde{\sigma}_{n+1}^-$

. Stop program when  $[\sigma_{n+1} = \underline{0} \ \& \ d^\pm = 1]$

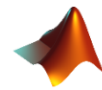


Figure 3.18 – Computational algorithm used to obtain unidimensional stress-strain diagrams (damage law)



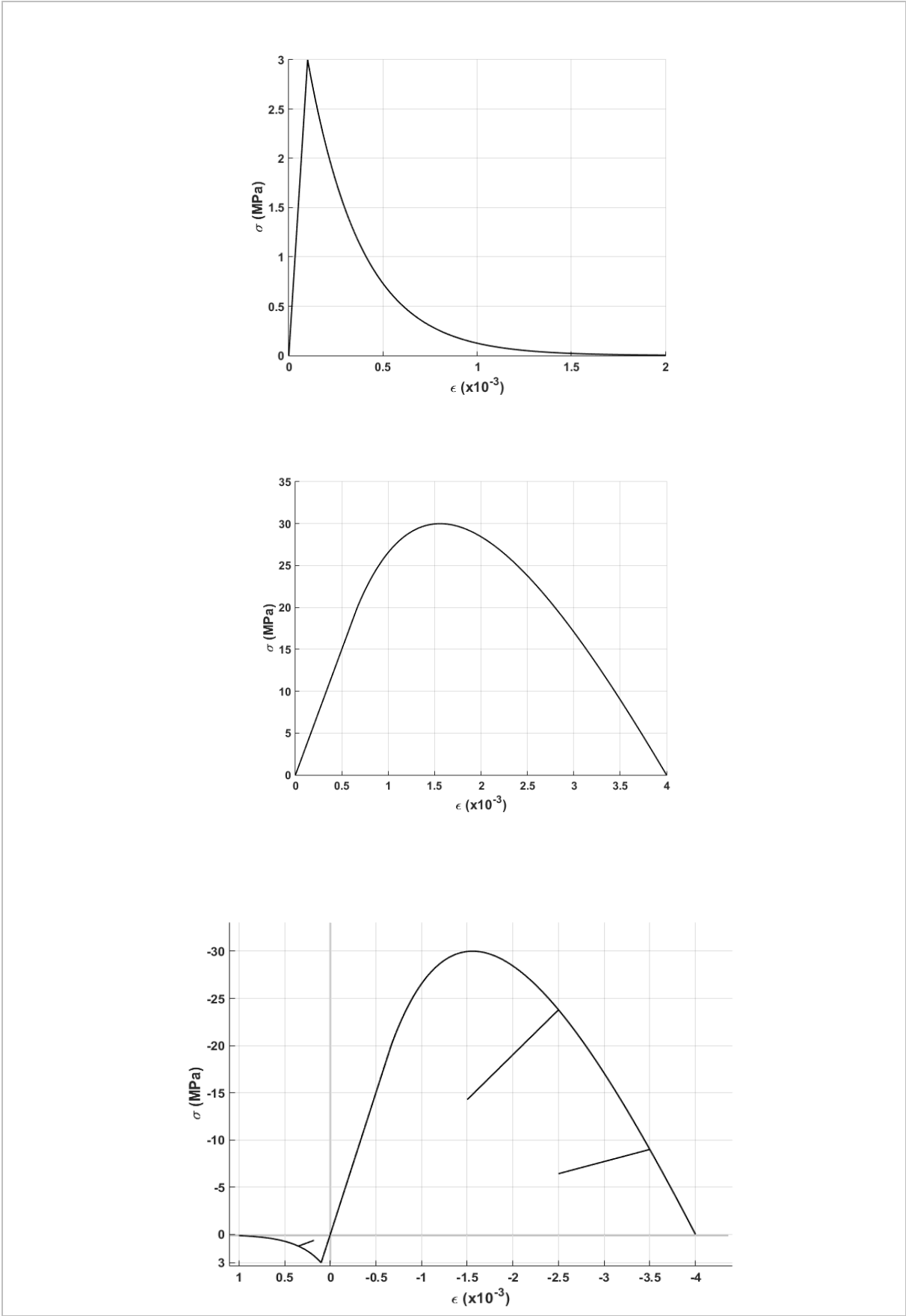


Figure 3.19 – Computed stress-strain diagrams for uniaxial strain increments: a) tension, b) compression and c) alternate tension and compression

## 4| Development of a 3D FE program for non-linear analysis of arch dams

### 4.1 General considerations

The development of computational tools to simulate the structural behaviour of dams is of the utmost importance to study their performance for different accident/incident scenarios and to support safety control studies for new and old dams. The implemented numerical models must be based on robust theoretical bases and formulations, using well defined parameters with clear physical meaning, in order to achieve accurate and reliable solutions. Additionally, it is important to seek to maximize computational efficiency in terms of performance and data storage, without compromising the quality of the obtained results, as well as to manage and present those results in a complete and comprehensible way.

In this chapter, the program developed for non-linear static analysis of arch dams, ***DamDamage3D1.0***, is presented. The main features and assumed hypotheses are addressed, and the program's algorithm is shown. In order to test and calibrate the developed code, non-linear calculations are conducted for a simple case study of a concrete frame structure with known expected behavior.

### 4.2 DamDamage3D1.0

***DamDamage3D1.0*** is a 3DFE program that was developed and optimized for non-linear static analysis of large concrete arch dams. The structural response is analysed for the static load combination including the self-weight (SW), assuming the body load to be applied simultaneously, and the hydrostatic pressure at the upstream face (HP), considering the water level at the crest height (full reservoir). The hypothesis of isotropic materials is considered. No joints or cracks are considered in the dam body nor in the foundation.

The discretization of the dam and the foundation is achieved using isoparametric elements with twenty nodal points and three degrees of freedom on each point. Based on the implemented FEM formulation (recall chapter 2), the self-weight and the hydrostatic pressure are computed as body forces on the dam volume domain and as boundary forces on the dam upstream face from chapter 2. The dam's stiffness matrix is calculated by summing the elementary stiffness matrices, considering the defined material properties. The foundation is simulated as an elastic body according to the massless approach, which means that its stiffness matrix is previously calculated and consequently condensed at the dam-foundation interface to introduce elastic supports at the dam base. With this approach the numerical calculations are performed only for the dam.

For linear static analysis, the displacement field is computed by solving the global equilibrium equation for the discrete system, while the stress tensors are calculated for all Gauss points over the domain, using the Gauss integration method

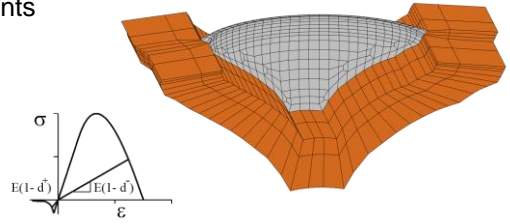
The non-linear analysis is carried out based on the stress-transfer iterative method (see section 2.4.4), considering the redistribution of unbalanced stresses (or forces) across the structure domain due to the material deterioration and consequent strength decrease. The aim in this procedure is to compute the displacements and the real stress tensors at each point over the domain, in order to assess the resistant capacity of the structure for the applied load. The concrete non-linear behaviour up to failure is simulated using an isotropic strain-softening constitutive damage law with 2 independent damage variables ( $d^+$  for tension and  $d^-$  for compression), which is incorporated into the stress-transfer code to compute the real stresses from the strain increments.

The inputs to this program are the FE mesh dam (nodes and elements), the material properties and other parameters, and info about the load combination. As outputs, the program provides high quality 3D graphical representations of the deformed shape and the stress field for linear and non-linear analysis. For the latter, the results obtained at the end of the stress-transfer process include 3D figures with tension and compression damage distributions and personalized notes concerning the convergence of the iterative method. The stress tensors and the damage variables are computed for every quadrature Gauss point of all elements of the mesh.

The computational algorithm developed for **DamDamage3D1.0** in MATLAB is presented in Figure 4.1.

## 1. Read input data file

- 1.1. Mesh data: nodes (coordinates) and finite elements
- 1.2. Material properties (dam and foundation)
- 1.3. Material properties (non-linear behaviour)



## 2. Foundation stiffness matrix

- 2.1. Compute the element stiffness matrices (Gauss integration):  $\underline{k}_f^e$
- 2.2. Compute the global matrix (assembly):  $\underline{K}_f = \sum_{e_f} \underline{k}_f$
- 2.3. Compute the condensed stiffness matrix at dam-foundation interface nodes:  $\underline{K}_{f,c}$

## 3. Dam stiffness matrix and force vector

- 3.1. Calculate element stiffness matrices, self-weight mass force vectors and hydrostatic pressure boundary force vectors (Gauss integration):

$$\underline{k}^e = \int_{\Omega_e} \underline{B}_u^T \underline{D} \underline{B}_u \underline{u}^e d\Omega, \quad \underline{f}_w^e = \int_{\Gamma_e} \underline{N}_u^T \underline{f} d\Gamma \quad \text{and} \quad \underline{f}_{r,e}^e = \gamma_w \int_{\Gamma_{t,e}} \underline{N}_u^T \cdot \underline{n}_{\Gamma_e}^T h_w d\Gamma$$

- 3.2. Compute global stiffness matrix and force vector (assembly):  $\underline{K} = \sum_e \underline{k}^e$ ;  $\underline{F} = \sum_e \underline{f}_w^e + \sum_{e_f} \underline{f}_{r,e}^e$
- 3.3. Calculate global elastic stiffness matrix (overlap of  $\underline{K}_{f,c}$  into  $\underline{K}$ ):  $\underline{K}_0$

## 4. Linear analysis

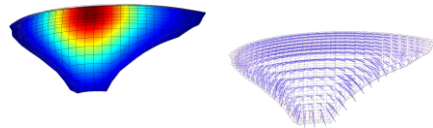
- 4.1. Compute the displacement vector  $\underline{u}$  by solving the equilibrium equation:  $\underline{K}_0 \cdot \underline{u} = \underline{F}$
- 4.2. Compute the elastic stress-tensors  $\underline{\sigma}$ , for every Gauss point of each FE:

$$\underline{u} \rightarrow \underline{u}^e \rightarrow \underline{\sigma}_{n_{GP}} = \underline{D} \underline{B}_{u,n_{GP}} \underline{u}^e$$

- 4.3. Analyse results (3D graphical representations)

4.3.1. Displacement field (values on all element nodes)

4.3.2. Stress field (values on all Gauss points)



## 5. Non-linear analysis: stress-transfer method & constitutive damage model

- 5.1. Define the applied load and compute the displacement vector:  $\underline{F}_{ap} = \lambda \cdot \underline{F} \rightarrow \underline{u} = \underline{K}_0^{-1} \cdot \underline{F}_{ap}$
- 5.2. Perform stress-transfer (iteration 1)
- 5.3. In every iteration  $n+1$

5.3.1. Read variables from previous iteration

- For all Gauss Points: effective stress tensor  $\underline{\tilde{\sigma}}_n$ , stress thresholds  $r_n^\pm$ , damage variables  $d_n^\pm$ , Cauchy stress tensor  $\underline{\sigma}_n$
- Unbalanced forces vector  $\underline{\Psi}_n = \underline{F}_{ap} - \underline{F}_{R,n}$ , corresponding displacements  $\underline{u}_{\Psi_n} = \underline{K}_0^{-1} \cdot \underline{\Psi}_n$



Figure 4.1 – a) Computational algorithm developed for DamDamage3D1.0 in MATLAB

### 5.3.2. For each FE

- Read material properties:  $E, \nu, K_v, G \rightarrow \underline{D}_0$ ;  $f_0^+, f_0^-, f_{0,2}^-, f_u^-$ ;  $G_f, w_b$ ;  $P_1(\sigma_1^-, \varepsilon_1^-)$ ,  $P_2(\sigma_2^-, \varepsilon_2^-)$
- Run **ParametersCDM.m**: calculate main parameters for the damage evolution laws
  - ✓ Tension:  $r_0^+, A^+$
  - ✓ Compression:  $R_0, K, r_0^-, B^-, A^-$
- Calculate the nodal displacements from the nodal unbalanced forces (iteration  $n$ ):  $\underline{u}_{\Psi_n}^e$
- For each Gauss Point  $\rightarrow$  run **CDamageModel.m**:
  - i. Compute strain increment (from the unbalanced forces):  $\Delta \underline{\varepsilon} = \underline{B}_{GP} \underline{u}_{\Psi_n}^e$
  - ii. Compute the effective stress tensor:  $\tilde{\underline{\sigma}}_{n+1} = \tilde{\underline{\sigma}}_n + \underline{D}_0 \cdot \Delta \underline{\varepsilon}$
  - iii. Compute equivalent effective stress tensors:  $\tilde{\tau}_{n+1}^+; \tilde{\tau}_{n+1}^-$
  - iv. Verify damage criteria and update stress thresholds
    - If  $\tilde{\tau}_{n+1}^\pm \leq r_0^\pm \rightarrow d_{n+1}^\pm = 0 \rightarrow r_{n+1}^\pm = r_0^\pm$
    - $\tilde{\tau}_{n+1}^\pm > r_n^\pm \rightarrow d_{n+1}^\pm > d_n^\pm > 0 \rightarrow r_{n+1}^\pm = \max(r_n^\pm; \tilde{\tau}_{n+1}^\pm)$
  - v. Calculate damage variables
    - Tension damage:  $d_{n+1}^+ = 1 - r_0^+ / \tilde{\tau}_{n+1}^+ e^{A^+ (1 - \tilde{\tau}_{n+1}^+ / r_0^+)} \geq 0$
    - Compression damage:  $d_{n+1}^- = 1 - r_0^- / \tilde{\tau}_{n+1}^- (1 - A^-) - A^- e^{B^- (1 - \tilde{\tau}_{n+1}^- / r_0^-)} \geq 0$
  - vi. Calculate Cauchy stress tensor:  $\underline{\sigma}_{n+1} = (1 - d_{n+1}^+) \tilde{\underline{\sigma}}_{n+1}^+ + (1 - d_{n+1}^-) \tilde{\underline{\sigma}}_{n+1}^-$
  - vii. Save main variables in global data matrices
- Calculate the elementary nodal resistant forces (Gauss integration):  $\underline{f}_R^e = \int_{\Omega_e} \underline{B}_u^T \underline{\sigma} d\Omega$

5.3.3. Calculate the global resistant load vector:  $\underline{F}_{R,n} = \sum_e \underline{f}_R^e$

5.3.4. Calculate the unbalanced forces vector:  $\underline{\Psi}_n = \underline{F}_{ap} - \underline{F}_{R,n}$

5.3.5. Compute the global displacement vector:  $\underline{u}_{n+1} = \underline{u}_n + \underline{u}_{\Psi_{n+1}} = \underline{K}_0^{-1} \cdot (\underline{F}_{ap} + \underline{\Psi}_{n+1})$

5.3.6. Convergence test:  $\underline{u}_{\Psi_{n+1}} = \underline{K}_0^{-1} \cdot (\underline{\Psi}_{n+1}) \Rightarrow \text{Norm}_{n+1} = \left( \frac{|\underline{u}_{\Psi_{n+1}}|}{|\underline{u}_{\Psi_1}|} \right) \times 100$

- If  $\text{Norm}_{n+1} > \text{Tol} \rightarrow$  Continue stress-transfer (repeat 5.3)
- If  $(\text{Norm}_{n+1} > \text{Tol} \ \& \ n+1 > n_{\text{iter,max}}) \rightarrow$  Stop stress-transfer (divergence)
- If  $\text{Norm}_{n+1} < \text{Tol} \rightarrow$  Stop stress-transfer (convergence)

5.4. Analyse non-linear results (3D graphical representations)

5.4.1. Displacement field (values on all element nodes)

5.4.2. Stress field (values on all Gauss points)

5.4.3. Tension and compression damage (values on all Gauss points)

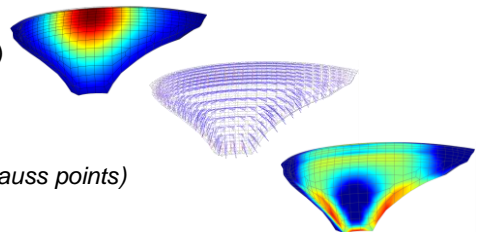


Figure 4.1 – b) Computational algorithm developed for DamDamage3D1.0 in MATLAB

### 4.3 Code validation. Test with a 3D structure

Aiming to calibrate and optimize the stress-transfer and the damage model codes for 3D structural calculations, non-linear tests were carried out for a simple structure with a controllable behaviour. This structure is a 3D frame structure with three columns ( $1 \times 1 \times 5 \text{ m}^3$ ), supporting a beam ( $5 \times 1 \times 1 \text{ m}^3$ ) at the top, with another beam acting as an elastic foundation. The upper beam is assumed to have infinite stiffness and strength, so it does not suffer any deformation. All remaining structural elements have Young's Modulus  $E = 30 \text{ GPa}$  and Poisson ratio  $\nu = 0,2$ . However, the central column is made of regular concrete, with and tension and compression strength of  $f_0^+ = 2 \text{ MPa}$  and  $f_0^- = -30 \text{ MPa}$ , while the lateral columns and the lower beam present much higher material strength, ensuring only linear elastic behaviour occurs. Also, high stiffness is assumed at the base of the lower beam to simulate a foundation behaviour with elastic supports. Therefore, according to above hypothesis, concrete failure is expected to occur only at the central column without causing the collapse of the structure, which remains in equilibrium.

3D FE mesh and material properties

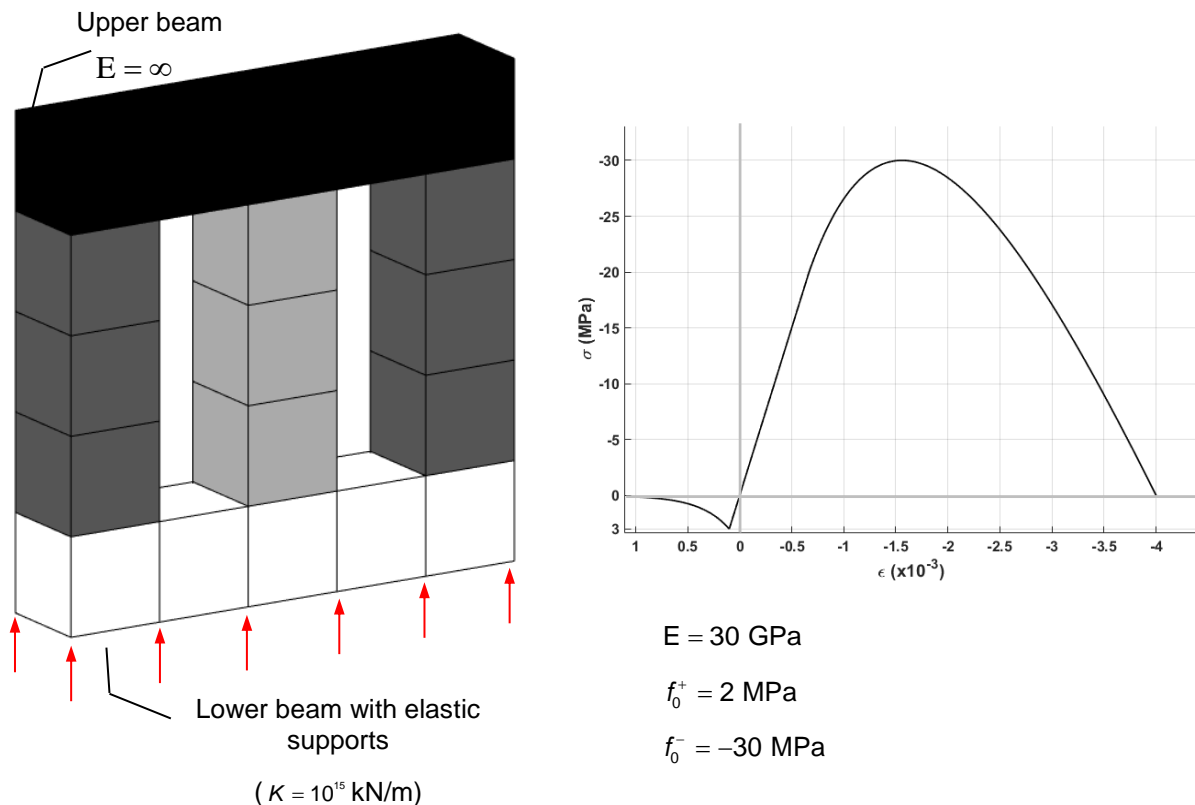


Figure 4.2 – Test structure: 3D FE mesh, properties and constitutive damage law for the central column

The non-linear analysis is studied by applying nodal vertical forces at the top of the upper beam, causing high stress values in the columns and hence concrete damage in the central column until its failure occurs. Consequently, the unbalanced stresses are to be redistributed to the remaining structural elements which will not present damage due to their high tension and compression strength. Also, even though the central column “collapses”, the structure is expected to present enough global resistant capacity to withstand it and redistribute all arising unbalanced stresses until equilibrium is reached. Two simulations are presented to analyse the effects of both tension and compression damage (stress and damage values are only shown for the three columns), with a convergence tolerance of 0.1% for the unbalanced forces.

The first test was carried out considering the application of nodal vertical traction force resulting in  $F_{ap}^+ = 10000$  kN. For the first iteration (Figure 4.3), a maximum vertical displacement of 0.43 mm and a maximum tensile stress of 4.08 MPa were computed at the central column. Given the effective (or elastic) stresses exceed the material tensile strength, tension damage occurs (from 0.1 to 0.4), and the stress-transfer procedure continues by redistributing the unbalanced stresses to the other structural columns. At the end of the stress-transfer (Figure 4.4), failure occurs at around mid-height of the central column, with tension damage values equal to 1, while the installed real stresses become approximately zero.

The second test was performed for nodal vertical compressive forces, in a total of  $F_{ap}^- = -100\ 000$  kN. The preliminary analysis (Figure 4.5) results in a maximum downward displacement of 4.36 mm and maximum compressive stresses of -40.85 MP, for the central column. Again, the computed effective stresses are greater than the compressive strength and thus compression damage occurs (values between 0.2 and 0.4). Again, resulting unbalanced forces are to be redistributed across the structure according to the global resistant capacity. At the end of the stress-transfer process (Figure 4.6), the central column collapsed due to concrete crushing at about half its height, where the damage value is equal to 1.

Naturally, in both simulations the stresses initially supported by the central column are transferred to the other structural elements and the maximum displacements increase until failure occurs. As expected, convergence is achieved, the structure reaches a state of global equilibrium upon the redistribution of all unbalanced forces and therefore, structure presents enough resistant capacity to support the applied forces.

In conclusion, the expected behaviour of the test structure under traction and compression forces was successfully simulated, i.e. the collapse of the central column occurred and the consequent redistribution of the resulting unbalanced stresses until global equilibrium was reached. Therefore, the program **DamDamage3D1.0** is a reliable tool for analysing the non-linear response of arch dams, considering the concrete tension and compression damage phenomena with a constitutive damage model.

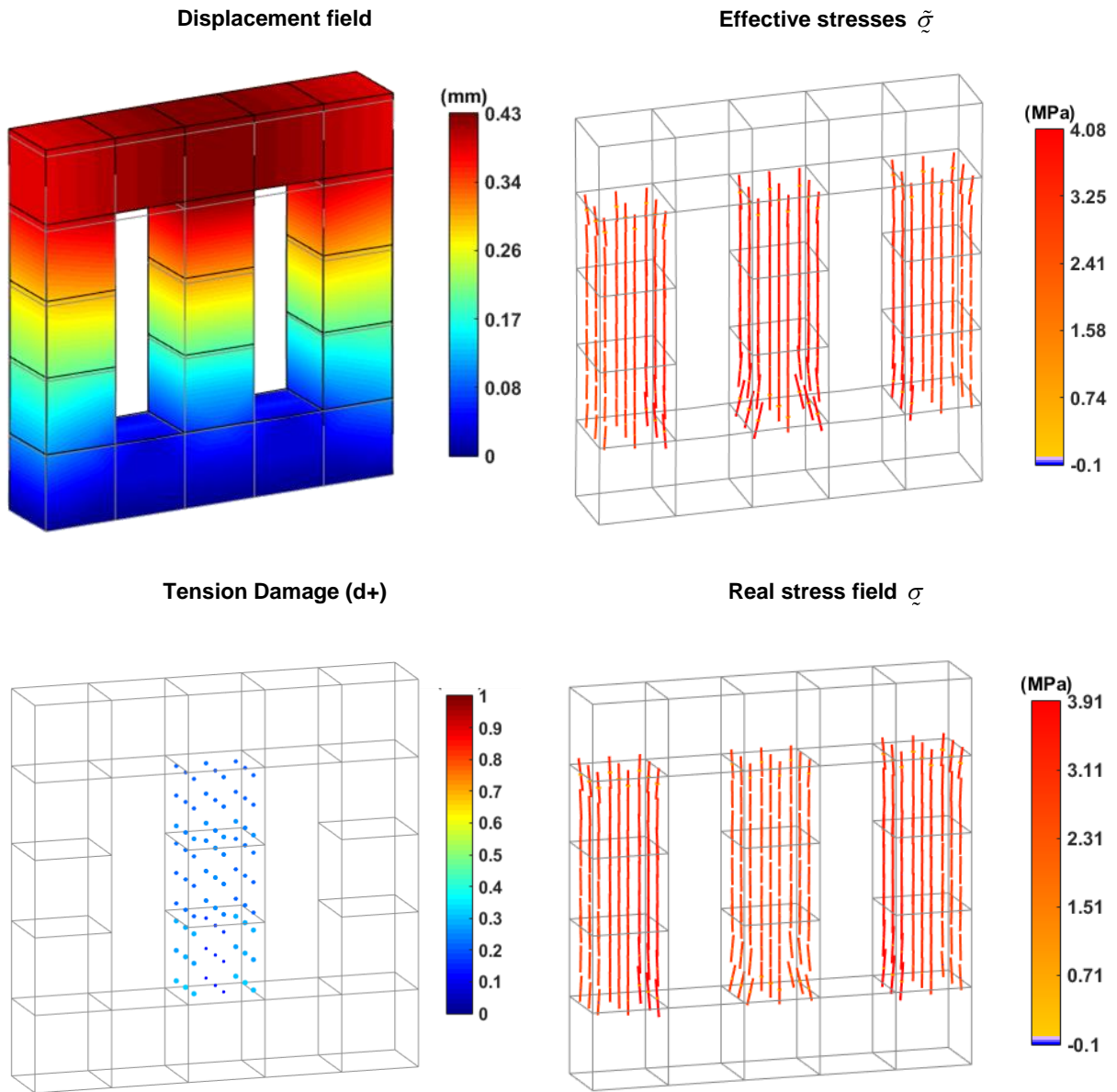


Figure 4.3 – Tension damage test. First iteration: displacement and elastic stress fields, tension damage values (d<sup>+</sup>) and real stress field



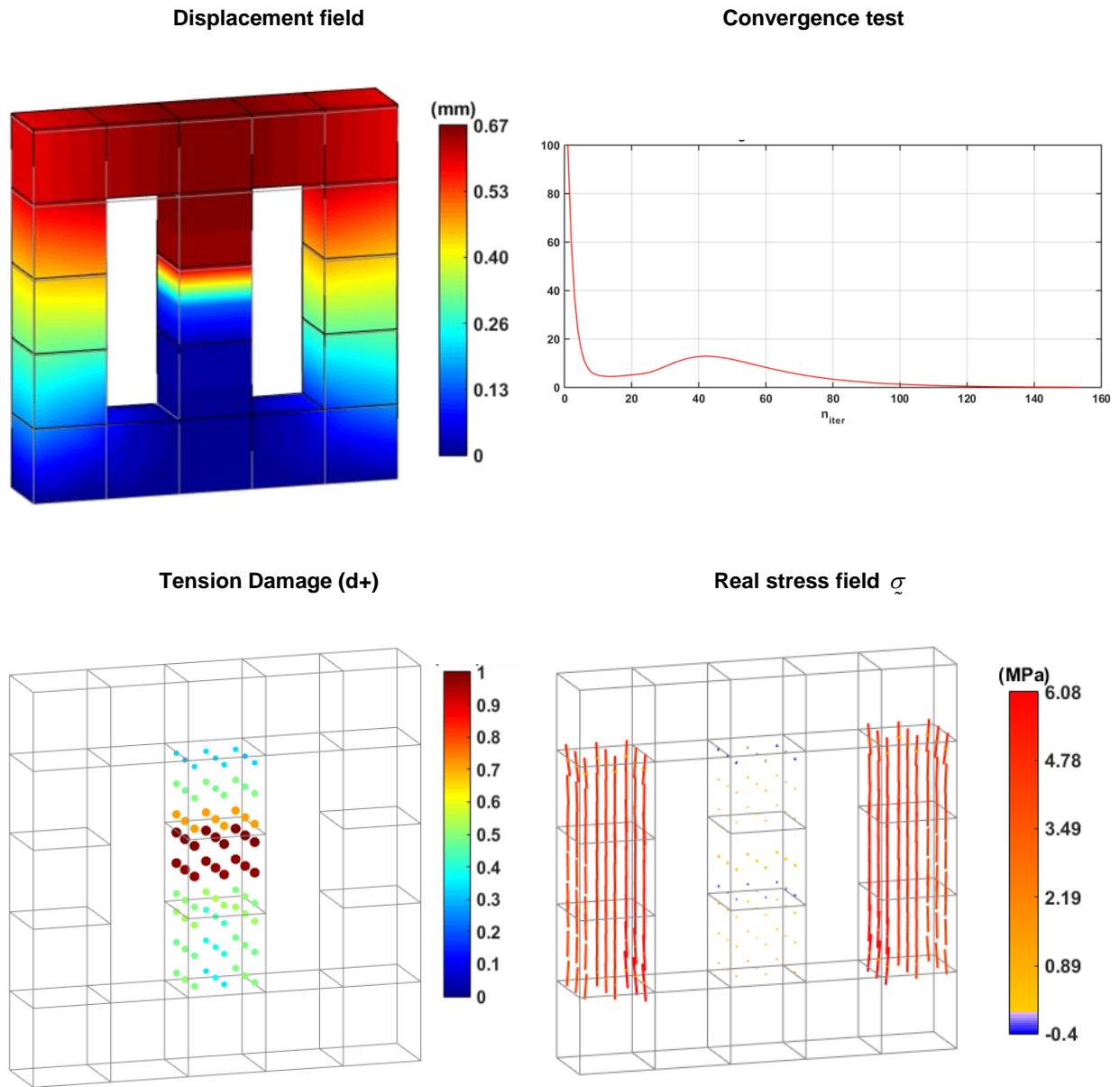


Figure 4.4 – Tension damage test. End of stress-transfer: displacement field, convergence test, tension damage values ( $d^+$ ) and real stress field

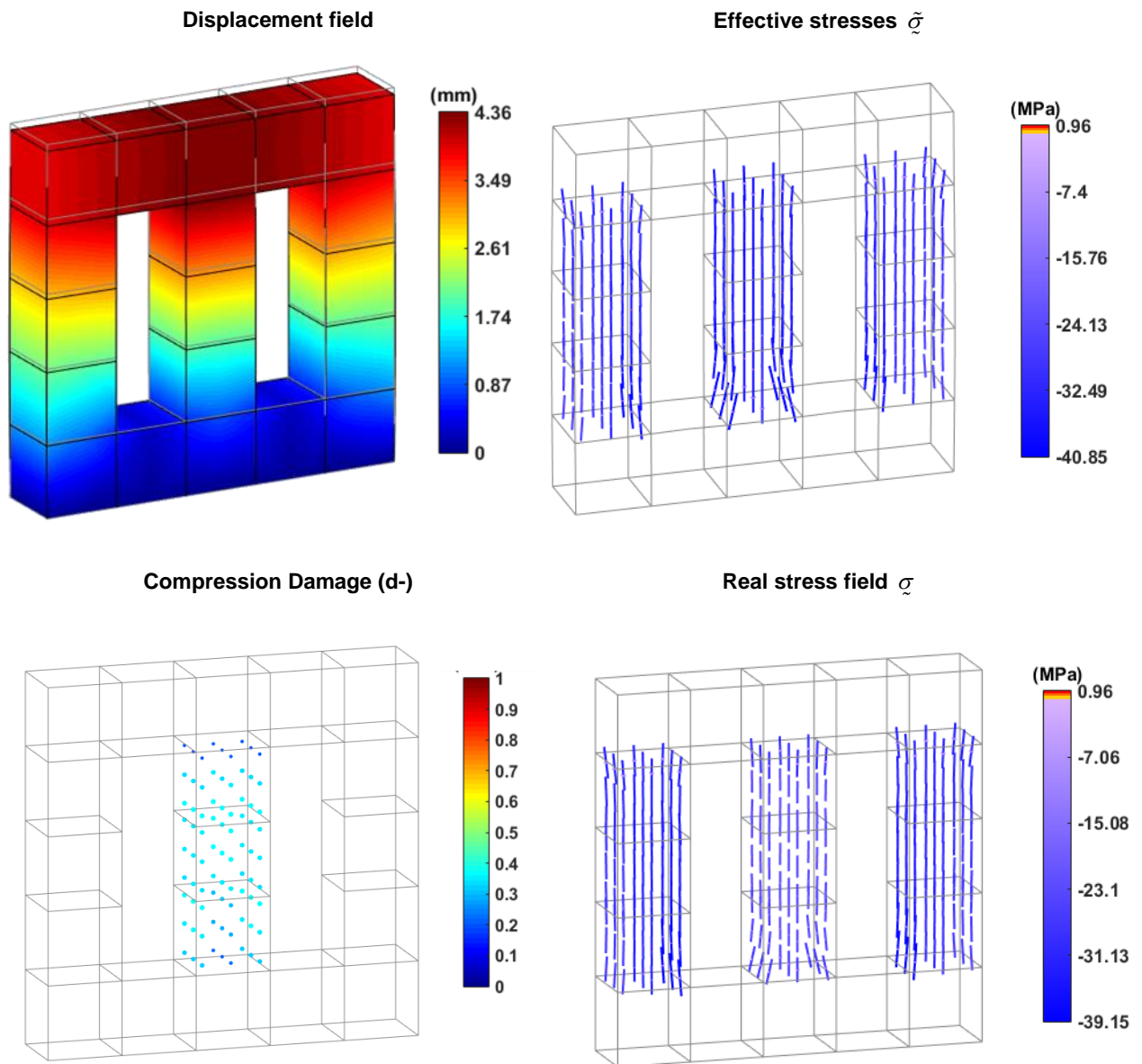


Figure 4.5 – Compression damage test. First iteration: displacement and elastic stress fields, compression damage values (d-) and real stress field

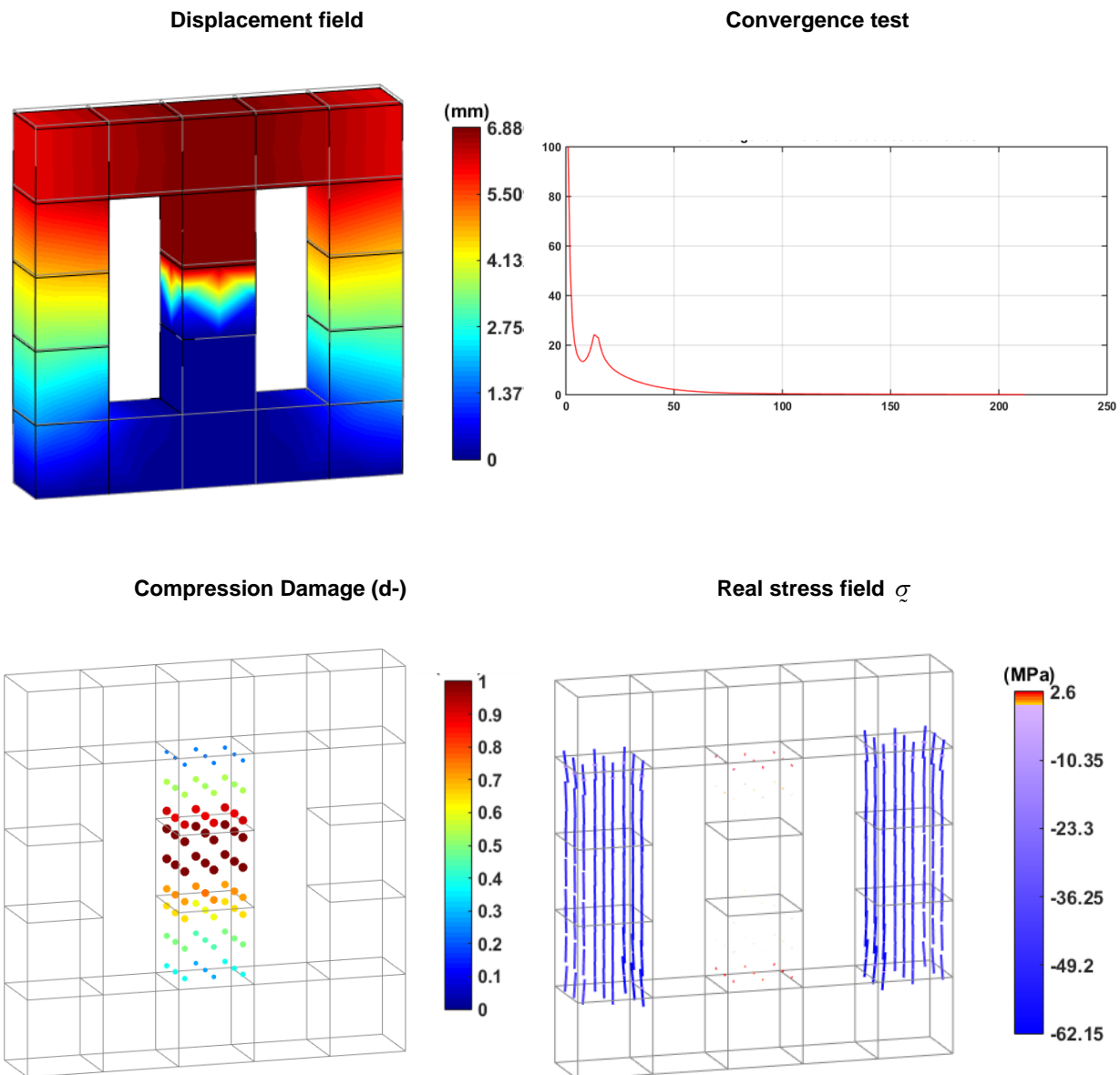


Figure 4.6 – Compression damage test. End of stress-transfer: displacement field, convergence test, compression damage values (d-) and real stress field

## 5| Non-linear analysis of a large arch dam. Study for the concrete strength decrease scenario

### 5.1 General considerations

In the scope of the structural safety control of large arch dams, it is common to study the main scenarios related to the foundation stability and to the integrity of the dam body, including the dam's structural safety verification for the concrete strength decrease scenario, with the goal of calculating a global safety factor, for the main operation static load combinations (self-weight, hydrostatic pressure, thermal gradients and eventually internal swelling processes). The concrete non-linear behaviour is considered, knowing that the material deterioration will cause a variation in the concrete properties, namely a stiffness decrease, and thus influence the dam's resistant capacity. It is also worth mentioning the importance of using different material properties to carry out comparative parametric studies.

The case study for this work is Cabril arch dam. The developed 3DFE model and the material constitutive laws are presented. The structural response of the dam is studied, considering both linear elastic and non-linear material behaviour. For the case of the non-linear analysis, the goal is to analyse the referred concrete strength decrease scenario and thus verify the structural safety of the dam, using two strain-softening constitutive laws to analyse the influence of the softening phenomenon. It is also carried out a comparison with results obtained with a refined mesh to further check the implemented damage model. As for the numerical results, the displacement and stress fields are presented, as well as graphical representations of the distributions of tension and compression damage (calculated in every Gauss point of each dam finite element). It is also worth mentioning that for the case of the stress fields, the principal stress values are only shown in some specific Gauss points to facilitate their interpretation.

With the study presented in this chapter it is intended to demonstrate the potential of the program *DamDamage3D1.0*, developed using MATLAB, to perform non-linear structural analysis and safety verifications of arch dams.

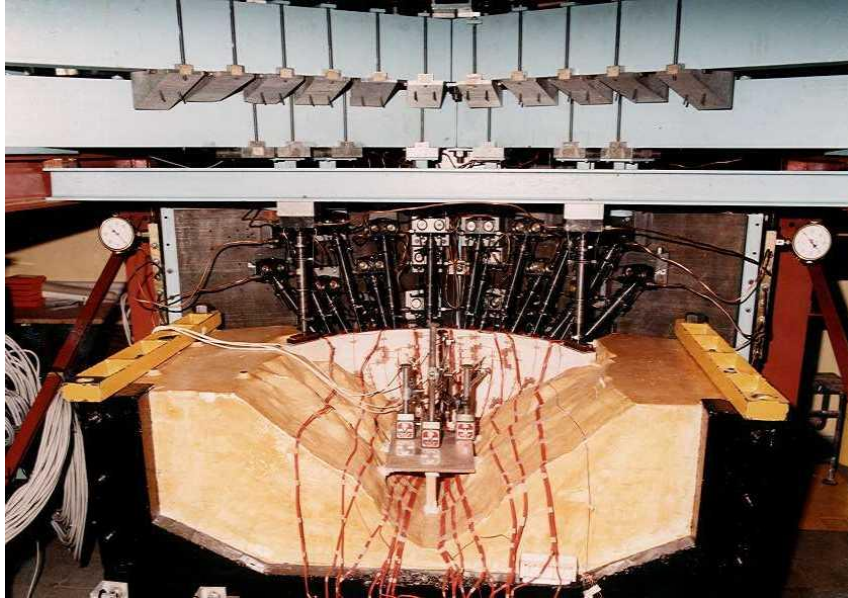
### 5.2 The concrete strength decrease scenario for arch dams

This failure scenario has been studied in LNEC for several decades (Figure 5.1) to assess the structural safety of concrete dams under static loads. Initially, by performing failure tests using physical scaled models (made of gypsum and diatomite) [LNEC, 1991; LNEC, 1993], and later, through the integrated use of physical and numerical computational models [LNEC, 2003, 2010, 2014]. This scenario is commonly studied by considering the operational static load combination including the dam's self-weight, and the hydrostatic pressure of the reservoir, which was simulated using hydraulic jacks in the physical models.

Based on the fundamental procedures of the first experimental failure tests with physical models, the goal of the referred study is to determine a safety factor ( $\lambda_s$ ), which is calculated as the maximum

multiplying factor ( $\lambda$ ) that can be applied to the static load combination without causing the dam to collapse, representing the maximum strength (peak stress) decrease that can occur. As previously referred, the safety factor is determined using this method of load amplification because it is not possible to reduce the material's strength in the physical models.

a)



b)

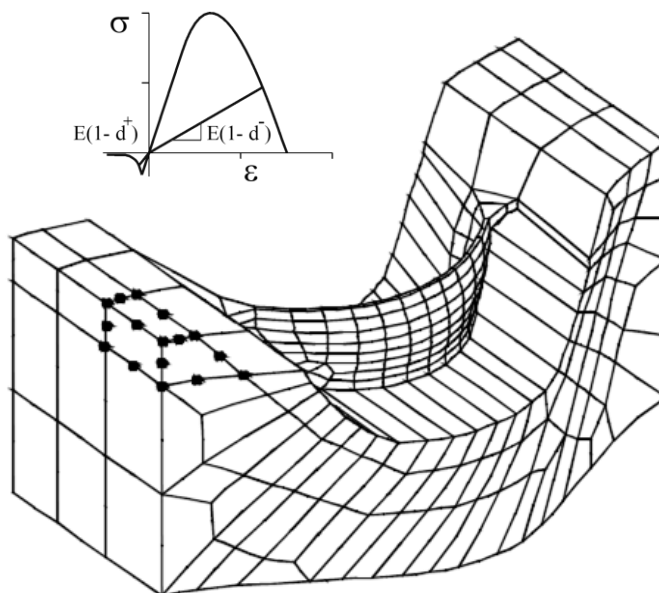


Figure 5.1 – Study of the concrete strength decrease scenario for Cabril dam: a) reduced scale physical model used in a failure test; and b) 3D FE model of Cabril dam and the material constitutive law

### 5.2.1 Structural behaviour and damaged zones

In terms of the observed structural behaviour, studies carried out for concrete arch dams in the CDD [LNEC, 2003, 2010, 2014] show a certain pattern in terms of the most commonly affected areas by material deterioration for the situation of imminent collapse. As for the displacement field, a gradual increase in the maximum displacement is typical, with the maximum displacements arising at the top of the central cantilever. Considering the concrete deterioration under tension, it is usual to observe the arising of cracks along the lower part of the upstream face, near the dam base, namely caused by high tensile stresses (mainly due to the hydrostatic pressures), and, in some cases [LNEC, 2003] at the upper area of the dam, where the maximum displacements occur. As for the damage under compressive stresses, the most severely damaged zones, where concrete crushing can occur, usually arise at the upstream face near the base, due to significant compressions in parallel with the insertion, as well as in the upper central volume of the dam body, caused by compressive stresses along the arch. Finally, the dam's structural behaviour can be influenced by its geometry and eventual asymmetries.

### 5.2.2 Compression damage in arch dams and its importance for the concrete strength decrease scenario. Numerical issues due to strain-softening

For most structural safety studies, the phenomena of concrete failure under compression is not as relevant as in the case of tension, due to its greater compressive strength (fragile material). This is also applicable for the case of concrete dams, being usual the arising of cracks due to high tensile stresses in the dam body, which might be important. Nevertheless, to study this specific failure scenario, it is essential to consider the concrete deterioration under compression up to failure, given that this phenomenon is more significant to the dam's collapse.

As is common in the numerical studies performed in CDD-LNEC [LNEC, 2003, 2010, 2014], the concrete deterioration is simulated using damage models that originate strain-softening constitutive laws, based on the smeared crack hypothesis and considering this phenomenon is associated to a certain energy dissipation. Therefore, given the importance of compression damage, one can recall the concepts regarding material failure under tension in section 3.4, namely referring to the energy dissipation during the failure process and the issues of damage localization. Thus, when performing FEM based calculations, the problem of mesh dependent results is applicable.

For problems of large dimensions, as is the case of large concrete dams, a typical solution to overcome these numerical issues consists in using a certain FE discretization, in order to guarantee that the volume associated to each Gauss point is of a similar size to the actual material volume involved in the failure process, which in the case of tension failure refers to the FPZ volume (for the concrete used in dams, where the maximum aggregate dimensions is of about 20 cm, one can consider the maximum FPZ's width to be  $w_b \cong 1$ ). Concerning the process of concrete crushing under high compressions, a similar assumption can be made. If this is true, then the stress-strain diagrams used in numerical calculations may be assumed to represent the "real" material constitutive laws, thus ensuring a realistic energy dissipation associated to the damage phenomenon and eliminating the dependence on the FE

mesh (an analogous analogous line of reasoning was followed to ensure an adequate simulation of the concrete's non-linear behaviour for the reduced scale models). Otherwise, when using finer or coarser meshes, one must implement a solution to overcome mesh dependence and guarantee the quality of the numerical results, such as the ones addressed in section 3.4.3 for large scale problems.

In any case, it should be stated that when this type of hypothesis is assumed, one should be aware of the simplifications assumed and of the resulting limitations of the numerical models when analysing the computed numerical results. However, based on previous studies, it must be noted that the abovementioned approaches have proven to be quite accurate, enabling to achieve satisfying results.

Regarding *DamDamage3D1.0*'s code, the above-mentioned principles were followed when developing the implemented algorithm, which does not automatically adjust the parameters that influence the energy associated to the failure process according to the FE mesh dimensions. Therefore, the FE models and the constitutive laws used in this work or in future studies must be developed in order to guarantee a consistent energy dissipation based on realistic constitutive laws and to ensure an accurate simulation of concrete failure.

### 5.3 Case study: Cabril arch dam (132 m high)

Cabril dam (Figure 5.2 and Figure 5.3), the highest arch dam in Portugal, is located on the Zêzere river. The dam was built between September of 1952 and December of 1953, while the reservoir filling took place from 1954 to 1956. This 132 m high double curvature arch dam (circular radius) is an impressive engineering work, with a total volume of about 360 000 m<sup>3</sup>. The crest reaches an altitude of 297 m and is 290 m long. The central cantilever has a maximum width of 20 m at the base of the dam and a minimum of 4.5 m at the upper part, 7 m below the crest, which was widened at the crest to allow the dam to be crossed by a road. The structure's transition to the insertion in the foundation was designed to provide a symmetrical shape to the dam.

The foundation consists on a granite massif of global good quality, which improves with depth. As for the reservoir, the water surface elevation ranges from 240 m (minimum required level for operating the dam) to a maximum storage level of 294 m (the maximum flood level is 296.3 m). The surface area is of about 20 000 km<sup>2</sup> with a total maximum capacity of 720 000 000 m<sup>3</sup>. A reinforced concrete intake tower with the same height of the dam was constructed next to the upstream face, which leans against the dam for lower water levels.

Regarding the dam's structural behaviour, it is important to refer a cracking phenomenon at a height of 280-290 m that occurred during the first filling of the reservoir, when the water elevation was close to the maximum level. This phenomenon was caused by high vertical tensions installed in the upper area of the downstream face, due to the greater crest width, leading to the opening of horizontal cracks. It should be noted that this set of cracks does not compromise the integrity nor the proper operation of the dam, which remains in good condition to this day.





3FE model of the dam-reservoir- foundation system

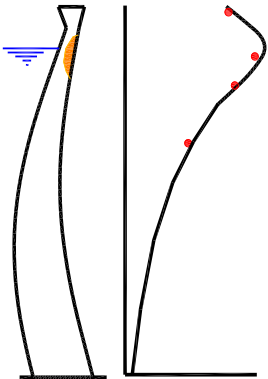
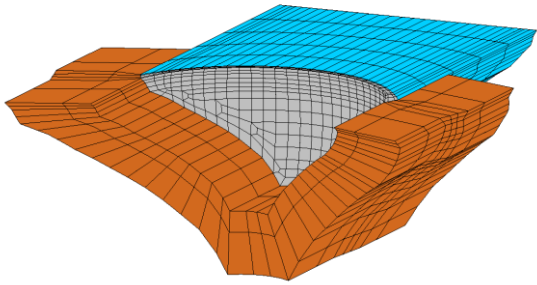


Figure 5.2 – Cabril dam (132 m high). Aerial view, downstream views, example of a 3DFE model and cracked zone detail



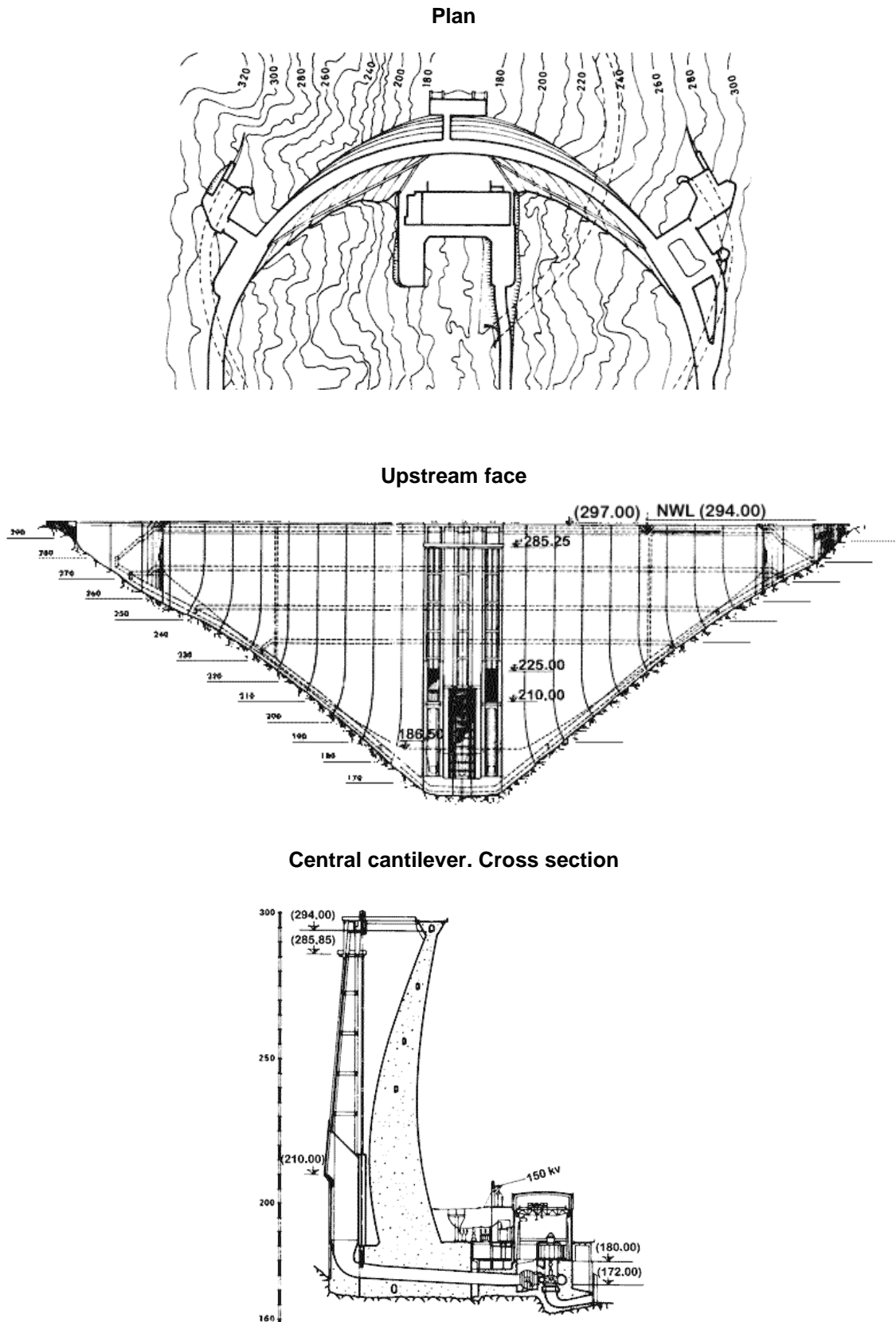
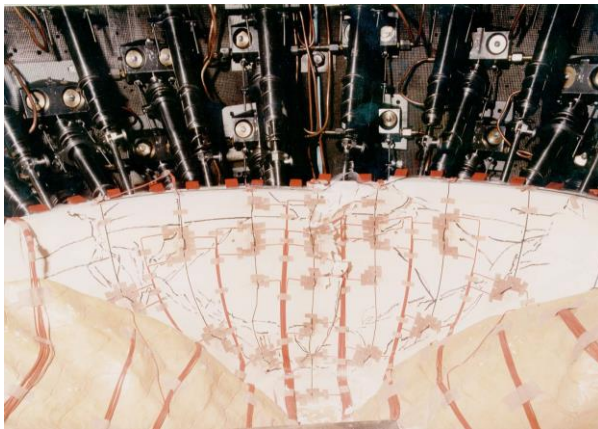


Figure 5.3 – Cabril dam. Technical drawings: Plan, upstream face elevation and central cantilever's cross section

Safety verifications for the concrete strength decrease scenario were carried out in the past in LNEC for Cabril dam, based on failure tests, with physical scaled models made of gypsum-diatomite [LNEC, 1991, 1993], and based on numerical studies, using 3D FE models [LNEC, 2003] (Figure 5.4).

For the experimental tests, the safety factors ranged from 7.8 to 8.8 according to different gypsum-diatomite ratios or different material properties attributed to certain zones of the scaled models, considering a compressive peak strength of 30 MPa. Regarding the numerical calculations, the safety factors varied between 7.2, for a constitutive law with an inferior ultimate strain (less softening up to failure), and 8.3, considering a constitutive law with a higher ultimate strain, both with a compressive strength of 30 MPa.

**Reduced scale model (gypsum-diatomite)**



**Coarse mesh. 3DFE model**

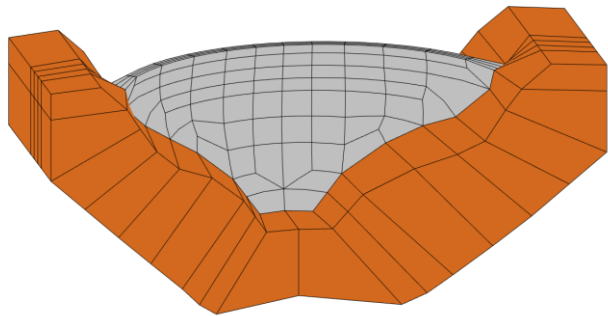


**Figure 5.4 – Cabril dam. The concrete strength decrease scenario: a) reduced scale model for failure tests; and b) 3DFE model used in previous numerical studies**

## 5.4 3DFE model, material properties and constitutive laws

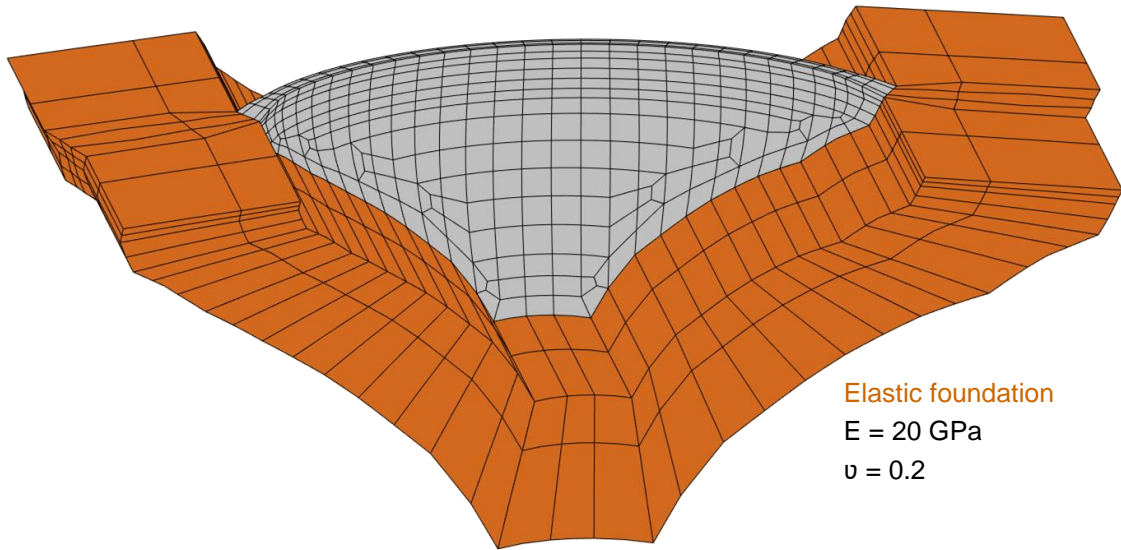
The numerical simulation of Cabril dam's structural behaviour was performed using a 3DFE model (Figure 5.5) based on the dam's real geometry. The presented mesh is a refined version of a coarser mesh used in previous studies carried out in LNEC [LNEC, 2003]. The discretization was carried out using 3D isoparametric FE with 20 nodal points, considering three elements in thickness for the dam body, resulting in a total of 909 elements and 4904 nodal points. The stress and damage fields are computed considering 27 Gauss points per element. The foundation is simulated based on the massless approach. Thus, a block of the foundation massif was discretized using the same type of FE, and, as mentioned in chapter 4, the foundation's stiffness is calculated at the dam-foundation insertion in order to simulate elastic supports at the dam base. With this approach, the structural analysis is performed only for the dam. Regarding the reservoir, the water level can be chosen as an input to compute the hydrostatic pressures at the upstream face.

The cracked zone, existing at a height of about 280-285 m, is not simulated in this study, in order to further check the developed model by attempting to simulate the stresses and thus the concrete damage that originate the actual cracks existing in the dam. The incorporation of the joint would eliminate the vertical tensions arising in that zone. Also, the vertical contraction joints in the dam body and the dam-foundation interface are not incorporated.

In terms of the material properties, the hypothesis of material isotropy, homogeneity and continuity are assumed for the dam body, with Young's modulus  $E = 20$  GPa and Poisson coefficient  $\nu = 0.2$ . The foundation is considered as a continuous and linear elastic medium, without any discontinuities and properties equal to the dam ( $E = 20$  GPa and  $\nu = 0.2$ ). The constitutive damage model with 2 independent damage variables ( $d^+$  for tension and  $d^-$  for compression) presented in section 3 is used to simulate the non-linear behaviour of concrete, considering a tensile strength  $f_t^+ = 3$  MPa and a compressive strength  $f_c^- = -30$  MPa.

To study the concrete strength decrease scenario for Cabril dam using the 3DFE model with no crack, two constitutive laws are used. The aim is to assess the influence of the compression softening branch in the overall non-linear behaviour of the dam. The type I constitutive law, intending to simulate a more fragile concrete failure by considering a sharper softening phenomenon, and the type II constitutive law, which considers a superior ultimate strain (less inclined softening branch) to model a more "ductile" behaviour of concrete up to failure. Finally, one should remind the assumptions addressed in sections 3.4.3 and 5.2.2 to state that the constitutive laws implemented in the numerical simulations ensure an adequate energy dissipation for concrete failure and may be considered equivalent to the real stress-strain diagrams of the concrete used in Cabril Dam.

**FE mesh**



**Dam concrete: material properties and constitutive laws**

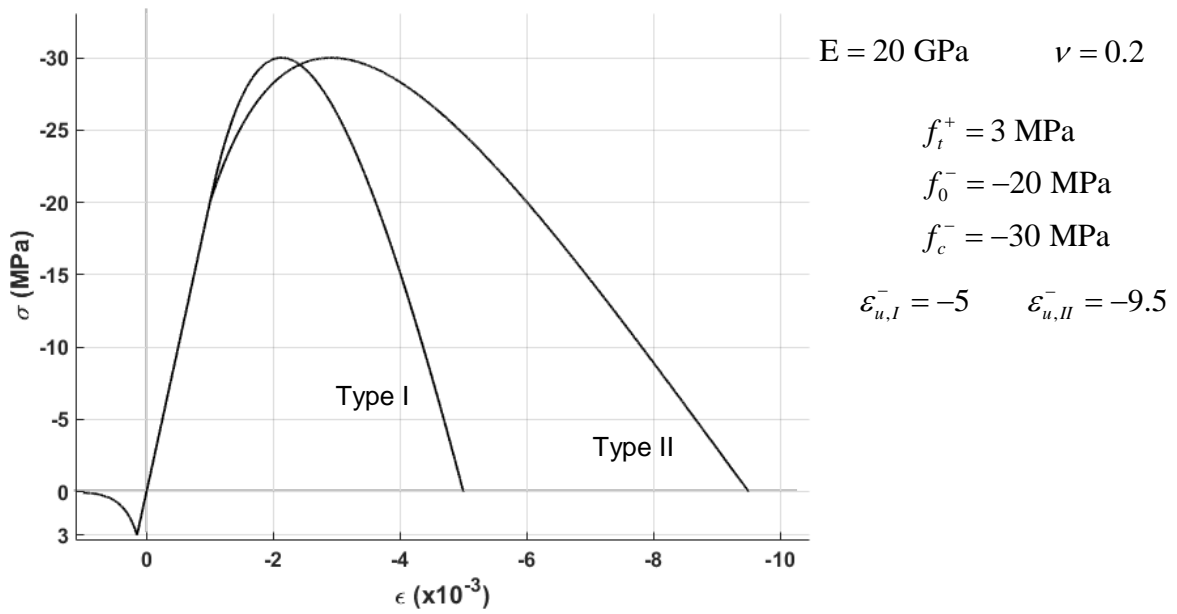


Figure 5.5 – Cabril dam: 3D FE mesh, material properties and constitutive law (type I and type II)

## 5.5 Static load combination and structural analysis

Cabril dam's structural response is analysed for the operational static load combination (Figure 5.6), including the self-weight (SW) of the dam, assuming it to be applied simultaneously, and the hydrostatic pressure (HP) at the upstream face, considering a water level  $H_w = 132$  m that corresponds to the full reservoir condition (water elevation of 297 m). No thermal variations or swelling reactions are considered in the present study. Therefore, the load combination used is henceforth referred to as SW+HP132.

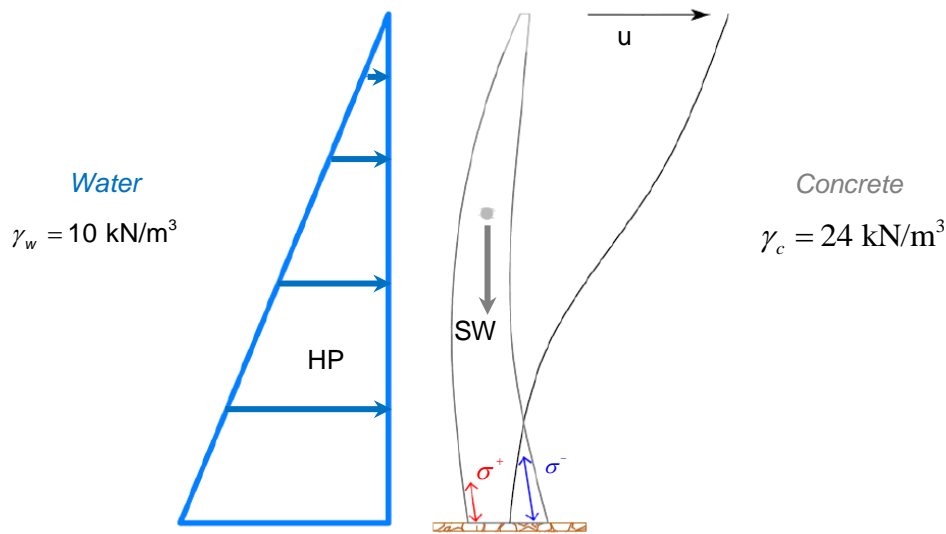


Figure 5.6 – Schematic representation of the static load combination SW+HP for an arch dam and the corresponding deformed shape

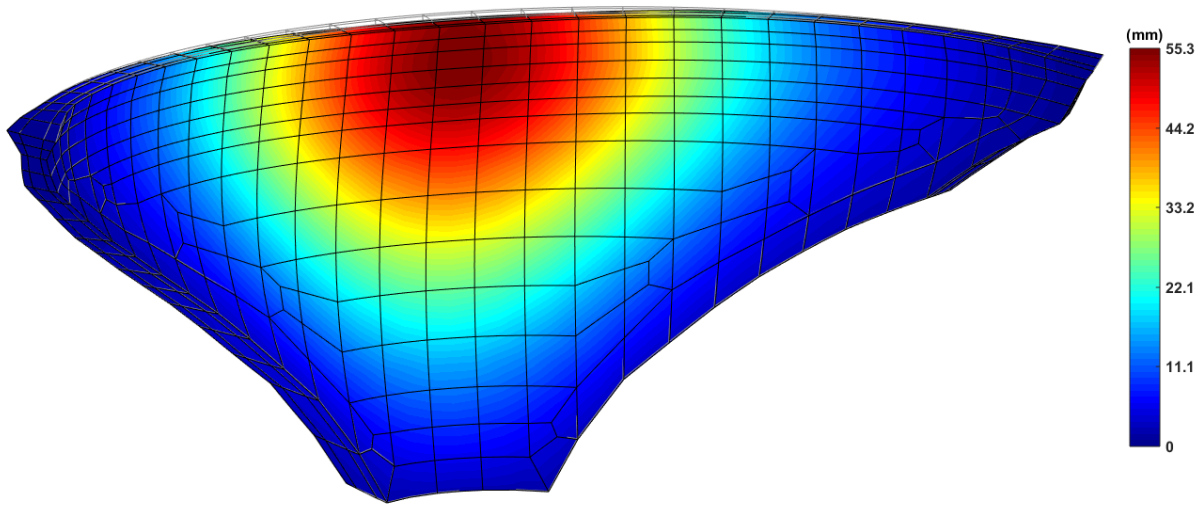
Cabril dam's linear response for SW+HP132 is presented in Figure 5.7, including the displacement fields and the principal stresses computed at the central Gauss points of each FE. The maximum displacement is of about 54 mm and occurs below the crest (at 285 m), with a significant radial component in the downstream direction, mainly due to the upstream downstream oriented water pressures. Regarding the stress state, the dam is globally under compressions, which means the dam's self-weight is responsible for compensating the high tensions caused by the water pressures.

Nonetheless, important tensile stresses normal to the insertion are installed at the dam's heel at the upstream face,  $\sigma_{\max}^+ = 2.6$  MPa ; vertical tensions ( $\sigma^+ \approx 1$  MPa) also arise near the crest.

The higher compressions arise near the dam base at the downstream face ( $\sigma_{\max}^- = -7.2$  MPa), oriented normally to the insertion, and in the upper part, with compressive arch stresses ( $\sigma^- \approx -5.5$  MPa).

### Linear analysis. Static load combination SW+HP132

*Displacement field*



*Stress field (upstream and downstream faces)*

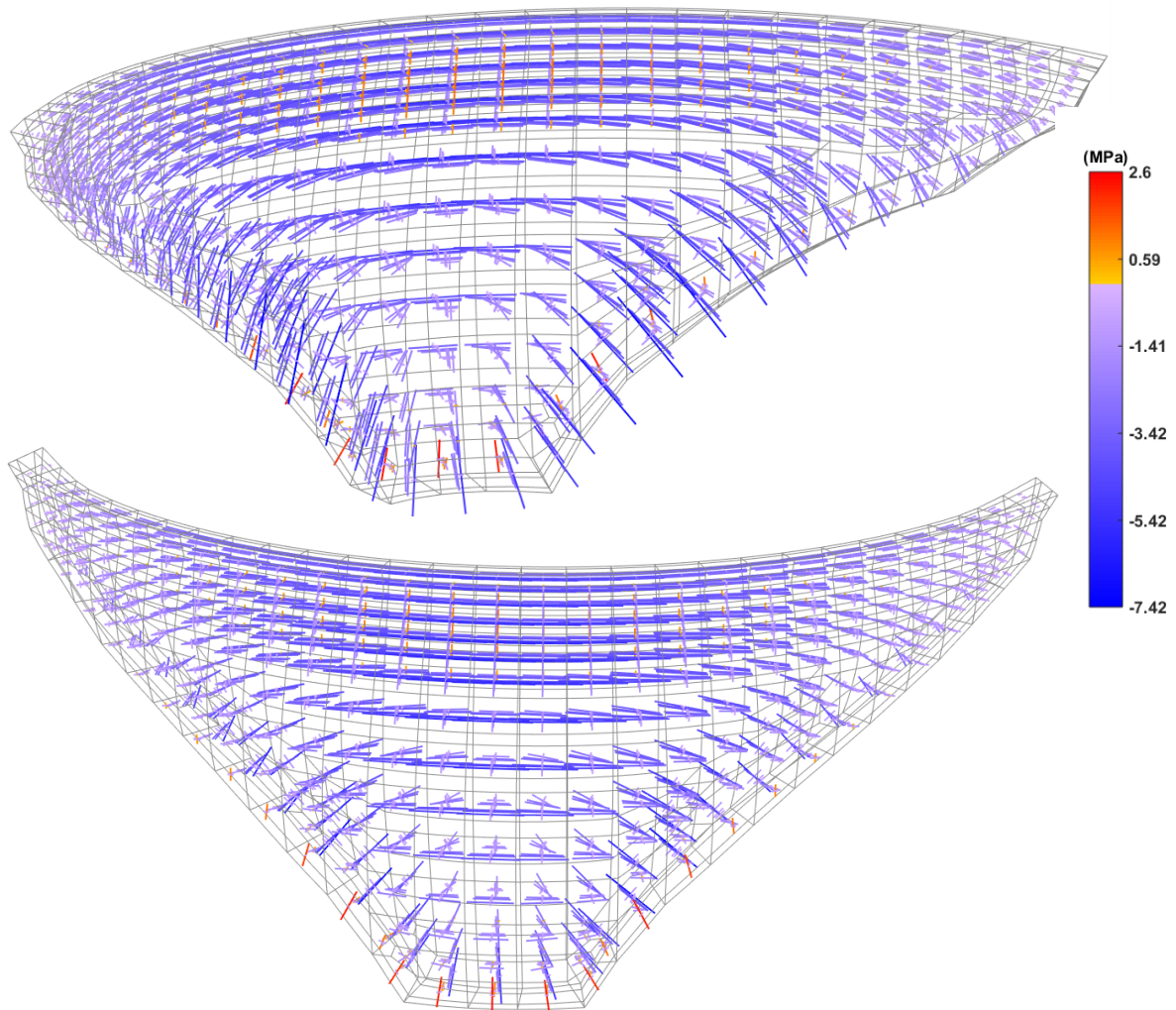


Figure 5.7 – Linear analysis. Static load combination SW+HP132. Displacement and stress fields

## 5.6 Safety verification for the concrete strength decrease scenario

The structural safety of Cabril dam is evaluated in this work for the concrete strength decrease scenario by analysing the non-linear response, considering the material deterioration up to failure under tension and compression. The aim of this study is to determine the global safety factors  $\lambda_s$  using different constitutive damage laws, in order to assess the influence of the compression softening branch in the stress redistribution process consequently in the overall response of the dam.

The referred collapse scenario is simulated through non-linear calculations, in which gradually increasing load multiplying factors ( $\lambda$ ) are applied to the static load combination,  $\lambda \times (SW+HP132)$ , in order to assess the global resistant capacity of the dam to support the installed stresses until collapse occurs. Thus, the global safety factor is determined as the last multiplying factor that does not result in the dam's collapse.

In this work, both constitutive laws presented in Figure 5.6 are used, considering a tensile strength of 4 MPa and a compressive strength of 30 MPa. For Cabril dam, the global safety factor for the concrete strength decrease scenario is  $\lambda_s = 7.4$ , using the Type I constitutive law, and  $\lambda_s = 8.1$ , considering the Type II constitutive law. One should emphasize that the obtained values in both cases are in accordance with the safety factors from failure tests in physical models and numerical studies performed previously in LNEC.

The main results from the numerical simulations of Cabril dam's non-linear response are presented herein (Figure 5.8 to Figure 5.13), including: a) the evolution of radial displacements along the central section of the dam, for a gradual increase of the applied load factor  $\lambda$ ; b) the deformed shape, obtained at the end of the stress-transfer iterative process; and c) the distributions of tension and compression damage variables, calculated on all Gauss points of the FE model, for the last calculation of the concrete strength decrease scenario, with  $\lambda = \lambda_s$ .

About the evolution of displacements on the central cantilever, a gradual increase in the radial displacements is computed. The maximum displacement occurs at the height 285 m: the values range from 54 mm ( $\lambda = 1$ ) to 545 mm, using the constitutive law I ( $\lambda_s = 7.4$ ), and to 734 mm, for constitutive law II ( $\lambda_s = 8.1$ ).

Tension damage starts to occur upstream along the base of the dam, due to high tensions normal to the insertion. Tension damage also occurs, for low values of  $\lambda$ , in the downstream face at height ~285 m, caused by vertical tensile stresses. When concrete failure under tension occurs, cracks would be expected to open. However, the dam still presents enough global resistant capacity to redistribute the resulting unbalanced stresses (convergent stress-transfer process). It should be mentioned that the zone at the upper part of the dam where failure under tension arises corresponds to the actual existing cracking phenomena in Cabril dam.

As the applied load increases and the compressive strength of the material is exceeded, compression damage starts to occur due to significant arch compressions in a substantial volume at the upper part of the dam body, with damage propagation towards the abutments and across the thickness; high compressions also arise near dam base at the downstream face, causing compression damage that



propagate towards the upper part of the dam. Therefore, the dam's failure would be expected to happen because of concrete crushing under compressions in a large section at the upper part of the dam body, as well as near the insertion, laterally. In comparative terms, by observing the tension and compression damage distributions near the collapse situation, it is obvious that when using the type II constitute law (i.e. more ductile concrete behaviour under compression) the dam has a greater capacity of redistributing the arising unbalanced stresses due to material damage and hence to withstand a larger volume of damaged zones, namely under compression). Therefore, the dam can support higher applied loads. This behaviour until collapse shows the influence of softening under compressive stresses in the non-linear response of the dam, namely by affecting the dam's capacity to redistribute the unbalanced stresses.

Finally, the non-linear response of Cabril dam predicted with ***DamDamage3D1.0*** and the calculated global safety factors correspond to the results obtained in the experimental failure tests and in previous numerical studies carried out in LNEC [LNEC, 2003, 2010, 2014], thus proving to be a reliable program for performing non-linear structural analysis of concrete arch dams.



**Concrete strength decrease scenario. Non-linear response for  $\lambda \times (\text{SW} + \text{HP132})$**

**Type I constitutive law:  $\lambda = \lambda_s = 7.4$**

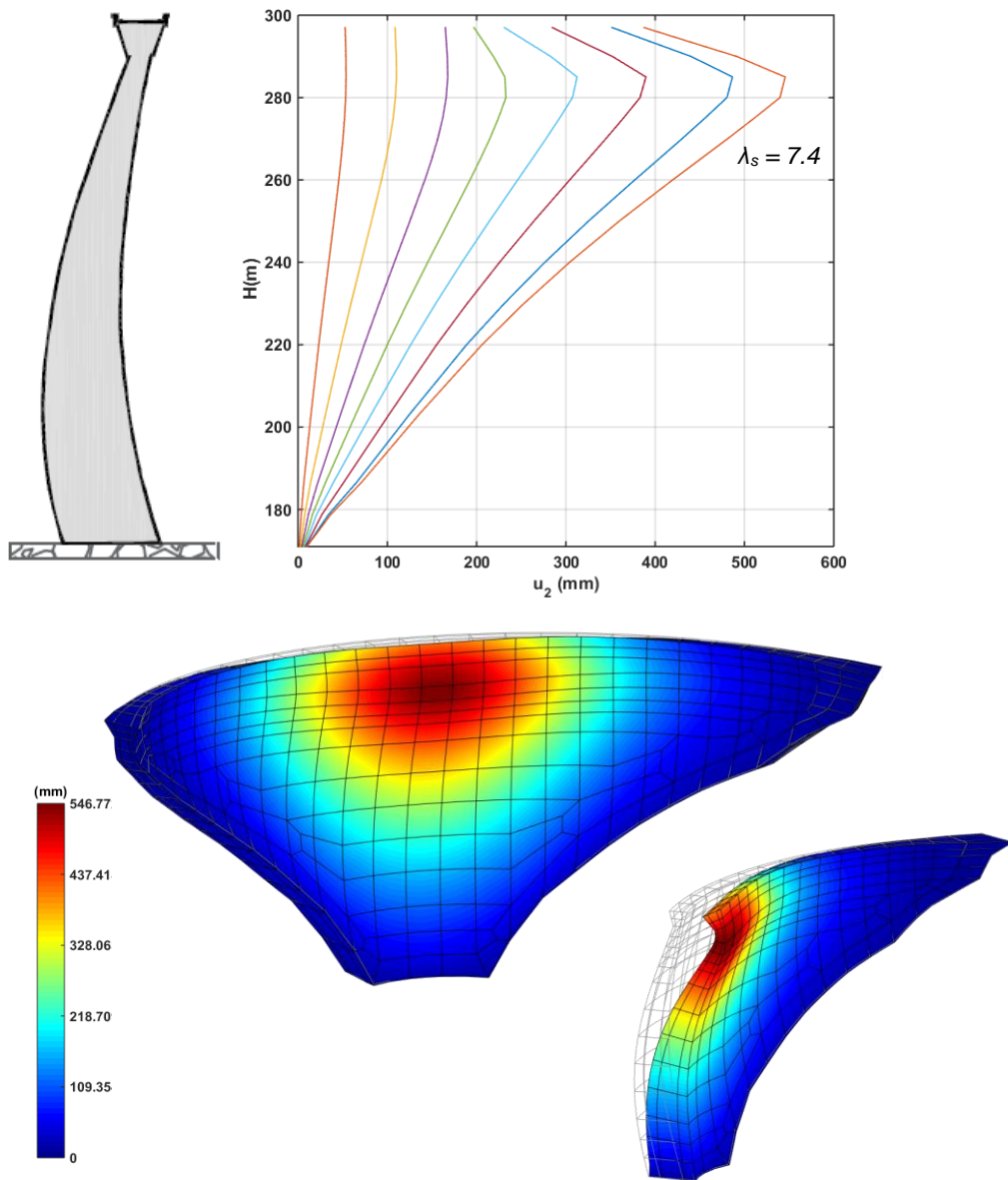


Figure 5.8 – Non-linear response: type I constitutive law ( $\lambda_s = 7.4$ ): evolution of the radial displacements (central cantilever) and displacement field at the end of the stress-transfer process

**Concrete strength decrease scenario for  $\lambda \times (\text{SW} + \text{HP132})$ . Non-linear response**

**Type I constitutive law:  $\lambda = \lambda_s = 7.4$**

*Tension damage: upstream and downstream faces*

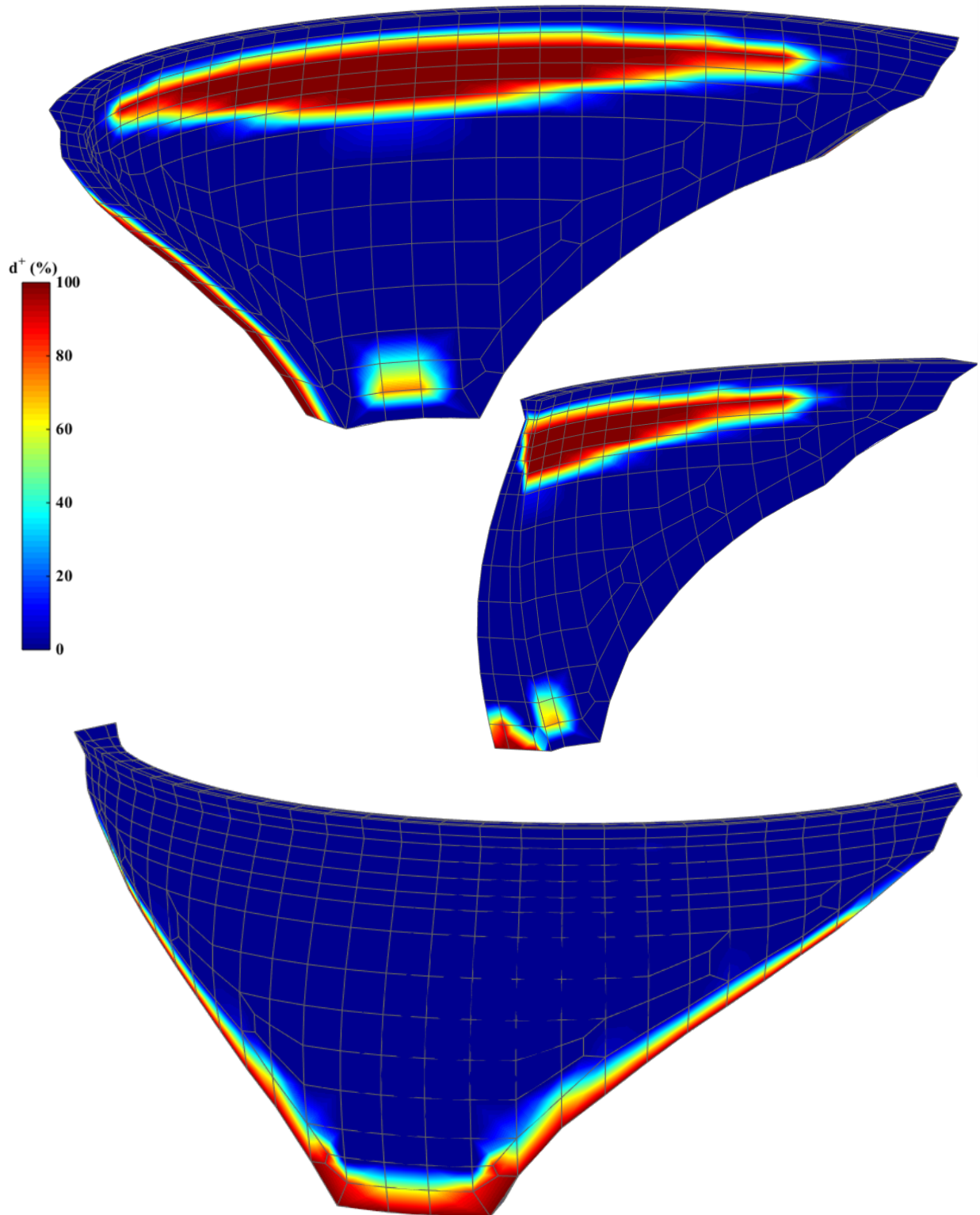


Figure 5.9 – Non-linear response: type I constitutive law ( $\lambda_s = 7.4$ ): tension damage distributions

**Concrete strength decrease scenario for  $\lambda \times (\text{SW} + \text{HP132})$ . Non-linear response**

**Type I constitutive law:  $\lambda = \lambda_s = 7.4$**

*Compression damage: upstream and downstream faces*

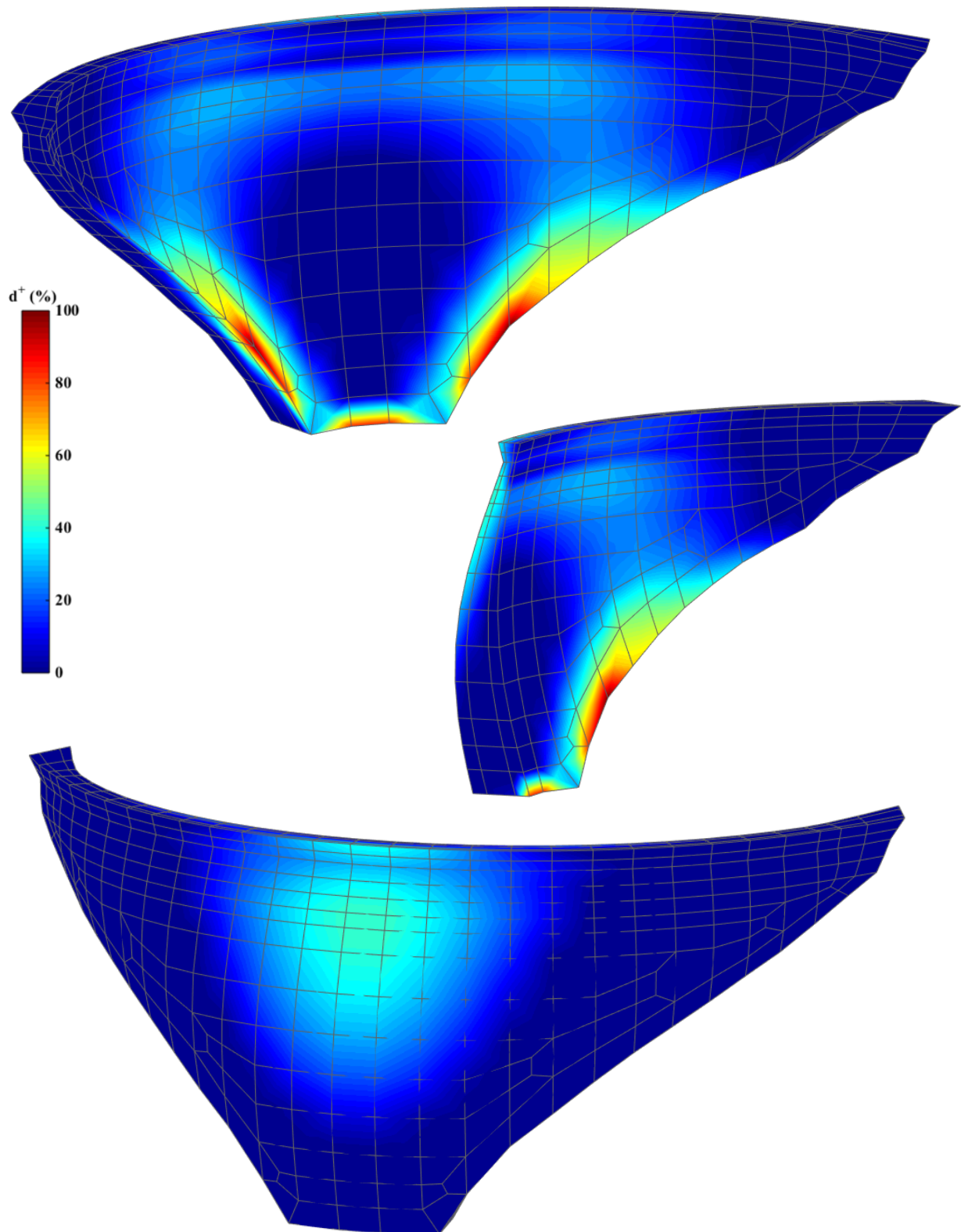


Figure 5.10 – Non-linear response: type I constitutive law ( $\lambda_s = 7.4$ ): compression damage distributions

**Concrete strength decrease scenario. Non-linear response for  $\lambda \times (\text{SW} + \text{HP132})$**

**Type II constitutive law:  $\lambda = \lambda_s = 8.1$**

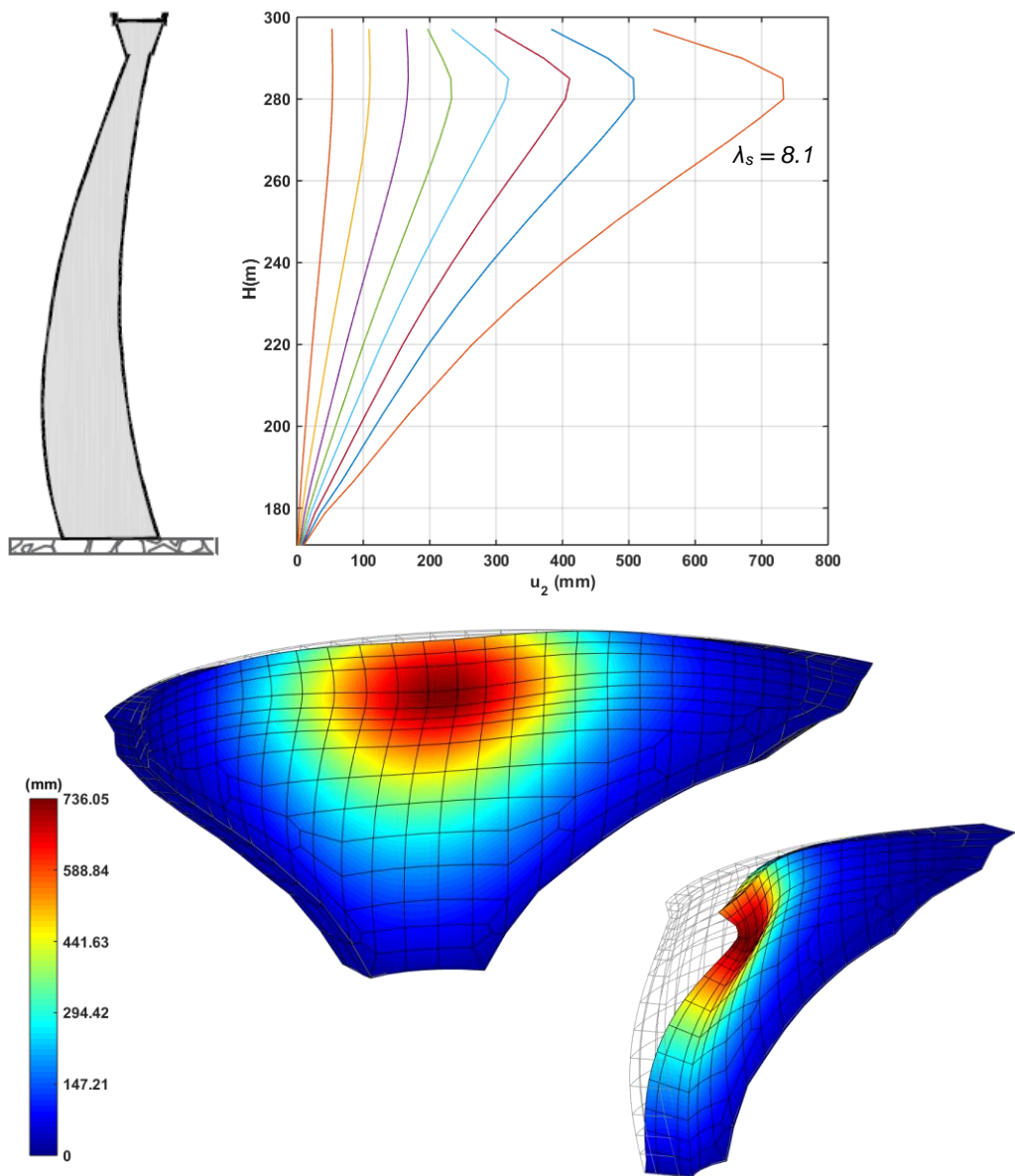


Figure 5.11 – Non-linear response: type II constitutive law ( $\lambda_s = 8.1$ ): evolution of the radial displacements (central cantilever) and displacement field at the end of the stress-transfer process

**Concrete strength decrease scenario for  $\lambda \times (\text{SW} + \text{HP132})$ . Non-linear response**

**Type II constitutive law:  $\lambda = \lambda_s = 8.1$**

*Tension damage: upstream and downstream faces*

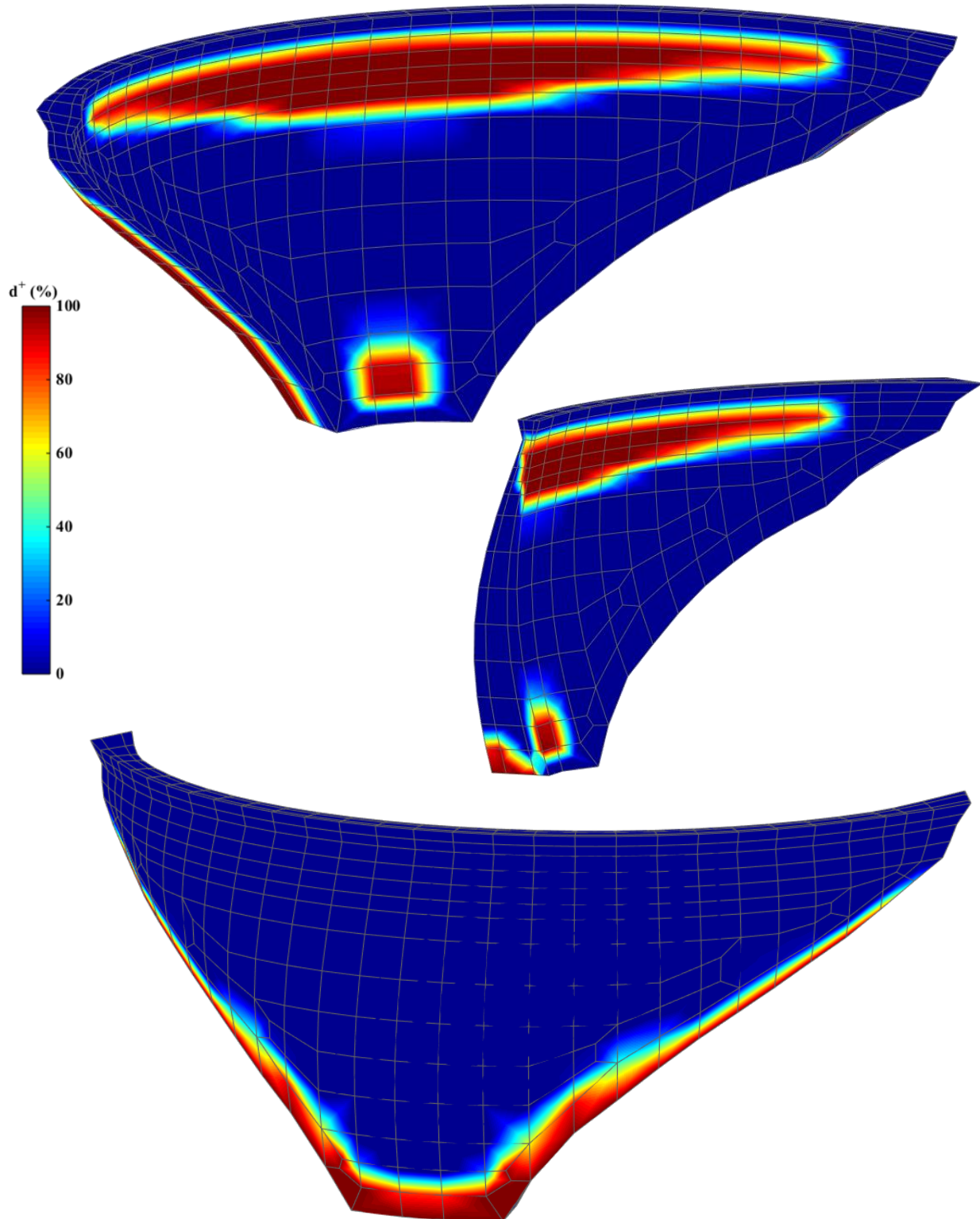


Figure 5.12 – Non-linear response: type II constitutive law ( $\lambda_s = 8.1$ ): tension damage distributions



**Concrete strength decrease scenario for  $\lambda \times (\text{SW} + \text{HP132})$ . Non-linear response**

**Type II constitutive law:  $\lambda = \lambda_s = 8.1$**

*Compression damage: upstream and downstream faces*

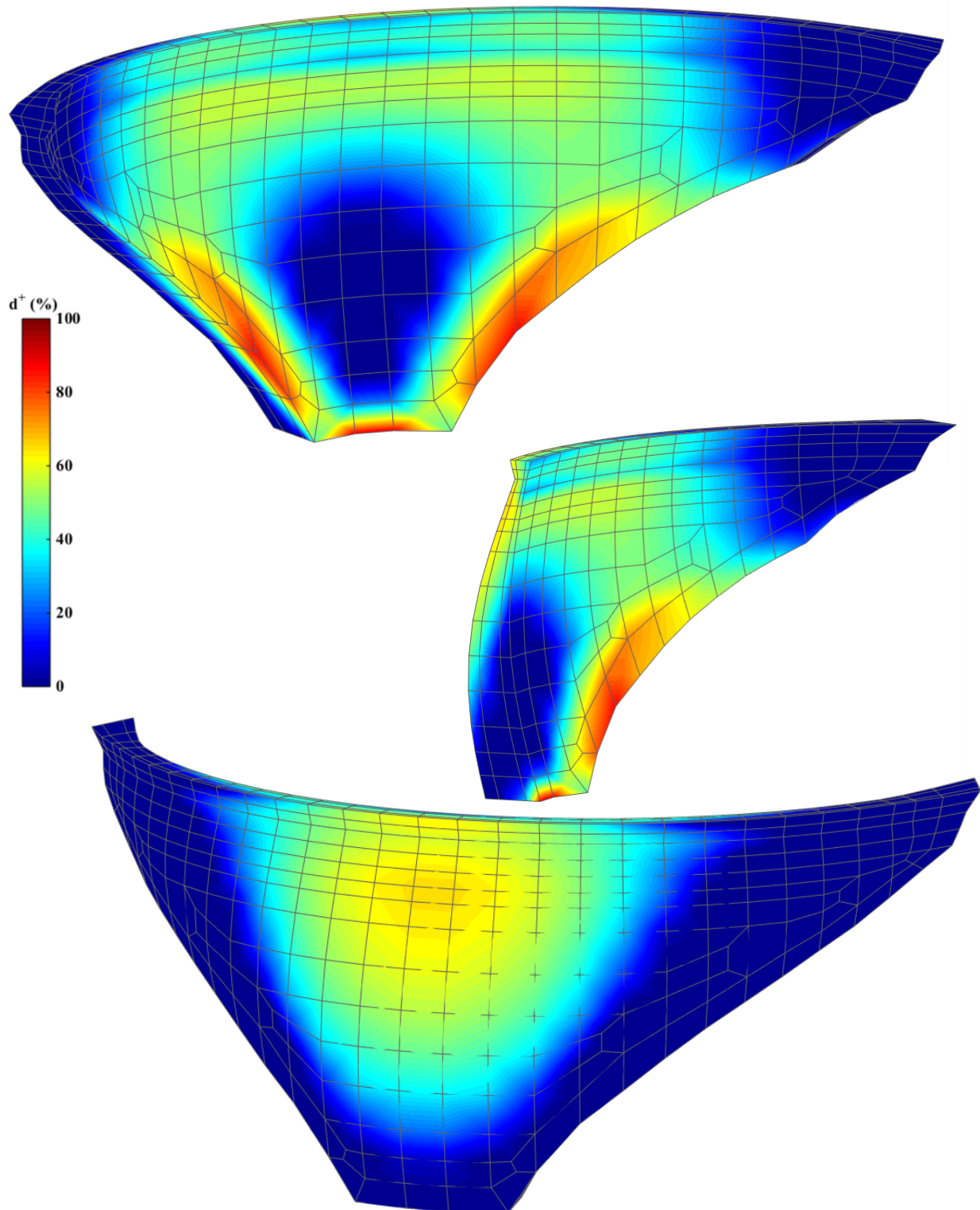


Figure 5.13 – Non-linear response: type II constitutive law ( $\lambda_s = 8.1$ ): compression damage distributions

## 6| Conclusions

The structural safety verification of large arch dams is a major issue in the field of Dam Engineering, in order to prevent incidents and accidents for the new large dams and for some of the older dams built several decades ago, in which deterioration problems (e.g. creep or internal swelling reactions) may have evolved over the years. This is particularly important considering that dams are civil engineering structures of great relevance for populations with a high potential risk.

In this scope, it is of the utmost importance to study the main failure scenarios, including the concrete strength decrease scenario to assess the structural safety of dam for the main operation static load combination. This scenario has been studied in LNEC over the last decades by conducting failure tests on physical models and based on 3DFEM numerical analyses, aiming to establish global safety factors that indicate the maximum material strength decrease that can occur without causing the dams' collapse. Also, the calculation of the safety factors enabled researchers to compare the performance of several dams with different shapes and characteristics for the referred failure scenario.

The numerical simulation of the non-linear analysis of arch dams was, and still is, a challenging subject, thus making it essential to seek the development of increasingly realistic models and efficient programs.

In this framework, ***DamDamage3D1.0***, a 3DFE based program for non-linear static analysis of arch dams was presented in this report. The theoretical bases that support the developed code were addressed in detail and the program's algorithm were shown. The non-linear calculations are carried out using the stress-transfer method, based on the redistribution of unbalanced forces. The non-linear behaviour of concrete up to failure is simulated using a constitutive damage law of two independent damage variables:  $d^+$  for damage under tension and  $d^-$  for damage under compression.

The developed program was tested and calibrated for the simple case of a 3D frame structure with three columns, under tensile and compressive forces. According to the material properties of structural elements, the concrete failure was expected to occur only at the central column without causing the global collapse of the structure. The expected non-linear behaviour was properly simulated with this test and thus the developed program was able to simulate the damage evolution phenomenon.

***DamDamage3D1.0*** was used to carry out a safety verification study of Cabril arch dam (132 m high) for the concrete strength decrease scenario, considering the material deterioration under tension and compression. This scenario was simulated by performing multiple non-linear simulations with gradual load amplification factors until a collapse situation was achieved (divergent stress-transfer process), enabling to determine the global safety factor  $\lambda_s$  as the maximum admissible factor applied to the static load combination  $\lambda_x(\text{SW}+\text{HP132})$ . This study was conducted using two constitutive damage laws to assess the influence of the compression softening phenomenon in the overall resistant capacity of the

dam: the type I constitutive law, to simulate a more fragile concrete failure, and the type II constitutive law, with a superior ultimate strain to model a more “ductile” behaviour of concrete up to failure.

For Cabril dam, considering a tensile strength  $f_t^+ = 3$  MPa and a compressive strength  $f_c^- = -30$  MPa, global safety factor  $\lambda_s = 7.4$  was determined using the Type I constitutive law and  $\lambda_s = 8.1$  using the Type II constitutive law.

Based on the numerical results presented in this report, one can note that concrete failure under tension would occur first, along the base of the dam and at the upper part at the height of the minimum width (around 280 to 290 m, a zone that corresponds to the actual horizontal cracking phenomena existing in Cabril dam). Subsequently, for higher load multiplying factors (equivalent to greater reduction in material strength) the concrete’s compressive strength would be exceeded and the dam’s collapse would occur because of concrete crushing under significant compressions in a large section at the upper part of the dam, as well as near the base, laterally.

Concerning the dam’s non-linear response using two different constitutive laws, the progression of the concrete deterioration throughout the dam body is similar, under both tension and compression. However, by analysing the damage distributions near the collapse situation, one can note that the dam has a greater capacity of redistributing the arising unbalanced stresses due to material deterioration and hence to withstand a larger volume of damaged zones, namely under compression, when using the Type II constitutive law. Therefore, it can be concluded that the dam would present a higher global resistant capacity and can support higher applied loads before collapse.

Finally, one should highlight that the predicted non-linear response of Cabril dam for the concrete strength decrease scenario (including the tension and compression damage distribution) and the corresponding global safety factors with **DamDamage3D1.0** agrees with the results obtained both in experimental failure tests and in previous numerical studies [LNEC, 2003, 2010, 2014]. Therefore, one can say that the developed program can accurately simulate the non-linear behaviour of arch dams, considering the concrete deterioration under tension and compression. As intend, this work enabled to demonstrate the potential of **DamDamage3D1.0** to perform non-linear calculations for large concrete arch dams, making it a useful tool to be used in the future in LNEC to verify their structural safety for the concrete strength decrease scenario.

Regarding the computational performance of the non-linear calculations carried out with the program **DamDamage3D1.0**. Using the fine Cabril dam mesh (4904 nodal points and 909 FE) global equilibrium is achieved (convergent stress-transfer process) in around 2 hours and 40 minutes, for about 400 stress-transfer iterations, using a computer with a 3.8 GHz processing capacity.



Lisbon, LNEC, November 2019

APPROVED

AUTHORS

The Head of the Modelling and Rock  
Mechanics Unit



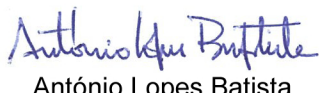
Luís Nolasco Lamas




André Alegre

Doctoral Research Fellow

The Director of the Concrete Dams Department



António Lopes Batista



Sérgio Oliveira

Assistant Researcher

## References

- ALFAIATE, J., 1992 – **Estudo e modelação do comportamento do betão fissurado**. Tese de doutoramento, IST. Lisboa.
- BATISTA, A. L., 1998 – **Análise do comportamento ao longo do tempo de barragens abóbada**. Tese de doutoramento, elaborada no LNEC. IST. Lisboa.
- COUTINHO, S.; GONÇALVES, A., 1994 – **Fabrico e propriedades do betão**. Vol. III, Edições LNEC (2ª edição). Lisboa.
- BAZANT, Z. P., 1986 – **Mechanics of distributed cracking**. Appl. Mech. Rev., ASME, 39(5), pp. 675-705.
- BAZANT, Z.P., 1987 – **Why continuum damage is non local: Justification by quasi-periodic crack array**. Mech. Res. Comm., Vol. 14, pp. 407-419.
- BAZANT, Z.P.; LIN, F.B., 1988 – **Nonlocal smeared cracking model for concrete fracture**. J. of Struct. Div., ASCE, V. 114, No. 11, pp. 2393-2510.
- BAZANT, Z.P.; OH, B.H., 1983 – **Crack band theory for fracture of concrete**. RILEM Mat. Struct. 16, pp. 155-177.
- BAZANT, Z.P.; PLANAS, J., 1998 – **Fracture and size effect in concrete and other quasibrittle materials**. CRC Press.
- BAZANT, Z. P.; PIJAUDIER-CABOT, G., 1987 – **Modeling of distributed damage by nonlocal continuum with local strain**. 4th Intern. Conf. on Numerical Methods in Fracture Mechanics, A. R. Luxmore, D. R. J. Owen, & M. F. Kanninen eds., San Antonio, Texas, Mar., pp. 411-432.
- BELYTSCHKO, T., FISH, J.; ENGELMAN, B.E., 1988 – **A finite element with embedded localization zones**. Computer Methods in Applied Mechanics and Engineering 1988, 70, pp. 59-89.
- DAVISON, L.; STEVENS, A.L., 1993 – **Thermomechanical constitution of spalling elastic bodies**. Journal of Applied Physics, Vol. 44, pp. 667-674.
- DE BORST, R.; SLUYS, L.J., 1999 – **Computational Methods in Non-Linear Solid Mechanics**. Faculty of Civil Engineering and Geosciences. Delft University of Technology, Delft.
- ESPADA, M., 2010 – **Desenvolvimento de Modelos para Análise Dinâmica de Estruturas. Aplicação a Barragens de betão e estruturas auxiliares**. Lisboa.
- FARIA, R., 1994 – **Avaliação do comportamento sísmico de barragens de betão através de um modelo de dano contínuo**. Tese de Doutoramento, FEUP, Porto.
- FARIA, R.; OLIVER, J., 1993 – **A rate-dependent plastic-damage constitutive model for large scale computations in concrete structures**. Monografia Centro Internacional de Metodos Numericos in Ingenieria (CIMNE), nº 17
- FARIA, R.; OLIVER, J.; CERVERA, M., 1998 – **A strain-based plastic viscous-damage model for massive concrete structures**. Int. J. Solids Struct., 35(14), pp. 1533–58.
- GEERS, M., 1999 – **Continuum Damage Mechanics. Fundamentals, Higher-order theories and Computational Aspects**. Lecture notes. Mechanics of Materials, Applied Mathematics and Technologies. Eindhoven University of Technology, Eindhoven.

- GRIFFITH, A., 1921 – **The phenomena of rupture band flow in solids**. Phil. Trans. Of The Royal Society of London, A221 pp. 163-197.
- HILLERBORG, A., 1985 – **Numerical methods to simulate softening and fracture of concrete**. In Fracture Mechanics of Concrete: Structural Application and Numerical Calculation, G.C. Sih and A. DiTomasso eds., Martinus Nijhoff Pub., Dordrecht, pp. 141-170.
- ICOLD, 2017 – **International Commission on Large Dams**. Retrieved from ICOLD: <http://www.icold-cigb.net>.
- INGRAFFEA, A.R.; SAOUMA, V., 1985 – **Numerical modelling of discrete crack propagation in reinforced and plain concrete**. In Fracture Mechanics of Concrete, G.C. Sih and A. DiTomasso eds., Martinus Nijhoff Pub., Dordrecht, pp. 171-225.
- JU, J.W., 1989 – **On energy-based coupled elastoplastic damage theories: constitutive modelling and computational aspects**. Int. Journal of Solids and Structures, V.25, pp. 803-833.
- KACHANOV, L.M., 1958 – **Time of the rupture process under creep conditions**. Izv. Akad. Nauk. USSR. OtdTekh.Nauk, N.8.
- KACHANOV, L., 1986 – **Introduction to continuum damage mechanics**. Martinus Nijhoff Pub., Dordrecht.
- LEMAITRE, J., 1984 – **How to use Damage Mechanics**. Nuclear Eng. And Design, Vol. 80, pp. 233-245.
- LEMAITRE, J; CHABOCHE, J. L., 1985 – **Mécanique des matériaux solides**. Dunod, Paris.
- LNEC, 1991 – **Estudo Experimental da Barragem do Cabril. Ensaios até à Rotura**. Rel. 216/91, NDE. Departamento de Barragens de Betão, Lisboa, Outubro.
- LNEC, 1993 – **Avaliação da Segurança de uma Barragem Abóbada com a Zona Superior Fissurada**. Rel. 143/93, NDE/NEE, Departamento de Barragens de Betão. Lisboa, Julho.
- LNEC, 2003 – **Observação da Barragem do Cabril (Período da fase de exploração de 1982 a 2001). Análise do Comportamento e Avaliação das Condições de Segurança**. 3º Relatório. Rel. 397/2003, NMMF/NO. Lisboa, Dezembro.
- LNEC, 2010 – **Análise do comportamento até à rotura da barragem de Foz Tua para o cenário de deterioração do betão. Modelação numérica com base em leis constitutivas de dano**. Rel. 190/2010 – NMMF. Departamento de Barragens de Betão. Lisboa, Maio.
- LNEC, 2014 – **Barragem do Alto Tâmega (segunda definição de formas). Estudo para o cenário de deterioração do betão modelação numérica com base em leis constitutivas de dano**. Rel. 000/2014 – NMMF. Departamento de Barragens de Betão. Lisboa, Janeiro.
- MAZARS, J., 1984 – **Application de la mécanique de l'endommagement au comportement non linéaire et à la rupture du béton de structure**. Thèse de Doctorat d'Etat, L.M.T., Univ. De Paris. France.
- MURAKAMI, S.; OHNO, N., 1981 – **A continuum theory of creep and creep damage**. Creep in Structures. Ponter and Hayhurst eds.
- NGO, D.; SCORDELIS, A.C., 1967 – *Finite element analysis of reinforced concrete beams*. J. Amer. Concrete Inst. 64, pp. 152-163.

- OLIVEIRA, E. A., 1975 – **Resistência dos materiais. Livro II - Elementos da Teoria da Elasticidade.** Ed. Ass. Estudantes do Instituto Superior Técnico, 2ª Edição 1999, Lisboa.
- OLIVEIRA, E. A.; PEDRO, J.O., 1986 – **The rise and decline of structural analysis as a research topic in structural engineering.** Conference on Recent Advances in Simulation of Complex Systems. Tóquio.
- OLIVEIRA, S., 2000 – **Modelos para a Análise do Comportamento de Barragens de Betão Considerando a Fissuração e os Efeitos do Tempo. Formulações de Dano.** Tese de Doutoramento, FEUP, Porto.
- OLIVEIRA, S., 2011 – **Mecânica dos Sólidos III.** Folhas da Unidade Curricular. Lisboa: ISEL.
- OLIVEIRA, S.; FARIA, R., 2006 – **Numerical simulation of collapse scenarios in reduced scale test of arch dams.** J. Eng. Struct. 28, pp. 1430–1439.
- OLIVER, J., 1989 – **A consistent characteristic length for smeared cracking models.** Int. Journal of Numerical Methods Eng., 28, pp. 461–74.
- OLIVER, J.; CERVERA, M.; OLLER, S.; LUBLINER, J., 1990 – **Isotropic Damage Models and Smeared Crack Analysis of Concrete.** Journal of Eng. Materials and Techn., Trans. Of the ASME, Vol. 105, pp. 99-105.
- PEDRO, J.O., 1977 – **Dimensionamento de barragens abóbada pelo método dos elementos finitos.** Tese para especialista LNEC (Memória nº 479), Lisboa, Portugal.
- PIJAUDIER-CABOT, G.; BAZANT, Z. P., 1987 – **Nonlocal damage theory.** J. Eng. Mech., ASCE, 113(10), pp- 1512-1533.
- PINA, C., 1988 – **Modelos de elementos finitos para estudo de barragens de betão. Cenários correntes e de rotura.** Tese de especialista, LNEC, Lisboa, Portugal.
- RAMTANI, S., 1990 – **Contribution à la modélisation du comportement multiaxial du béton endommagé avec description du caractere unilatéral.** Thèse de Doctorat présentée à l'Univ. Pierre et Marie Curie, Paris. France.
- RASHID, Y.R., 1968 – **Analysis of prestressed concrete pressure vessels.** Nuclear Eng. Des. 7, pp. 334-344.
- RSB, 2018 – **Regulamento de Segurança de Barragens.** Decreto-Lei Nº 21/2018 de 28 de março.
- ROCHA, M.; SERAFIM, L., 1960 – **O problema da segurança das Barragens Abóbada.** LNEC, Memória nº 42, Lisboa.
- SIMO, J.C.; JU, J.W., 1987 – **Strain- and Stress-Based Continuum Damage Models – I. Formulation / II. Computational Aspects.** Int. Journal of Solids and Structures. Vol. 23 nº 7, pp. 821-840 / pp. 841-869.
- WESTERGAARD 1933 – **Water pressures on dams during earthquakes.** Transactions, ASCE; 98:418-433.
- ZIENKIEWICZ, O. C., 1967 – **The Finite Element Method in Structural and Continuum Mechanics.** McGraw-Hill Ed.
- ZIENKIEWICZ, O. C., 1977 – **The Finite Element Method.** McGraw-Hill Ed., 3<sup>rd</sup> edition.
- ZIENKIEWICZ O.C.; TAYLOR R.L.; ZHU, J.Z., 2005 – **The Finite Element Method: Its Basis and Fundamentals.** 6<sup>th</sup> edition, Elsevier Butterworth-Heinemann.